ABSTRACT

YEH, JACQUELINE S. Effect of Varying Hydrodynamic Shear and Extracellular Polymeric Substances on Aerobic Granulation. (Under the direction of Dr. Francis Lajara de los Reyes III).

Conventional activated sludge (AS) has been a central part of the wastewater treatment system since its development. The efficiency of AS could be improved by converting the slow-settling flocs to larger, denser, and more regularly shaped microbial aggregates known as aerobic granular sludge (AGS). The advantages of AGS over AS include higher settling velocity, increased toxicity tolerance, and higher biomass residence time. Previous research has shown that AGS formation is affected by hydrodynamic shear force, organic loading rate, and hydraulic selection pressure. However, although these factors are important to the granulation process, their impacts are not fully understood. This project aims to determine whether variations in hydrodynamic shear force and extracellular polymeric substances (EPS) are necessary factors for aerobic granulation by comparing the formation of AGS within Couette-Taylor Bioreactors (CTBs) and a control sequencing batch reactor (SBR). The SBR represents varying shear due to aeration solely occurring at the bottom of the reactor while the movement of concentric cylinders in CTBs allows a consistent total average shear due to the aeration and rotation. Three CTBs were compared to the SBR: one with lower, one with equal, and one with higher total average shear to the SBR. Granules were determined to be particles with an equivalent diameter above 200 um and roundness (a measure of elongation) above 0.6. The results showed the SBR achieving a higher percentage of granules than each of the CTBs, which did not consistently accumulate AGS. The SBR granule percentage peaked around day 40. EPS was extracted and measured as a ratio of protein (PN) and polysaccharide (PS) components found in soluble, loosely-, and tightly-bound EPS. Trends in the PN/PS ratio measured from the types of EPS indicate that destabilization of aerobic granules may be followed by an increase in the

polysaccharide component of soluble EPS, perhaps making the polymer matrix too stiff to allow for sustained granule growth by aggregation. Additional trends indicate that tightly-bound EPS trends follow the formation of granules, suggesting higher proportions of polysaccharides to proteins in this layer are beneficial for granule formation.

Effect of Varying Hydrodynamic Shear and Extracellular Polymeric Substances on Aerobic Granulation

by
Jacqueline S Yeh

A thesis submitted to the Graduate Faculty of
North Carolina State University
in partial fulfillment of the
requirements for the degree of
Master of Science

Environmental Engineering

Raleigh, North Carolina

2018

APPROVED BY:

_____	_____
Dr. Joel J. Ducoste	Dr. Douglas F. Call

_____
Dr. Francis Lajara de los Reyes III
Chair of Advisory Committee

DEDICATION

To my parents, David and Khue, and my brothers, Andy, Victor, and Carter,

Thank you for your unconditional love and support.

And for pretending to look interested when I explained my research project.

BIOGRAPHY

Jacqueline Yeh was born in Plano, Texas on June 27, 1994 to David and Khue Yeh. She spent half her childhood in Plano before moving to Cary, North Carolina in 2005. In 2012, her undergraduate journey began at North Carolina State University. During her time as an undergraduate student, Jacqueline was in the University Honors Program, served as co-director of Engineers' Week within Engineers' Council, studied abroad at the Prague Institute in Prague, Czech Republic, and enjoyed pottery classes at the Craft Center. Jacqueline completed her Bachelor of Science in Environmental Engineering and Minor in Design Studies at North Carolina State University in 2016. After an interest in research was sparked as an undergraduate, she began her Master of Science degree in Environmental Engineering in the same department in the fall of 2016 under the supervision of Dr. Francis Lajara de los Reyes III.

ACKNOWLEDGMENTS

With immense gratitude, I would like to acknowledge my advisor, Dr. Francis de los Reyes, for introducing me to the world of research and for guiding me during my graduate studies. I am grateful for all the advice and opportunities shared along the way.

Additional gratitude for Dr. Joel Ducoste for his support, advice, and knowledge shared during research meetings and for his constant enthusiasm.

Sincere thanks as well for my committee member, Dr. Douglas Call, for the suggestions made and time set aside during this thesis development.

I am very grateful to Joseph Weaver, Ling Wang, Yi-Chun Lai, and Austin Burke for their help with the lab work involved with my reactor operation. This project would not have been possible without your assistance.

Further thanks to Dr. Lisa Castellano, the Environmental Engineering Lab Manager who helped me process numerous samples and develop my experimental procedures.

Many thanks to Jake Rhoads for his expertise and help in building and fixing the reactors.

Additional thanks to the Staff of North Cary Water Reclamation Facility for always being eager to answer my questions and for providing the seed sludge for this project.

Thank you to the National Science Foundation for the funding of this project.

Lastly, to all who sit in the Mann Hall 319A office and the rest of the environmental engineering graduate student family, thank you for the support, laughs, and sanity you provided along this journey.

TABLE OF CONTENTS

LIST OF TABLES

LIST OF FIGURES

CHAPTER ONE – Introduction

The conventional activated sludge treatment process is one of the most prominent and long-lasting technologies of the wastewater treatment industry though there are many areas where inefficiencies could be improved. Typical activated sludge steps must include two basins, requiring a large footprint. Typical aerobic sludge becomes flocculent in the aeration basin and is allowed to slowly settle in the secondary clarifiers and be returned to treat the new flows of influent wastewater. These characteristic fluffy floc structures may require long settling periods. A common operational disadvantage is for facilities to experience periods of bulking and foaming which prevents the sludge from settling effectively. In addition, the microbes in conventional activated sludge may not be able to handle unexpected loads or toxic shocks. Thought there are still questions regarding how and why certain reactor characteristics lead to their formation, aerobic granules have been developed over the past two decades as a more efficient alternative to the conventional activated sludge system.

Granules are self-immobilized microbial aggregations with larger and more consistent size, density, and shape factors, formed without additional media. The higher density and size of granules allows them to settle faster than flocs, leading to better retention. The microbial layers within an aerobic granular particle also allow for simultaneous nitrogen and phosphorous removal by the chemical reactions shown in the following figure.

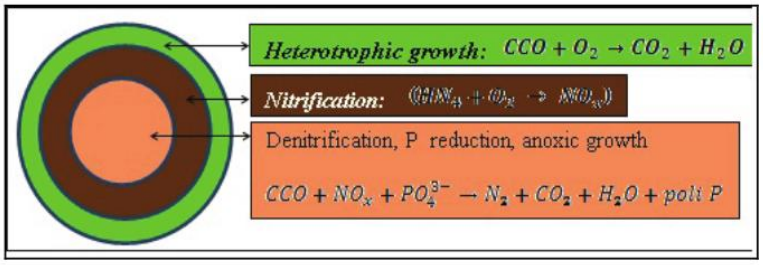

Figure 01. Possible chemical transformation processes in activated sludge granules (Cornea, Cr, & Dinu, 2013)

In addition, the granular sludge structure is better suited to deal with high organic loading rates and shock loadings. Previous research has been conducted to determine whether fundamental characteristics such as hydrodynamic shear, organic loading rate, and flow characteristics due to reactor configuration influence aerobic granular formation (Xiao, Yang, & Li, 2008).

Thus far, only one instance of aerobic granular sludge technology has been implemented at a full-scale facility, the Nereda® technology, developed at Delft Tech University in collaboration with Ryal HaskoningDHV (Rewell & Seccombe, 2012). Under specific conditions, Nereda® may be grown using a mix of bacteria able to remove biological oxygen demand (BOD), nitrogen, and phosphorous from wastewater.

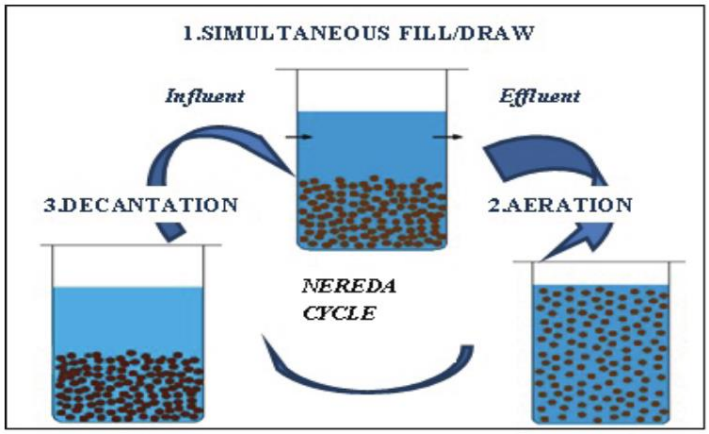

Figure 02. Nereda® cycle (Cornea et al., 2013)

The granules produced by the Nereda® system are dense and settle ten times faster than conventional activated sludge processes, which allows plants with the technology to operate with a smaller reactor volume and overall footprint (Rewell & Seccombe, 2012). The more efficient granules have achieved up to 40 percent lower energy consumption and reduces operational costs because little additional chemicals are needed, fewer tanks are required, and less aeration is

needed (Rewell & Seccombe, 2012; S. J. Sarma & Tay, 2018). Full-scale plants with Nereda® technology can achieve high effluent quality with less than 5 mg/L total nitrogen and about 0.3 mg/L total phosphorous (S. J. Sarma & Tay, 2018). Though this is an advance toward making aerobic granular sludge a reality for many treatment facilities looking to improve their treatment process, it is mostly suited for small plant sizes, batch configuration, specific types of wastewater, and specific loadings and removal requirements. The test plant in South Africa that piloted the full-scale demonstration of Nereda® treated four million liters per day of high strength influent (Rewell & Seccombe, 2012). High strength septic influent and municipal wastewater with high contributions of industrial waste from slaughterhouses have been successfully treated by aerobic granular sludge but at flows limited to 4000 to 36000 m^3/day (Li, Ding, Cai, Huang, & Horn, 2014). Thus far, few detailed reports have been released about the ability of the aerobic granules at these plants to withstand changes in process conditions, which has been an issue seen during lab-scale experiments and may be an issue for full-scale plants (S. J. Sarma & Tay, 2018). Improvements that the Nereda® team suggest include improving the type of influent the granular sludge is able to treat and widening the types of facilities that may be retro-fit with such technology, since Nereda® granules are only applicable under batch configurations, limiting the number of plants which may utilize the technology. Though there are several full-scale plants that operate with aerobic granular sludge technology in the Netherlands, Portugal, and South Africa, operational conditions of the technology are still limited by reactor configuration, substrate composition, selecting pressure, volume exchange ratio, hydrodynamic shear force, organic loading rate (OLR) feast-famine regime, feeding strategy, and cycle time (Li et al., 2014).

It is often concluded that the relatively circular upflow patterns seen in column reactors are homogenous enough to be represented by a single, average hydrodynamic shear value (Y. Liu & Tay, 2002). However, column reactors with a high ratio of reactor height to diameter display a variation in shear throughout a reactor system from high to low moving away from aeration ports. Higher levels of hydrodynamic shear are important for inducing the excretion of extracellular polymeric substances (EPS) which forms a sticky matrix and for driving the aggregation process (Feng et al., 2016). The EPS quantification is typically represented as a ratio of proteins (PN) and polysaccharides (PS) and it is widely assumed that these polymeric substances are important factors that lead to the formation of long-lasting granules (Liang, Li, Yang, & Du, 2010; H. Tay & Liu, 2001; B. Bin Wang et al., 2014). Despite recent interest in EPS, there is no consensus regarding the dominant polymers during the formation and steady-state operation of aerobic granular sludge technology or which type of EPS, soluble or bound, contributes the most to the granulation process (Laspidou & Rittmann, 2002). This project aims to determine if there is a distinguishable effect of variation of hydrodynamic shear, extracellular polymeric substances, and microbial community on the formation of granules. The results of this experiment could help treatment plant engineers and researchers better understand whether these factors are necessary to transform conventional activated sludge into aerobic granular sludge and push the field towards implementing this technology.

CHAPTER TWO – Background

2-1 Activated Sludge

Activated sludge is the most common biotechnology used during the secondary treatment process of wastewater due to its reliable performance of organics removal. This step requires the use of an aeration tank, for the removal of organic carbon, ammonium, and phosphate, and a secondary clarifier for the separation of solids (Martins, Pagilla, Heijnen, & Van Loosdrecht, 2004). While it has been widely used, there are areas for improvement in the technology. Potential improvement could be made to reduce the production of excess sludge, size of the unit process footprint, time of settling period, and operational problems.

A common operational problem that can arise with conventional activated sludge processes is bulking due to the sludge being unable to settle apart from the clear supernatant in the settling tank. This problem is often due to the presence of filamentous microorganisms which prevent the flocs from compacting and settling out (Martins et al., 2004). Alternative treatment methods have been developed and researched to avoid such problems and to meet increasing demand placed on existing facilities using existing infrastructure. Aerobic granulation has been studied as an improvement to the conventional activated sludge system with superior settling ability, high biomass retention, and tolerance for high organic loading rates.

2-2 Goal of Secondary Treatment

After primary treatment, which removes suspended solid waste and reduces BOD, secondary treatment uses biological processes to remove the remaining organic matter after primary treatment. Some common secondary treatment technologies include constructed wetland systems, stabilization ponds, and the most common – activated sludge. For each system, the last

step involves a settling process to separate suspended solids from treated water which is where there are inefficiencies with settling times and basin size and number required. By tailoring the sludge to settle faster through the formation of larger, denser granules, the secondary treatment footprint may be reduced, and shorter settling periods may be achieved.

2-3 Aggregation

The basis for many microbial processes in wastewater is aggregates: microbial communities that form biofilms or flocs which utilize extracellular polymeric substances (EPS) to stick together. Attached growth processes rely on a biofilm structure to achieve retention of the microbial community while suspended growth processes rely on the gravity settling ability of the floc particles to retain their microbial communities (Grady Jr., Diagger, Love, & Filipe, 2011). Though there are aspects of the complex aggregation process that are not fully understood, it has been concluded that EPS is important to the aggregation of flocs and biofilms due to their assistance with the retention of water, storage of nutrients, accumulation of enzymatic activity, and protection against toxins (Grady Jr. et al., 2011).

2-4 Extracellular Polymeric Substances

Extracellular polymeric substances (EPS) are sticky materials excreted by cells that primarily consist of polysaccharides, proteins, glycoproteins, nucleic acids, phospholipids, and humic acids with polysaccharides and proteins being the major constituents (Grady Jr. et al., 2011; Y.-Q. Liu, Liu, & Tay, 2004). The presence of proteins, lipids, and nucleic acids in EPS are due to the release of intracellular polymers from cell lysis (Y.-Q. Liu et al., 2004). Past research has shown that EPS are significant to adhesion phenomena, formation of matrix structure, microbial physiology, and granule stability (Y.-Q. Liu et al., 2004). The materials

excreted by cells forms a three-dimensional matrix that entraps bacteria, nutrients, and microbial debris, acting as a stabilizing and protective barrier between cells and the environment. Within the protective matrix, the EPS can also trap organic materials, providing the cells with a readily-available energy source, and enzymes, which hydrolyze the sorbed organic matter (Laspidou & Rittmann, 2002). While present in both flocculent and granular sludge, research has shown the EPS content of granules to be much higher than both conventional flocs and biofilms due to higher stress conditions necessary for the formation of granules (Y.-Q. Liu et al., 2004). Though reported as controlling factors related to membrane fouling of submerged membrane bioreactors (MBR), EPS is theorized to play an important role in the formation of aerobic granules (Z. Wang, Wu, & Tang, 2009). Several operational conditions, including reactor type, substrate composition and loading rate, hydraulic retention time, hydrodynamic shear force, settling time, feast-famine regime, and influent and operational temperatures can stimulate cells to produce additional EPS (Y.-Q. Liu et al., 2004).

Regarding biogranules, EPS can be divided into three types based on their proximity and interaction to the biomass. Soluble EPS (Sol-EPS), primarily consisting of soluble macro-molecules, colloids, and slimes, may be found in the bulk liquid, not attached to any particular microbial community. Loosely-bound EPS (LB-EPS) and tightly-bound EPS (TB-EPS), composed of sheaths, capsular polymers, condensed gel, loosely bound polymers, and attached organic material, are found close to microbial communities with TB-EPS being the layer closer to and more difficult to separate from the microbes (Laspidou & Rittmann, 2002; More, Yadav, Yan, Tyagi, & Surampalli, 2014). Ratios of bound and soluble EPS may change drastically depending on the growth conditions and consistency of operation (Y.-Q. Liu et al., 2004). The presence of EPS between microbial cells and bulk liquid forms concentration gradients for the

flocs and biofilms, also resulting in ecological zones (Grady Jr. et al., 2011). Separation of the soluble portion of EPS may be achieved by centrifugation as the soluble polymers are transferred to the supernatant, leaving the bound polymers attached to the biomass pellet (Y.-Q. Liu et al., 2004). Thus far, research has not been able to determine whether the EPS is made initially, leading to bacteria being able to stick together, or whether bacteria are able to adhere prior to the production of EPS.

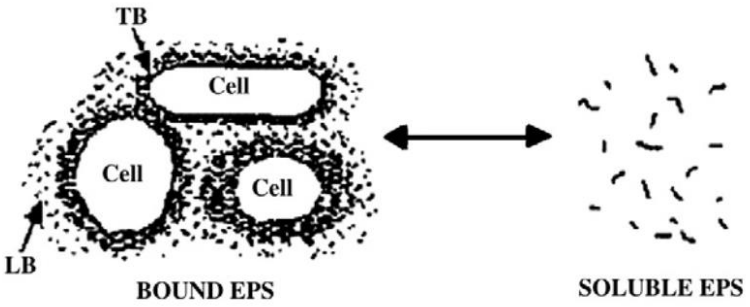

Figure 03. Sketch of EPS structure (Sheng, Yu, & Li, 2010)

Past research has produced contradictory reports on the ratio of carbohydrate to protein found in granule EPS with some reporting higher protein components (Fukuzaki, Nishio, & Nagai, 1995) and other reporting higher carbohydrates (Fang, Liu, & Zhang, 2002) though it is agreed that the quantity and composition of EPS produced by granules depends on the present species, limiting substrate, oxygen limitation, ionic strength, shear force, and phase of the batch cycle, among other operational conditions (Y.-Q. Liu et al., 2004). It has been reported by Tay et al. (2001) that aerobic granule formation corresponds to a sharp increase in cellular polysaccharides, leading the EPS polysaccharide to protein ratio to fall in the range of 2-16 g/g (J. H. Tay, Liu, & Liu, 2001). Since protein has more negatively-charged amino acids, it is thought to be more involved in electrostatic bonds with multivalent cations than polysaccharides; these electrostatic bonds are important to the stabilization of the aggregate structure (Laspidou &

Rittmann, 2002). While there are contradicting reports regarding the dominant components of granular EPS, it should be noted that there is not one standard EPS extraction method - there are many different EPS extraction methods, including EDTA extraction, ultracentrifugation, steam extraction, formaldehyde (RCF) and regular centrifugation, and sonication, among others, which makes it difficult to compare EPS found in different granular sludges treating different types of influent (Y.-Q. Liu et al., 2004; Pellicer-Nàcher, Domingo-Félez, Mutlu, & Smets, 2013). In general, it has been found that a protein/polysaccharide (PN/PS) ratio of 3.4:6.2 is present in the EPS matrix, not separated by different EPS types (Grady Jr. et al., 2011). It is thought that the β-polysaccharides and alginate are responsible for mechanically stabilizing the granules (Grady Jr. et al., 2011). While generally it is understood that the production of EPS affects the formation of larger aggregates and mature granular sludge, there is still more that is not understood about its formation – including whether a particular species produces the majority of the EPS or if all the microorganisms making up the granules produce EPS at similar rates. Additional work that needs to be performed includes EPS characterization to determine the individual polymers extracted as proteins or polysaccharides. Knowing which individual polymers are present may help determine which are the most important for granulation (Grady Jr. et al., 2011).

Though EPS components help organisms 'stick together' in stable arrangements, bioflocculation is also affected by the environment provided by the bulk liquid. Environmental parameters that affect bioflocculation include ionic strength, divalent ions, and solids retention time. Bulk liquid must have an ionic strength high enough for individual cells to get close enough for EPS to bridge between the cells but not high enough to lead to deflocculation; it has been suggested that an ionic strength in the range of 0.005 to 0.050 is optimum for stable floc formation (Grady Jr. et al., 2011). Divalent ions are thought to bridge between the negatively

charged cell surface and EPS with a minimum concentration of 0.7 to 2.0 meq/L of calcium and magnesium being suggested, though the actual required concentration would depend on the ionic strength of the particular wastewater being treated (Grady Jr. et al., 2011). Calcium, Ca^{2+}, ions may crosslink anionic polysaccharides in the EPS and play a role in stable granule formation while phosphate ions, which act as ion chelating agents, have been found to dissolve crosslinks found in calcium-alginate gels (Grady Jr. et al., 2011). This observation has led to the conclusion that chelating agents, such as phosphate ions, amino acids, peptides, or organic acids, found in wastewater may be responsible for destabilizing aerobic granules (Grady Jr. et al., 2011). In addition to having a recommended concentration of divalent ions, it is important for the ratio of divalent to monovalent cations to be above 0.5 as the competition between the two cations for the binding sites on the cell surfaces and the EPS can cause lower formation of settling characteristics (Grady Jr. et al., 2011). Operating above a minimum solids retention time (SRT) is important to allow the rate of EPS production by the floc-forming bacteria to match the rate of bacterial growth with new surface area; if the SRT is too short, the bacterial growth rate may exceed the EPS production and prevent optimal conditions for bioflocculation from being reached.

Bulk liquid characteristics can also affect surface characteristics of cells which affects the bound EPS components that accumulate on the surface of microorganisms. Cell surface hydrophobicity, surface charge density, binding site availability, and overall surface morphology can be affected by the production of EPS (Y.-Q. Liu et al., 2004). Some research has proposed that EPS may help reduce the strength of the negative charge found on cell surfaces, allowing adjacent cells to be physically bridged, as seen Figure 04. Other groups have found that EPS

increases the softness of cell surface and further reduce the negative surface density charge of cells by transferring some of the negative charge to the EPS itself (Y.-Q. Liu et al., 2004).

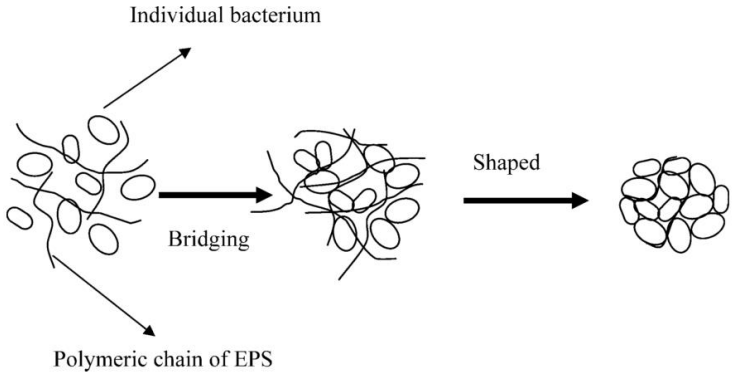

Figure 04. Schematic representation of extracellular polymeric substance (EPS)-enhanced biogranulation (Y.-Q. Liu et al., 2004)

The overall process that relates EPS production to the aggregation and formation of aerobic granules comes from the role of EPS as a capsular material correlated to cell-to-cell adhesion. It has been found that when exopolysaccharide synthesis was blocked, microbial aggregation was also prevented, strengthening the argument that EPS is a necessary factor related to microbial adhesion (Cammarota & Sant'Anna, 1998). The formation of the EPS matrix also provides a larger surface area for bacterial binding and additional sites for the attraction of organic and inorganic materials (Sponza, 2002; J. H. Tay et al., 2001). Though the exact functions of EPS related to granules have yet to be confirmed, microscopic observation has led researchers to discover EPS within the intercellular spaces in granular microcolonies and surrounding both aerobic and anaerobic granules (J. H. Tay et al., 2001). Compiling these experimental results, it seems likely that EPS plays a role in maintaining the structure and integrity of granular sludge.

2-5 Granules and Activated Sludge

Granular sludge technology began with anaerobic granules in 1976 for wastewater treatment with aerobic granular technology being reported and researched beginning in 1991 (Saurabh Jyoti Sarma, Tay, & Chu, 2016). The success of anaerobic granular technology with upflow anaerobic sludge blanket (UASB) reactors is often marred by the long start-up period of two to eight months for anaerobic granular sludge development and its inability to be applied for nutrient removal of wastewater; comparatively, the relatively new aerobic granules have a shorter start-up period and may be used for nutrient removal (Y.-Q. Liu et al., 2004). Thus far, aerobic granules have been almost exclusively developed in sequencing batch reactor configurations.

Aerobic granules are self-immobilized microspheres with multispecies microbial layers that typically grow to 1-3 mm in diameter and must be cultivated under specific operational conditions with strong selective pressure (Y. Q. Liu & Tay, 2007; S. J. Sarma & Tay, 2018). Without specific operational conditions, the self-aggregation without the presence of media would not begin the granulation process (Y.-Q. Liu et al., 2004). Due to an outer layer of aerobic microorganisms and an inner layer of facultative and obligate anaerobic microorganisms and dead biomass, aerobic granules are able to achieve nutrient removal (S. J. Sarma & Tay, 2018). The process to grow ideal granules containing certain species of autotrophic ammonia-oxidizing bacteria, which perform better nitrogen removal, and *Accumulibacter,* which can couple denitrification with phosphorous uptake, and the factors leading to these granules' formation still needs to be determined. To date, mature aerobic granules with stable COD removal efficiency have been formed in sequencing batch reactors over a period ranging from one week to several months, an improvement relative to anaerobic granule start-up.

The compact and dense nature of aerobic granules allows short settling times to be used and reduces the necessary size of settling tanks to about one-fifth of that required by conventional activated sludge systems (S. J. Sarma & Tay, 2018). The sludge volume index (SVI) is generally used as the main quantitative factor used to evaluate sludge settling properties and shows large differences between aerobic granules and flocs formed from conventional activated sludge (Deng, Wang, & Su, 2016). It has been increasingly common to compare a five-minute and thirty-minute SVI (SVI_5 and SVI_{30}) to show the superior settling of granules over flocs (Pronk et al., 2015; S. J. Sarma & Tay, 2018; Wei, Ji, Li, & Qin, 2012). Due to the high biomass concentration, the desired removal of contaminants is much faster than in conventional activated sludge or larger volumes may be treated in a smaller amount of space (J. H. Tay, Liu, & Liu, 2002). Direct analysis of the SVI_5 also helps correlate operational events to granule behavior; for instance, decreases in SVI_5 just after inoculation of reactors with conventional activated sludge could indicate slow adaptability to the new configuration and operation or washout of suspended biomass due to strong selection pressures (Wei et al., 2012). The fast settling of aerobic granules also allows about three to five times greater biomass retention, as the granules tend not to be washed out in the effluent, and a reduction in sludge volume which allows larger volumes of wastewater to be treated under the same period (S. J. Sarma & Tay, 2018). The improved biomass retention also reduces the amount of biomass that makes it to the treated effluent stream, reducing the cell-bound pollutants and nutrients that are released with the effluent (Saurabh Jyoti Sarma et al., 2016).

The theorized granulation process begins with cell-to-cell contact due to physical movement initiated by hydrodynamic forces, diffusion forces, gravity, Brownian movement, or cells' mobility (Y. Liu & Tay, 2002). Once the cells are close enough to interact with one

another, adhesion due to proton translocation, surface charge neutralization, cell surface hydrophobicity, and van der Waals forces takes place (Y. Liu & Tay, 2002; S. J. Sarma & Tay, 2018). The gradual development of the microaggregates is followed by growth of the multispecies clusters and EPS production, due to environmental stressors such as fluid shear or nitrogen starvation, which helps form larger aggregates by mediating cohesion and adhesion of cells (Adav, Lee, & Lai, 2007). The final steps lead to mature granule formation, involving compaction and growth to a diameter between 1 to 3 mm as well as strengthening of the aggregate structure. At steady-state, hydrodynamic shear forces lead the three-dimensional structure of the granules to be more regular. From the innermost to outermost layers, the granule consists of a core of anaerobic and facultative anaerobic microorganisms and dead microbial cells and an outer layer of aerobic microorganisms. Though aeration is needed for the growth of aerobic granules, it reduces the nitrogen and phosphorous removal efficiency; this has led the determination that granule development and use in wastewater treatment should be treated as separate processes to keep both efficient (S. J. Sarma & Tay, 2018). The layers present around aerobic granules may protect the innermost bacteria, allowing granules the resilience to withstand toxic shocks and changes in pH (Y. Q. Liu & Tay, 2007).

This process is sensitive to many factors, including reactor geometry, substrate type, and nucleating agents. Most aerobic granules produced under lab conditions have come from sequencing batch reactors with a large height to diameter ratio though the practical implementation of aerobic granular sludge in treatment plants will often involve low height to diameter ratios (S. J. Sarma & Tay, 2018). Selection pressure, or the set of environmental factors including temperature, dissolved oxygen (DO), chemical oxygen demand (COD), and settling time which favor the growth and dominance of a certain group of microorganisms, is known to

be one of the driving forces behind aerobic granulation; however, the actual molecular mechanisms that lead these forces to affect granulation are not fully understood (Grady Jr. et al., 2011). While aerobic granules can be produced without the addition of media for the biomass growth to begin on, nucleating agents such as granular activated carbon have been used to speed up the formation of granules by acting as locations for cell attachment and granule growth to begin (S. J. Sarma & Tay, 2018).

Since aerobic granules have a better retention time than conventional activated sludge, it may more effectively be able to remove pollutants via bioaccumulation or adsorption, which increases its ability to effectively remove emerging contaminants, persistent organic pollutants, nanomaterials, and heavy metals present in wastewater at low concentrations (Saurabh Jyoti Sarma et al., 2016).

Another aspect of granulation that is being researched is how to predictably maintain healthy and stable granules. Stability of granules may be defined as the ability of microbial aggregates to resist hydrodynamic and mechanical shear which may erode the surface of the particles and affect the separation of the solid and liquids (Sheng et al., 2010). Currently, the mechanisms leading to aerobic granule disintegration have not been identified. The increase in granules' size as a result of microbial growth prevents the dynamic size and shape characteristics of particles during granulation from being predictable since not much is known about the growth rates of the microorganisms found in aerobic granules. Though microbial communities vary throughout different the formation of granules under different conditions, it is suggested that the formation of EPS is more significant to the formation and strength of granules than microbial composition (Quarmby & Forster, 1995). In order for aerobic granules to be a reliable technology, more research will be needed regarding conditions needed to keep efficient granules

under steady-state conditions. As mentioned earlier, a possible mechanism for destabilization is the presence of phosphorous ions which act as chelating agents and precipitate out calcium and magnesium as calcium or magnesium phosphate, respectively, and rendering the cations useless for crosslinking with the EPS matrix polymers (Grady Jr. et al., 2011). Other studies have suggested that granule disintegration may be due to anaerobic ammonium-oxidizing bacteria (Grady Jr. et al., 2011) or EPS-deficient conditions (Quarmby & Forster, 1995). As granules disintegrate, it has been observed that the protein to polysaccharide ratio of EPS content will also correspondingly decrease with disintegration events (Kang & Yuan, 2017). Adav et al. (2007) discovered that the proteins and dead cells were the main components in the core layer of aerobic granules while active cells and α-polysaccharides were found along the outer layers of the granules and β-polysaccharides were found throughout the granules; from this experiment they theorized that the protein found in the core of the aerobic granules and the β-polysaccharides found throughout were important for the stability of the granules (Adav et al., 2007). Confirmation of this theory has been hindered by the difficulty to accurately separate layers of extracellular and intercellular polymers. Current literature includes some reports that the protein component of EPS found on aerobic granules is essential for the stability and settleability of granules while other experiments report that the polysaccharide component of EPS is responsible for the gel-like properties that lead to denser and more stable granule formation (Kang & Yuan, 2017). Thus, more research and consistent results are needed to determine which primary component of EPS is essential to the successful formation of aerobic granules.

EPS formation over the course of aerobic granulation is also followed as changing portions of protein to polysaccharide (PN/PS) ratios which are used to determine how EPS production changes as a result of organic loading rates and hydraulic retention times. Kang et al.

(2017) reported that EPS production was increased because lower OLR and led to more compact granules formation (Kang & Yuan, 2017). The same experiment also reported that higher PN/PS ratios were achieved for lower OLR and confirmed that starvation times during batch operation of reactors led to higher EPS production. Some theorize that increasing protein components of EPS are secreted to protect cells from the shock of nutrient deficiencies while increasing polysaccharide components assist aggregates in becoming denser and more regularly shaped (Deng et al., 2016). This increase of EPS for nutrient deficiencies was also seen during the starvation phase of batch operation to allow the microorganisms to continue to consume nutrients though the COD fed during the influent period had already been removed (Deng et al., 2016).

When assessing the viability of aerobic granular sludge technology, it is important to compare the timeline of start-up between developing granules and adapting conventional activated sludge. Conventional activated sludge typically takes between 30 and 40 days to acclimate to a particular wastewater (Pronk et al., 2015; Wei et al., 2012). If additional biomass is required to treat the wastewater to regulation levels, the start-up period required may be longer. When planning for the necessary biomass volume, a plant must consider the ability to treat the highest load at the coldest temperature the plant, which leads to longer start-up times. Thus far, the start-up times required for aerobic granular sludge plants have been similar (Pronk et al., 2015). Depending on the stringency of effluent requirements, plants may need to operate with gradually increasing stepwise influent flows to achieve effluent quality requirements during start-up.

Granules have been observed to form effectively under a variety of different substrates (i.e. glucose, acetate, etc.) and with many different organisms, such as methanogens, acidifying bacteria, nitrifying bacteria, denitrifying bacteria, and aerobic activated sludge (J. H. Tay et al.,

2002), which leads to the conclusion that granulation is primarily related to the operational parameters chosen for reactors (i.e. settling period, hydraulic retention time, aeration, hydrodynamic shear, etc.). Although there are still fundamental questions remaining around the aerobic granulation process, laboratories have made efforts to determine how other operational parameters such as organic loading rate, shear stress, aeration, hydraulic retention time, and selection pressure affect the granulation process. Though these factors have warranted many different experiments, the granulation process is still unpredictable and not fully understood.

2-6 Hydrodynamic Shear in Reactors

In biological reactors, hydrodynamic shear force can come from gas or liquid flow and particle-particle collision and is an important operational parameter for the effective formation and stability of granules under aerobic and anaerobic conditions due to its influence on the structure, metabolic behavior, and kinetic behavior of microorganisms present in granular sludge (Tay et al., 2002). Though high shear has been observed to be necessary for the formation of a strong biofilm, and low shear has led to heterogeneous, porous and weaker biofilm structure, less is known about how hydrodynamic shear affects the formation of granules. Studies have shown that granulation failed to occur under low shear conditions, but there is not a consensus about how hydrodynamic shear force mechanisms lead to effectively produced granules (Liu et al, 2002). Additional research has shown that higher superficial air upflow velocity leads to higher polysaccharide to protein (PS/PN) ratios of EPS in three-phase fluidized bed reactors and it has been generally shown that polysaccharide production increases with higher hydrodynamic shear forces (Liu et al., 2002; Adav et al., 2007). This increased production of EPS components is beneficial for the initial cell-to-cell adhesion that is an early step in the aerobic granulation process.

It has also been reported that within upflow sludge blanked reactors (USBR) with low superficial air velocities around 0.008 m/s, only fluffy flocs were formed, and it was not until an superficial air velocity of 0.025 m/s was reached that granules were reported (Tay et al., 2001). It was similarly reported by Beun et al. (1999) that superficial air velocities of 0.014 and 0.02 m/s did not lead to granulation while higher superficial air velocities of 0.041 m/s did lead to stable aerobic granulation under SBR conditions. Adav et al. (2007) also reported that low aeration rates of 1 L/min did not produce stable granules in comparison to granules with filamentous growth under 2 L/min aeration and 1.0 to 1.5 mm diameter granules were produced in reactors with high aeration rates of 3 L/min. Operational deficiencies in dissolved oxygen or nutrients due to lower aeration may be more favorable to filament growth which affects the stability and performance of granules. High shear may be responsible for the surface erosion that leads to smoothing and promotion of denser aerobic granules, though further research needs to be performed to fully understand how the shear affects granulation at a molecular level.

High hydrodynamic shear conditions with experimental SBRs may lead to the breakup of filamentous granules that are often seen soon after inoculation with conventional activated sludge; the filamentous granules are not stable and usually break apart after a few days but may be important nucleation sites for stable granules (Beun et al., 1999). These filamentous pellets likely lyse due to oxygen limitations in the center of the pellets. The appearance of higher superficial gas velocities also led to the smoothing of granules which displayed filamentous outgrowth, leading to higher shape factors and a more regular appearance of the formed granules. Thought the originally filamentous pellets lyse, the bacterial aggregates of multispecies microorganisms are able to continue to grow and form colonies because they are also able to become large enough to settle quickly and will eventually grow large enough to form granular

media and dominate reactors under the right operational conditions (Beun et al., 1999). Paired with high COD loading and short settling periods, high shear can lead to the formation of stable granules in an SBR.

Several reported experiments have contrasted the view that higher aeration, and subsequent hydrodynamic shear forces, are necessary for the formation of aerobic granules by reporting that compact granules were successfully achieved with lower hydrodynamic shear rates. Kang et al. (2017) achieved such granules with a superficial upflow air velocity of 0.43 cm/s and Henriet et al. (2016) also achieved granulation with dynamic shear rates of 0.42 cm/s. The apparent granulation achievement of these experiments may indicate that it is not an average hydrodynamic shear that leads to granule formation, but rather the inclusion of a variation in hydrodynamic shear within a reactor that offers ideal conditions for granulation. The experiment performed for this project aimed to address whether this variation in hydrodynamic shear is necessary for aerobic granule formation within an SBR.

While previously believed that column reactors with a high ratio of reactor height to diameter led to relatively homogenous circular flow along a reactor's height (Liu et al., 2002), it is known that there is variation in shear due to the reactor configuration. Thermodynamically, the circular flow found in column reactors forces granules to be sheared into more regularly shaped aggregates to develop minimum surface free energy, similar to how benthic round-shaped boulders are formed in flowing river systems (Liu et al., 2002).

2-7 Sequencing Batch Reactors vs. Couette-Taylor Bioreactors

Sequencing batch reactors (SBR) are a common reactor type due to their cost effectiveness and efficiency. They utilize operational cycles consisting of fill, aeration/reaction,

settle, and decant times to treat wastewater though suspended growth biomass. These reactors are often use for lab-scale aerobic granulation experiments because each step of the cycle can be easily tailored to favor the formation of larger, denser particles, increased EPS production, and the microbial communities that lead to aerobic granules.

Taylor-Couette flow is the flow between the narrow gap of two coaxial cylinders where one or both of the cylinders are rotating (Masuda, 2018; Qiao, Yan, Teoh, Tong, & Wang, 2018). This type of flow has been used in industrial applications for the cooling of rotary machines, filtration, particle classification, and blood detoxification and for food and bioprocesses due to its improved mixing and heat transfer (Masuda, 2018). Taylor-Couette reactors are also chosen for many bioreactors because the produce less agitation and sparging than traditional stirred and aerated bioreactors which can produce high stress and lead to undesired breakup of fragile cells (i.e. mammalian cells without cell walls) (Qia, Yan, Teoh, Tong, & Wang, 2018). In many cases, only one of the coaxial cylinders will be allowed to rotate to simplify the system. For this experiment, the inner cylinder, or wall, remained stationary while the outer cylinder rotated. This system of movement meant that the fluid velocity was highest adjacent to the inner wall and lowest near the outer wall, leading to the circular movement of fluid from the inner to the outer wall. These small eddys produced a more laminar flow than if the inner wall had been the rotating surface, as illustrated in Figure 05. This was desirable as it led to a more homogeneous mixture of the fluid within the reactors which allowed for average shear comparison between the CTBs and the SBR which had spatially varying shear. The vortices produced by Taylor-Couette flow are affected by density and viscosity of the fluid, buoyancy, speed of rotation, and operational parameters of the specific setup.

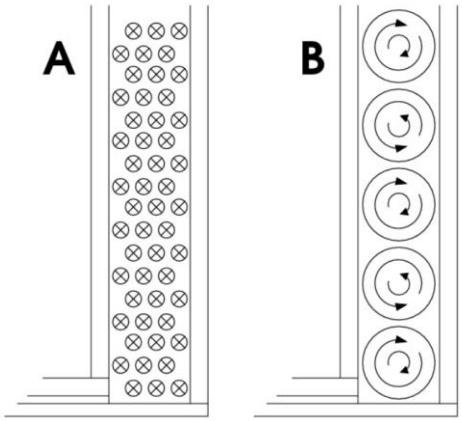

Figure 05. Fluid motion within an annular gap; (A) For a rotating outer cylinder, laminar streamlines flow into or out of the page with no z-component; (B) For a rotating inner cylinder, turbulent Taylor vortex motion is observed (Williams, 2004)

2-8 Stokes' Law of Settling

Settling velocity of aerobic granules, and conventionally for particle aggregates in water and wastewater treatment processes, follows Stokes' law for porous but impermeable microbial granules, which is a generalization applicable for a wide range of Reynolds numbers (Wei et al., 2012).

$$U_s = \left(\frac{4g(\rho_a - \rho_l)d}{3\rho_l C_d}\right)^{1/2} = \left[\frac{8gf}{\pi}\left(\frac{1}{\rho_l} - \frac{1}{\rho_a}\right)\frac{W_d}{C_d d^2}\right]^{1/2} \quad \text{Eq. 1}$$

Where ρ_a and ρ_l are the densities of the aggregate and the surrounding liquid, respectively, g is the gravitational constant (9.81 m/s^2), d is the diameter of the aggregate, C_d is the empirical drag coefficient adjusted for Reynolds numbers above 1, f is a dimensionless ratio between the wet mass and dry mass of the cells with the aggregate, and W_d is the dry mass of the bacterial aggregate (Wei et al., 2012). The empirical drag coefficient is adjusted according to the following equation, using Reynolds numbers (Xiao et al., 2008).

$$C_d = \frac{24}{Re} + \frac{6}{1+\sqrt{Re}} + 0.4 \qquad \text{Eq. 2}$$

Settling rate of particles is dependent on the size and density of particles due to Stokes' Law of Settling. Under sequencing batch reactor configurations, the desired settling period will allow larger, granular material to settle below the effluent discharge point while more flocculent, slow-settling sludge is washed out of the effluent port.

2-9 Key Players in Conventional vs. Granular Aerobic Sludge

Though much research has been performed to determine how various process parameters affect the formation of granules, there is also little known about the microbial communities found within the layers of a granules' structure. Thus far, few experiments have been performed analyzing community structures found within aerobic granules and corresponding reactor performance. Granules developed for swine wastewater treatment showed *Nitrosomonas* and *Nitrosococcus* as the dominant bacteria populations for both flocs and granules, though the diversities of the dominant populations were not significantly different (Mota et al., 2014). Understanding how the ecology of influent wastewater affects the microbial communities and their nutrient removal performance would allow for more tailored treatment operation and control. Aerobic granules degrading tert-butyl alcohol have been found to have stable communities with α, β, and δ subdivisions of *Proteobacteria* and the *Cytophaga-Flavobacteria-Bacteroides* (CFB) group (Zhuang, Tay, Yi, & Tay, 2005). Under influent primarily consisting of methyl *tert*-butyl ether (MTBE), *Sphingomonals*, *Methylobacterium*, and *Hyphomicrobium* vulgare, have been found to be the dominant members (Zhang, Chen, & Fang, 2008). Other analyses of pyridine-phenol aerobic granules have found *Acinetobacteor* sp. to be the dominant species (Adav et al., 2007). Though these studies have reported dominant species, the

wastewaters being treated in the experiments are not representative of typical municipal or industrial waste which the majority of treatment plants would receive. Additionally, there has not been extensive research looking at whether there is a consistent community structure that makes up aerobic granules regardless of the dominant component of substrate to be treated. An example of a microbiological study regarding granules that could be done includes how autotrophs, which can store excess nutrients in the form of glycogen or polyhydroxyalkanoates (PHA), contribute to granule formation (Grady Jr. et al., 2011). Determining which microbial 'key players' are necessary to the formation of granules can help determine which process parameters should be tweaked to achieve fast and efficient granule formation.

2-10 Knowledge Gaps Preventing Aerobic Granular Technology from being Implemented

Before aerobic granular sludge technology may be implemented further into industry or municipal wastewater treatment the granulation process needs to be predictable and reproducible under different reactor configurations and should be able to treat a wide range of wastewater. It should be further understood how process parameters such as aeration rates and primary substrate concentrations affect the growth and stability of aerobic granules. Since anaerobic granules were developed before aerobic granules and have been successfully studied and understood, it has been suggested to identify the common factors involved in both anaerobic and aerobic granule formation as the 'primary factors' which should be further investigated as the basic requirements for granulation in general. Examples of primary factors include EPS synthesis, quorum sensing, cell-surface hydrophobicity, and ionic bridging (Grady Jr. et al., 2011). From there, the secondary factors, which may only affect the quality or appearance of the granules, which are not common between anaerobic and aerobic granule formation should be identified and studied. An example of a secondary factor is substrate type of the wastewater;

acetate-fed microbes produce slightly different granules to propionate-fed microbes. So, although the two types of substrate form granules with differing qualities, both types do form granules. This approach would allow research to focus on developing an understanding of how the basic mechanisms, the primary factors, affect granulation.

During lab-scale experiments revolving around the growth and developing stability of aerobic granules, it has been found that the pH of the influent wastewater effects the structure and microorganism dominance of the granules (Xiao et al., 2008). Generally, influent with a low pH and alkalinity produces filamentous and fungi-dominated granules while reactors fed by high-alkalinity influent tend to produce denser granules dominated by rod-shaped bacteria (Xiao et al., 2008). The species that dominates aerobic granules is important because the structure affects the settling velocity and operational parameters. For instance, fungi-dominated granules tend to be larger, looser, and impermeable which leads to settling velocities that are not as fast as denser granules characteristic of bacteria-dominated granules when evaluated using Stokes' law. Thus far, paying attention to the alkalinity of the influent and regulating pH can help determine the dominant species during the aerobic granulation process (Xiao et al., 2008). To improve the viability of this technology in industry, conditions leading to the consistent formation of granules need to be determined to favor species needed to effectively treat the wastewater to regulation standards.

One of the major setbacks in the quest to implement the more efficient aerobic granular sludge technology includes the current inability to develop consistent and stable aerobic granules under continuous operational condition, as opposed to batch conditions. The development of a solution to this problem is essential since most plants that could be retrofit with aerobic granular

sludge technology must operate under continuous conditions to meet demand. Future research will need to adapt what is known about aerobic granulation for continuous reactor setups.

2-11 Hypothesis

With this project, we want to address our hypothesis that variation in shear, not just an average shear, within a reactor is necessary for aerobic granulation and determine whether extracellular polymeric substances play a role in the granulation process. To compare consistent and variable shear within a reactor, Couette-Taylor bioreactors and a sequencing batch reactor were used, respectively. For the Couette reactors, aeration and rotation of the outer wall provide shear while only aeration operates as the shear source for the SBR. To examine whether variation in shear or a minimum shear is required for the formation of aerobic granules, the SBR operated as the control while three CTBs are operated at a lower, equal, and higher total average shear to the control SBR. Samples taken during the operation of the four reactors were tested for the polysaccharide and protein components of soluble, loosely-, and tightly-bound EPS to allow trends related to granulation to be determined. Findings from this project should be able to help treatment plants looking to implement aerobic granular sludge technology to understand what kinds of shear variation, flow patterns, and EPS levels are favorable for inducing aerobic granulation.

CHAPTER THREE – Materials and Methods

3-1 Introduction

To address the primary operational variable of hydrodynamic shear variability, four lab-scale sequencing batch reactors were operated in parallel. The control reactor was a tall, narrow, cylindrical Sequencing Batch Reactor (SBR) similar to typical setups prepared where aerobic granules have been developed. The other three reactors were Couette-Taylor bioreactors (CTBs), used to examine reactor conditions where there was a uniform average shear throughout the reactor body. The CTB configuration is also known as an annular gap bioreactor, further discussed in Section 3-2 of this chapter. One CTB was run at a lower average total shear than the SBR, one at an equal total average shear to the SBR, and one at a higher total average shear to the SBR. Activated sludge, sampled from the North Cary Water Reclamation Facility, was placed in each reactor as inoculum. Influent concentration and flow, discussed in Section 3-5, were the same for every reactor and aeration provided by fine bubble diffusers and stones were adjusted to ensure the desired total average shear in the CTBs was appropriate with the limits of the pottery wheels providing rotation to the CTBs.

3-2 Reactor Setup

This experiment was run using a control sequencing batch reactor (SBR) and three experimental Couette-Taylor Bioreactors (CTBs). The SBR system has been used in other laboratory studies to reliably form granules and displays the variation in shear that was desired to be explored. Couette-Taylor bioreactors were chosen because of their unique setup with a stationary inner cylinder and rotating outer cylinder. To provide the rotation, the outer wall of each CTB was placed on a pottery wheel with clockwise rotation while the inner cylinder was

clamped aloft within the larger cylinder by an upper shelf. This movement creates small eddys moving in small flow patterns from the inner wall towards the outer wall in a laminar manner. This hydrodynamic behavior of fluid inside a CTB allows even shear to be found throughout the reactor body. In the case of a CTB, hydrodynamic shear originates from both the movement of the reactors and from the provided aeration. Since the SBR had a larger diameter opening than the CTBs, an air stone was placed at the bottom of the SBR to provide compressed air to the reactor. Since the CTBs had a narrower opening and were constantly in motion during the fill and reaction cycles, a thin bubble wand, which had moldable, perforated foam sides, was fit around the curve of the inner cylinder to provide aeration. To compare to the SBR setup, the CTBs were set up to have lower, equal, and higher total average shear to the SBR.

3-3 Experimental Setup Schematics and Configurations

The experimental setup in Broughton Hall Environmental Engineering Lab at North Carolina State University is shown in Figure 06. The height difference between the SBR and CTBs can be seen along with the different relative diameters between the different types of reactors.

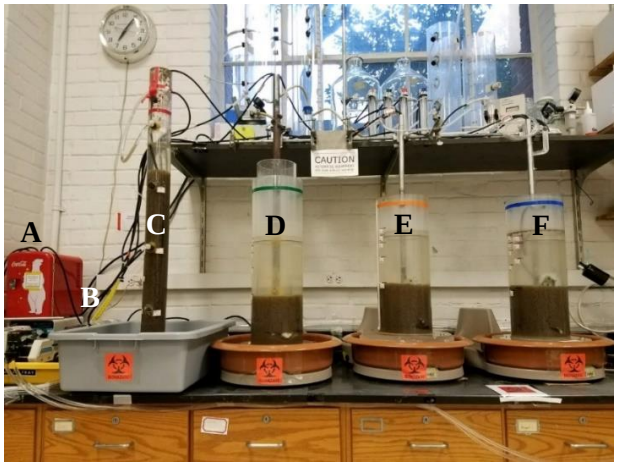

Figure 06. Experimental setup showing a) refrigerated influent, b) inline mixers, c) SBR, d) CTB1 with lower average total shear to SBR, e) CTB2 with equal average total shear to SBR, f) CTB3 with higher average total shear to SBR

The basis of each reactor came from previously designed and used reactors. The CTBs were made of two concentric acrylic cast cylinders to provide the annular gap. Each cylinder had a height of 45.5 cm. The outer cylinders, which became the rotating outer wall, had an outer diameter of 18.4 cm and an inner diameter of 17 cm. To provide rotation, the outer cylinders were connected to a base plate of acrylic that could be connected to a pottery wheel via screws, similar to a pottery throwing bat. The inner cylinders, which were clamped to a shelf to remain stationary, had an outer diameter of 13.8 cm and an inner diameter of 12.5 cm. These cylinders were clamped to the upper shelf by a steel shaft with and inner diameter of 1.5 cm and height of 78 cm that was set into the middle of the inner cylinder with synthetic urethane rubber compound PMC-790, which was poured into the base of the inner cylinder. These dimensions provided an annular gap of 1.6 cm which provided a total available volume of 3.5 L. To prevent accidental overflow due to slight variations in peristaltic pump operation, the working volume was 2.6 L.

For the operation of the CTBs as batch reactors, 2.54 cm holes were drilled in the shaft to provide access for tubing to reach influent, effluent, and aeration ports. The influent port was located 3.5 cm below the top of the inner cylinder. The effluent port was put at 16.5 cm above the base to provide a 50% exchange ratio. The aeration port was placed 2.5 cm above the base to allow the 45.7 cm flexible bubble wands to be placed at the bottom of the reactors, so the fine air bubbles would travel the entire reactor space. Norprene tubing, size 16 (Cole-Parmer, Vernon Hill, IL) was used to connect the ports to the necessary locations and Masterflex L/S peristaltic pumps (Cole-Parmer, Vernon Hill, IL) for influent and effluent flows. The pottery wheels (DichBlick, New York, NY) used to provide the outer cylinder with rotation were able to be adjusted between 0-220 RPM which fit the range needed for desired shear.

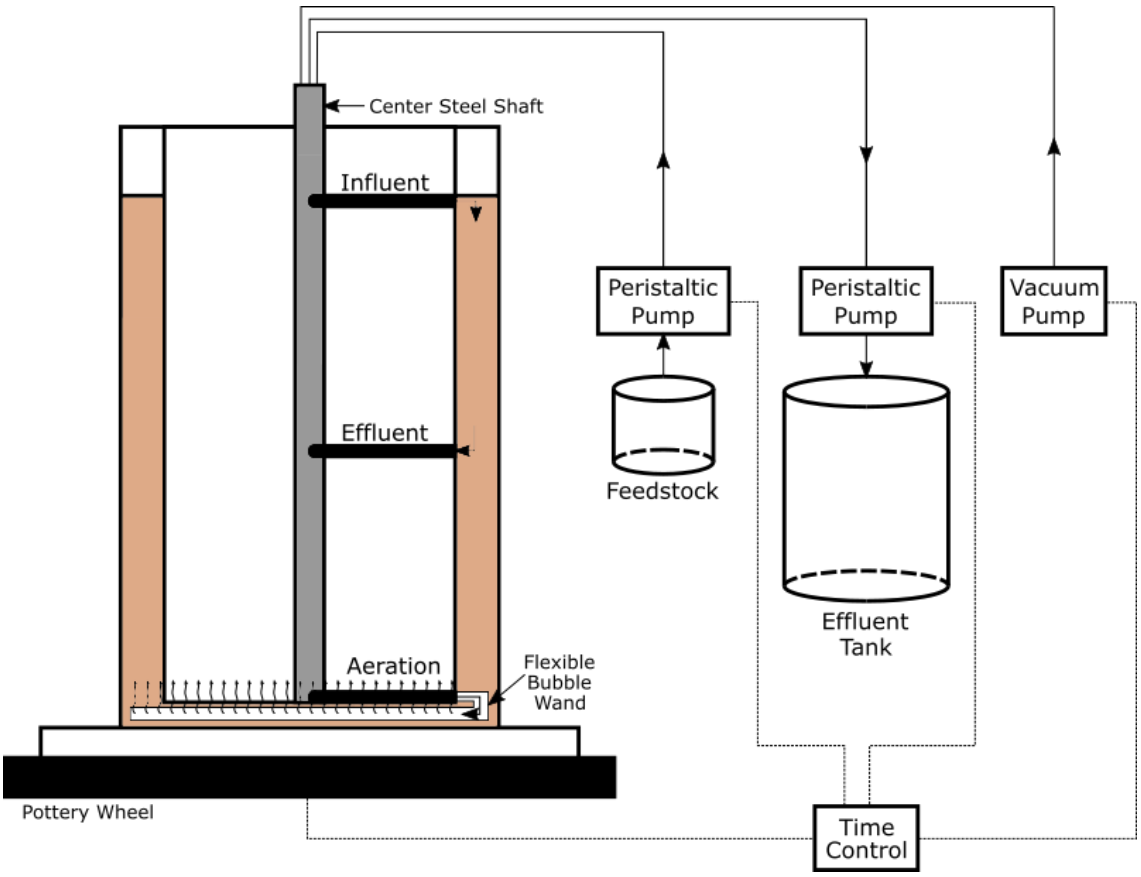

Figure 07. Couette-Taylor bioreactor setup

The control SBR consisted of a narrow acrylic cast tube with a high height-to-diameter ratio. The nominal diameter was 6.35 cm and the height was 102 cm. Large height-to-diameter (H/D) ratios have primarily been used in past research to meet the minimal settling velocity for granule formation (Li et al., 2014). To keep the reactor upright, the acrylic tube was placed on a plexiglass base. Five holes with a 2 cm diameter were drilled 20.4 cm apart along the length of the reactor with only the top and center ports being utilized for influent and effluent ports, respectively. The other ports were plugged with rubber stoppers and sealed with silicone. Masterflex Tygon Lab tubing, L/S 25 (Cole-Parmer, Vernon Hill, IL) was used to connect the ports with the necessary locations. To provide a sealed connection between the reactor and the tubing, short segments of hard plastic tubing were inserted into the rubber stoppers with center

holes in the ports which connected to influent and effluent basins via the Tygon tubing. Aeration was provided by a two-inch limewood airstone (Lee's Wooden Air diffuser, San Marcos, CA) placed at the base of the reactor tube and was connected to a vacuum pump via tubing that sat through the length of the reactor.

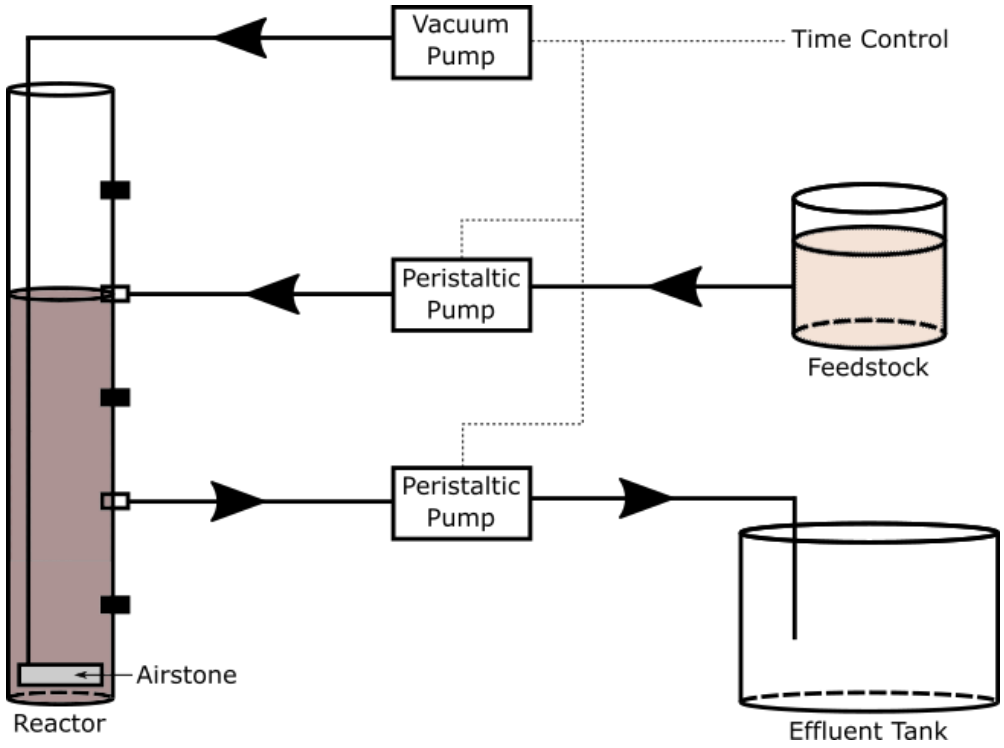

Figure 08. Sequencing Batch Reactor setup

Tubing on each reactor was replaced after about 50 days to prevent excess wear due to the peristaltic pumps from creating a hole in the tubing and to get rid of biofilm growth due to nutrients becoming trapped in the influent lines. Reused tubing connections were cleaned for 10 minutes in a 10% bleach bath and rinsed in deionized water before further use.

3-4 Experimental Matrix (table for aeration and shear levels within reactors)

The experimental setup dealt with variation of hydrodynamic shear, fixed aeration, and settling pressure. The experimental reactors varied from the control reactor in that the flow

patterns of CTBs results in laminar eddys, with more even estimates of shear throughout when compared with tall, narrow SBRs with base aeration. In addition, since aeration affects the hydrodynamic shear, each reactor had a different upflow gas velocity, listed in Table 01.

The setup of the reactors included one control Sequencing Batch Reactor (SBR) and three Couette-Taylor bioreactors (CTB): one below the SBR average total shear rate, one equal to the average total shear rate (including that due to aeration and velocity), and one equal to the aeration shear rate above the average total shear rate of the SBR. The average shear rates compared between the control and experimental reactors were determined based on aeration and/or rotation rates, keeping all other parameters constant. The volumetric power dissipation is related to bulk liquid density and standard gravity, in Eq. 3, and mean shear rate is calculated by Eq. 4 (Sánchez Pérez, Rodríguez Porcel, Casas López, Fernández Sevilla, & Chisti, 2006):

$$\frac{P}{V} = g\rho U_g \qquad \text{Eq. 3}$$

$$\gamma = \left(\frac{1}{K} g\rho U_g\right)^{\frac{1}{n+1}} \qquad \text{Eq. 4}$$

Where n is 1 and K is μ for Newtonian fluids, ρ is density, and g is the acceleration of gravity.

Table 01. Experimental Matrix

	Control	Higher SBR Shear Rate	Equal Total Shear Rate	Equal Aeration Shear Rate
	SBR	**CTB1**	**SBR**	**SBR**
Mean shear rate (s^{-1})	**204**	**135**	**204**	**249**
U_g (cm/s)	0.424	0.123	0.326	0.424
Aeration shear rate (s^{-1})	204	110	159	204
SBR	--	50	90	90
Rotation shear rate (s^{-1})	--	25	45	45

1. U_g is superficial gas velocity, given as the gas volume flow rate divided by the reactor cross sectional area

Both the SBR and Couette reactors were operated in parallel. 12 L of seed sludge was collected from an aeration basin at the North Cary Water Reclamation Facility during the aeration period to ensure a well-mixed sample was pulled. Prior to the inoculation of each reactor, the seed sludge was aerated in a large bucket and pulse-fed the equivalent of one day's worth of concentrated influent and allowed to acclimate to the laboratory conditions for two days. After the acclimation period, 2.6 L of the well-mixed seed sludge was poured into each reactor and allowed to settle below the effluent port so 1.3 L of the supernatant could be removed before the addition of the synthetic wastewater. This was to allow the initial biomass concentration to remain the same after the addition of the synthetic wastewater, rather than have the sludge become diluted to half its original concentration.

3-5 Influent and Mixing Feed Process

To eliminate a previous problem of developing unknown growth in the two-day batches of feedstock kept in a 42 gallon drum at room temperature, the influent feed during this experiment was concentrated and pumped from a refrigerator kept at 4°C. The original volume of synthetic wastewater fed per cycle was 1.3 L and was adjusted so that the concentrated volume fed to each reactor was 15.6 mL. This concentrated volume of feed was then brought up to a total volume of 1.3 L during the feeding phase of the batch cycle by being mixed with deionized water. Two different peristaltic pumps were used to pull the concentrated media, from the refrigerator, and deionized water, kept in a 55 gallon drum, through a static inline mixer (Cole-Parmer) with 24 turns to ensure that each reactor received the same concentration of feed. Air was pumped through the bottom of the 1 L beaker containing the current batch of concentrated feed to ensure that all nutrients in the feedstock remained suspended. Inline three-

way valves were placed just before each reactor to sample the influent COD. Tubes and inline mixers were replaced every 50 days to prevent microbial growth.

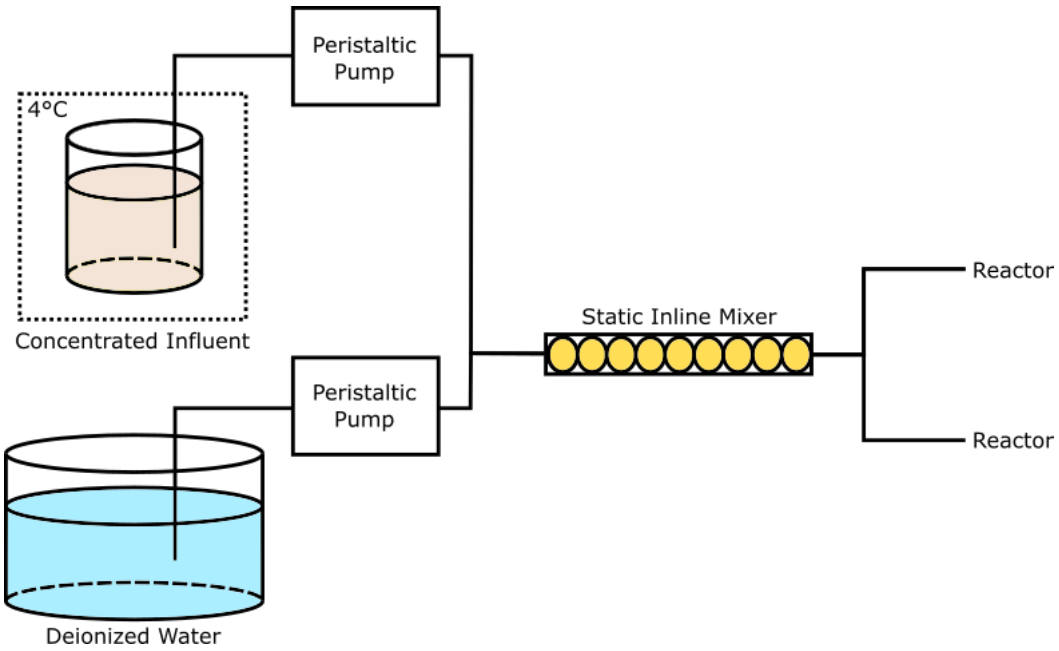

Figure 09. Schematic showing the influent mixing process (use of inline mixer) used in duplicate

3-6 Components of Influent Feed

The synthetic wastewater formula used was adapted from Adav et al. (2007) and consisted of the components listed in Table 02. Concentrations for listed macronutrients were adjusted to fit the desired 15.6 mL volume of feed which was then diluted to the original concentrations when the concentrated macronutrients and micronutrients were brought up to the necessary 1.3 L batch of feedstock using deionized water during operation. The micronutrient components of the influent feed were prepared separate to the macronutrient components in 1 L batches and added to each batch of influent feed prepared.

Table 02. Influent feed components

Macronutrients		
Component Name	**Chemical Formula**	**Concentration [mg/L]**
Sodium acetate	CH_3COONa	600
Ammonium sulfate	$(NH_4)_2SO_4$	500
Sodium chloride	NaCl	100
Magnesium sulfate heptahydrate (Epsom salt)	$MgSO_4 \cdot 7H_2O$	100
Iron(III) chloride	$FeCl_3$	10
Calcium chloride	$CaCl_2 \cdot 2H_2O$	5
Dibasic potassium phosphate	K_2HPO_4	825
Potassium dihydrogen phosphate	KH_2PO_4	675
Micronutrients [1 mL/L synthetic wastewater]		
Component Name	**Chemical Formula**	**Concentration [g/L]**
Boric acid	H_3BO_3	0.05
Zinc chloride	$ZnCl_2$	0.05
Copper(II) chloride	$CuCl_2$	0.03
Manganese sulfate	$MnSO_4 \cdot H_2O$	0.05
Ammonium molybdate tetrahydrate	$Mo_7SO_4 \cdot 4H_2O(NH_4)_6$	0.05
Aluminum chloride	$AlCl_3$	0.05
Cobalt(II) chloride hexahydrate	$CoCl_2 \cdot 6H_2O$	0.05
Nickel chloride*	$NiCl_2$	0.05

* Note that the original influent feed formula from Adav et al. (2007) incorrectly listed Nickel chloride as NiCl instead of $NiCl_2$.

Theoretical influent COD was 460 mg/L COD and total nitrogen was approximately 110 mg/L. With the influent flow, organic loading rate was 3.6 g COD/day and the hydraulic retention time was 8 hours. In each cycle 1.3 L of supernatant was decanted and replaced with 1.3 L of fresh synthetic wastewater, consisting of the concentrated and deionized water components mixed directly before injection into the reactors via static inline mixers. Due to the concentrated nature of the feed, air was bubbled through the concentrated batches of influent to ensure all nutrients were completely mixed prior to the feeding period.

3-7 Novel pH Control

Due to previous projects in this lab experiencing low pH, each reactor was closely monitored for pH during this run. Around 25 mL of mixed liquor samples were collected daily after the feeding phase and measured for pH. After measurement, the samples were returned to

each reactor. If the pH of a reactor was measured as below 6.5 for two consecutive measurements, a buffer of 1M magnesium hydroxide ($Mg(OH)_2$) was added – generally, no more than 10 mL was necessary – and pH was measured again at the next cycle to ensure that the pH had returned to a near neutral point.

3-8 Measured Parameters During Run

Parameters measured over the run included total suspended solids (TSS), volatile suspended solids (VSS), chemical oxygen demand (COD), pH, nitrate, nitrite, total nitrogen, ammonia, and additional samples were collected for later EPS extraction and 16S rRNA gene sequencing work. Mixed liquor and effluent samples from each reactor were collected every Monday, Wednesday, and Friday for further analysis using the following materials and methods for each parameter:

- **Total and Volatile Suspended Solids (TSS/VSS):** Solids parameters were determined according to Standard methods, test number 2540D (APHA, 2015). 15 mL of mixed liquor was used for each measurement; each sampling point was analyzed in triplicate.
- **Soluble Chemical Oxygen Demand (COD):** HACH (Loveland, CO) COD kits for high range (0-1500 mg/L) and low range vials (0-150 mg/L) were used to measure the COD. Samples were filtered through 0.45 μm membranes held in place by filter holders.
- **pH:** To monitor the pH of each reactor environment, samples of the mixed liquor were taken during the aeration/reaction phase of the batch cycle and analyzed using a pH meter. When the pH was below 6.5 for two consecutive measurements, the pH was adjusted according to Section 3-7.
- **Nitrate and Nitrite:** For this parameter, one mL of collected effluent was filtered through 0.45 μm membranes held in place by filter holders into clean 1.5 mL ion chromatography vials and capped and clamped with an IC filter cap. Samples were stored

at 4°C just prior to analysis on a Dionex IC unit (Sunnyvale, CA) using an IonPac AS4A-SC 4 mm column. For every batch, extra sample for a few sampling points were filtered to provide matrix spikes for at least every 10 samples.

- **Total Nitrogen:** Nitrogen was measured using HACH (Test ‘n Tube, Loveland, CO) total nitrogen reagent set (0-25 mg/L). Each vial required 2 mL sample volumes for the total nitrogen test.
- **Ammonia:** For ammonium measurements, HACH (Test ‘n Tube, Loveland, CO) high range ammonium sets (0-40 mg/L) were used. The vials required 100 μL of sample for the ammonium test.
- **Sludge Volume Index (SVI):** The sludge volume index for each reactor was measured three times a week according to Standard Methods, test number 2710D (APHA, 2015). Due to the limited working volume of each reactor, 2.6 L, the volume of mixed liquor required for this test was altered from 1000 mL to 100 mL. Over a period of 30 minutes, the volume occupied by the sludge was measured in milliliters every five minutes and SVI was calculated according to the following equation:

$$SVI\left[\frac{mL}{g}\right] = \frac{settled\ sludge\ volume\ [mL/L]\times[1000\ mg/g]}{suspended\ solids\ [mg/L]} \quad \text{Eq. 5}$$

To capture the 5-minute SVI (SVI_5), Eq. 5 was modified so that the settled sludge volume used was the sludge volume measured after 5, rather than 30 minutes, of settling.

- **Particle size distribution:** Particles from mixed liquor samples were embedded in Bactoagar gel and imaged with a camera attached to a stereomicroscope. The Microsoft Image Composite Editor (ICE) software was used to stitch images from the same plates together and ImageJ software was used to analyze the stitched images and collect particle size data. Initial thresholds used to assess percent granulation within each reactor were

size greater than 200 μm and roundness above 0.6. Roundness was determined by the following equation:

$$Roundness = 4\frac{Area}{\pi \times Major\ Axis^2} = \frac{1}{Aspect\ Ratio} \quad \text{Eq. 6}$$

A detailed description of the image analysis techniques used may be found in the Appendix.

- **Extracellular Polymeric Substance (EPS):** Extraction of each EPS component was performed according to the protocol listed by Pellicer-Nàcher et al. (2013), specifically following the sonication methods for both loosely-bound and tightly-bound EPS extraction. A more detailed description of the extraction and analysis methods are listed in Section 3-9 of this chapter and full procedure is listed in Appendix A-3.
    - **Protein analysis:** Quantification of the protein fraction within the EPS was done by BCA Assay kit from Frølund (1996), adapted for use with 0.2 mL 96-well microplates, incubation in a PCR cycler at 37°C for 30 minutes, and read by a microplate reader (Tecan, Männedorf, Switzerland) at 560 nm.
    - **Polysaccharide analysis:** Carbohydrate analysis was performed using the anthrone-sulfuric acid assay method by Dreywood, 1946 (referenced by Pellier-Nàcher et al., 2013) adapted to be performed on 0.2 mL 96-well microplates (Fisherbrand) and incubated at 90°C in a PCR cycler and cooled on ice before being read by a microplate reader (Tecan, Männedorf, Switzerland) at 620 nm.
- **Community analysis (DNA):** DNA will be extracted and prepped for Illumina sequencing by the Genomic Sciences Lab on Main Campus of North Carolina State University.

3-9 Batch Tests

The following batch tests were performed to analyze reactor performance during a cycle. Mixed liquor samples were taken to perform these tests and returned to the reactors once finished.

- **Parameters during a cycle:** Towards the end of the run, samples from each reactor were pulled to measure a few of the monitoring parameters, COD, ammonia, nitrite, and nitrate, were over a 4 hour cycle. These parameters were measured to provide insight into the behavior of the reactors.
- **Oxygen Uptake Rate:** A respirometry test was performed based on the procedure from Eliosov and Ellis to measure the extant kinetic parameters (μ and k_s) (Eliosov & Ellis, 2002). Mixed liquor samples were tested within 2 hours of removal from the reactors and were returned to the corresponding reactor after testing.

Note that the growth tests were not conclusive due to the low oxygen levels that were bubbled through the mixed liquor samples prior to analysis of the injection of COD and analysis of the uptake. Figures A-02 through A-05 in the Appendix show the attempted curve fits for oxygen uptake using Matlab.

3-10 Length of Run

The run was concluded when the reactors showed signs of sustained failure such as excessive algae growth, wear on rotors, or sludge degradation which caused unrecoverable conditions (e.g. continuous inability to reach >90% COD removal) within single or multiple reactors. CTB1 had the most issues with algae growth, after about 90 days of operation (after the cutoff point for the experimental parameters). CTB2 and CTB3, which had the higher RPM

operation, had more issues with wear on the pottery wheel rotors due to the weight of the reactors and continuous operation and needed a replacement wheel to sustain operation.

3-11 Extracellular Polymeric Substance Measurement

To determine whether the excreted extracellular polymeric substances (EPS) from the sludge microbes played a role in the development of more granular biomass, samples from each reactor were regularly taken and analyzed for different EPS components. 15 mL mixed liquor samples were collected every 3-4 days over the course of the run to quantify the three EPS components. The samples were processed to separate soluble, loosely-bound (LB-), and tightly-bound (TB-) EPS according to the method described in Pellicer-Nàcher et al. (2013), though slight modifications were employed to tailor the procedure available lab equipment. Prior to extraction, 1 L batches of extraction buffer, see Table 03, were prepared in deionized water.

Table 03. Extraction buffer components

Component Name	**Component Formula**	**Concentration**
Trisodium phosphate	Na_3PO_4	2 mM (0.327 g/L)
Monosodium phosphate	NaH_2PO_4	4 mM (0.479 g/L)
Sodium chloride	NaCl	9 mM (0.5259 g/L)
Potassium chloride	KCl	1 mM @ pH 7 (0.0745 g/L)

Gentle sonication at 50 J/mL and immediate formamide addition at 6 ul/mL was used to separate LB-EPS from the biomass. Each sample was centrifuged for 2 minutes at 4500 RPM in a swing-bucket rotor, then at 12,000 g in a fixed angle rotor, and finally at 5000 g in a fixed angle rotor prior to filtration through 0.2 μm membranes. Following LB-EPS extraction, biomass pellets resuspended in extraction buffer underwent sonication at 150 J/mL to separate the TB-EPS from the biomass. Due to the use of a microtip probe on the sonicator, an amplitude percentage of 20% was employed on a QSonica 500 watt converter during both LB- and TB-EPS extraction to provide the gentlest sonication and maximize prevention of cell lysis. To input the

larger amount of energy per unit volume for TB-EPS extraction, the samples were sonicated for a longer period of time, see Appendix for full extraction procedure (Pellicer-Nàcher, 2013). TB-EPS extraction procedure from sonication to the end of centrifugation was performed in triplicate, resulting in TB-1, TB-2, and TB-3 replicates for each original mixed liquor sample. Previous work done by Pellicer-Nàcher et al. (2013) did not show significant differences in the TB-EPS replicates using the sonication technique but were able to recover more EPS than other extraction methods with minimal cell lysis. All EPS samples were filtered through 0.2 um filter membranes and stored in 1.5 mL microcentrifuge tubes at -20°C prior to analysis. Pellets were resuspended to the original volume in extraction buffer after each procedure.

Previous studies primarily examine the protein and carbohydrate components of EPS and compare the subsequent ratio (PS/PN) as the other EPS components, humic acids, nucleic acids, glycoproteins, and phospholipids, are present in relatively small amounts in comparison. Protein quantification followed the Frølund et al. procedure, adapted for absorbance to be performed on a microplate reader (Tecan, Männedorf, Switzerland) using a BCA kit with albumin as the standard (Frølund, Palmgren, Keiding, & Nielsen, 1996). Carbohydrate quantification followed the protocol listed in the Pellicer-Nàcher et al. (2013) method using anthrone and sulfuric acid to determine polysaccharide content via colorimetric methods and adapted for absorbance measurement using a microplate reader (Pellicer-Nàcher et al., 2013). D-Glucose was used as the standard for the carbohydrate quantification with a sufficient number of standards provided to determine a standard curve.

CHAPTER FOUR – Results

4-1 Introduction

Chapter Four will discuss the results obtained from the physical-chemical methods and batch tests detailed in Chapter 3. The performance of the three Couette-Taylor bioreactors will be compared to the control sequencing batch reactor to assess the differences between reactors with varying and homogeneous shear.

4-2 Notes about General Operation

Over the course of the reactor run, the pH was one of the quantitative parameters used to immediately assess the health of the microbes in the reactor. During periods where the pH was consistently lower than 6.5, pH was measured and the magnesium hydroxide buffer was added during multiple cycles per day, as seen in Figure 10.

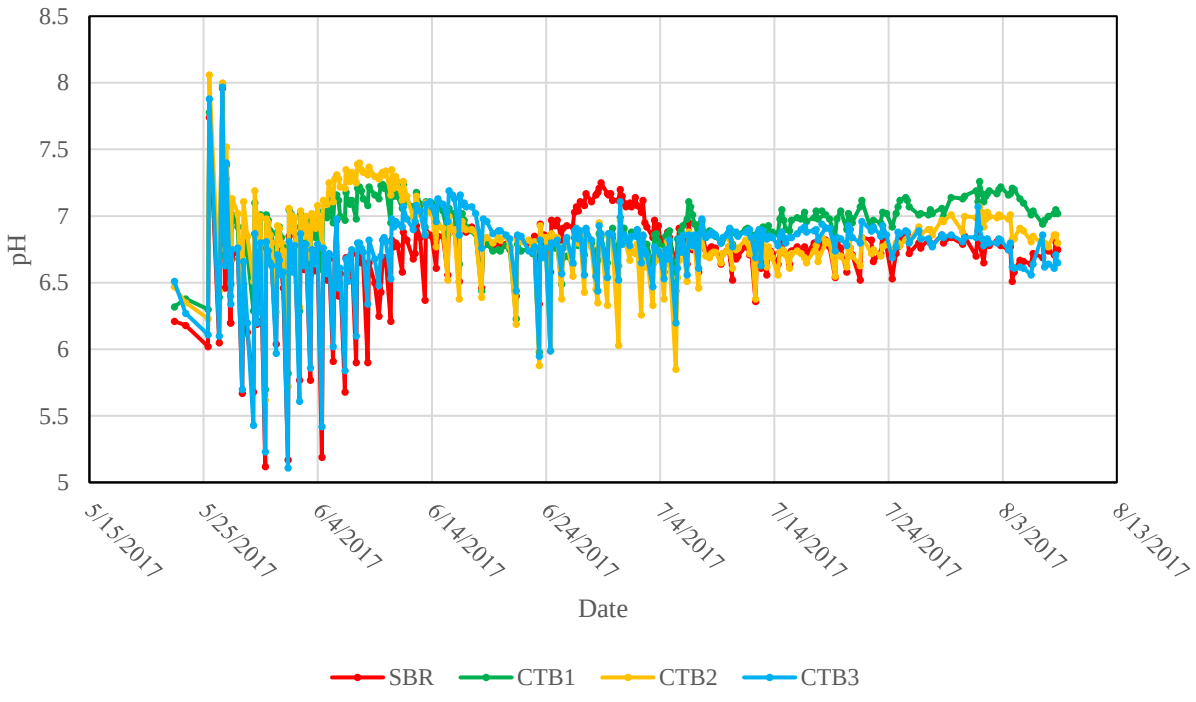

Figure 10. pH of each reactor during operation

Once the pH had stabilized between 6.5 and 7.25, buffer was no longer added and the pH remained within the desired range, the frequency of measurements taken for monitoring purposes was decreased.

An additional parameter used to assess the performance of reactor was the organics removal, measured as COD removal within each reactor. Given the influent COD of 460 mg/L and tests looking into the actual COD being fed into each reactor the percent COD removed could be calculated. As seen in Figure 11, the percent removal for all reactors remained above 95% for the duration of the run, indicating good performance from all reactors.

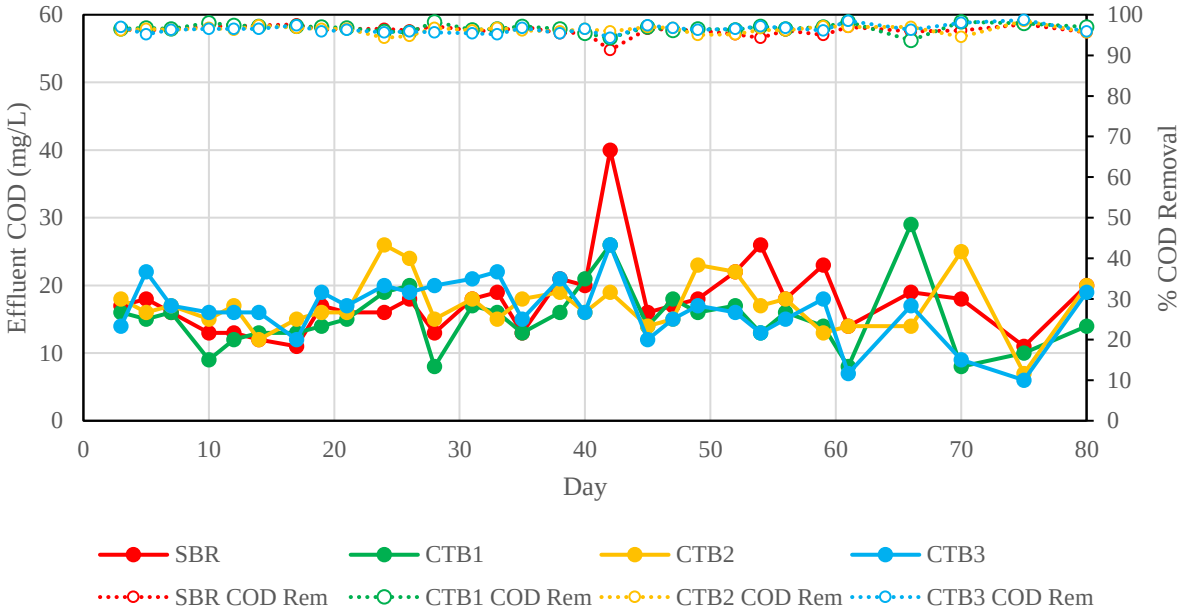

Figure 11. COD removal performance

4-3 Mixed Liquor Suspended Solids (MLSS)

During the first two weeks of operation, the total suspended solids (TSS) behavior between all four reactors was about the same. After this point, the solids measurements began to diverge, with the SBR following a decreasing solids trend to approximately 2.5 g/L while the

three CTBs tended to remain around or above 3.5 g/L. This difference between the SBR and CTBs could be due to the wasting of smaller particles in the SBR as faster-settling particles were produced.

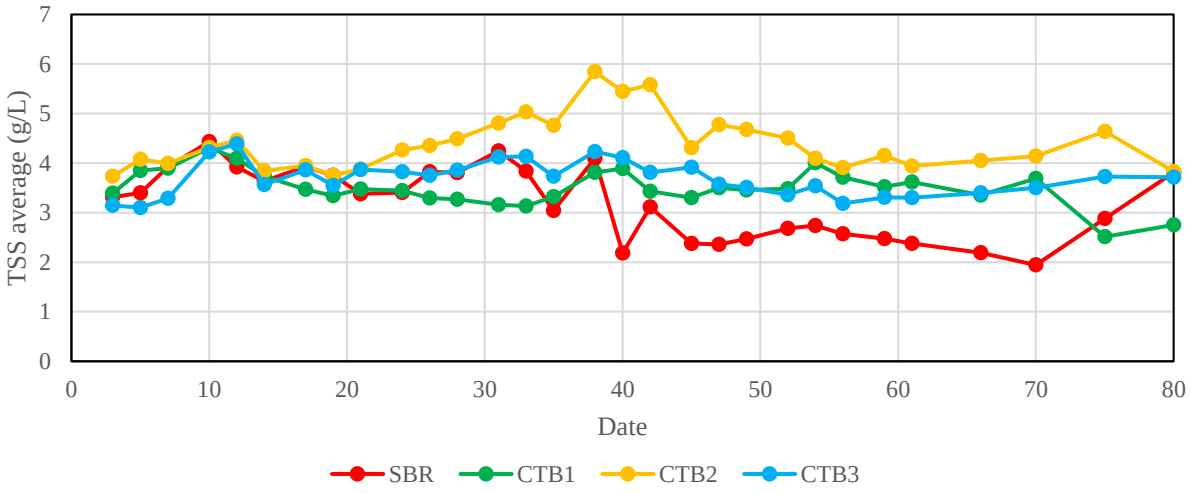

Figure 12. Total Suspended Solids measured for each reactor

The uptick in TSS seen in the SBR between days 70 and 80 may be due to the growth of the larger particles.

4-4 Sludge Volume Index

The primary parameter used to assess the settling characteristic of the particles within each reactor was sludge volume index (SVI). Good settling is represented by SVI measurements less than 100 mL/g biomass. Past research and at plants where Nereda® granules have been implemented, the difference between the 5-minute and 30-minute SVI has been increasingly used as a method for monitoring granule formation and stability. The relative simplicity of a SVI test and clear difference between the excellent settling ability of larger, denser granules and slower settling of smaller, lighter particles allows the small difference between measurements at 5 (SVI_5) and 30 (SVI_{30}) minutes while the fluffier particles with poor settling ability will display

large differences in the two measurements since it will take these particles longer to reach their final settled position (Pronk et al., 2015; S. J. Sarma & Tay, 2018; Wei et al., 2012). This difference is clearly displayed using ribbon plots which graph the difference between two variables at a given x-value, in this case time. The SBR was the only reactor within this experiment that achieved the formation of particles with good settling characteristics (Figure 13), as seen by the thin red ribbon representing the SBR performance. In comparison, each of the CTBs display continually wide ribbons for the duration of the experiment, indicating that the sludge in these reactors contained slow-settling particles. It should be noted that the locations within the plot that show the CTBs having thinner ribbons, for instance CTB1 (green) at day 32 and CTB2 (orange) between days 40 and 60, are still due to poor settling. The ribbons appear thinner because the sludge did not settle well over the 30-minute SVI measurement period, which while still leading to small differences between the SVI_5 and SVI_{30}, are characterized by large recorded sludge volumes during the SVI test.

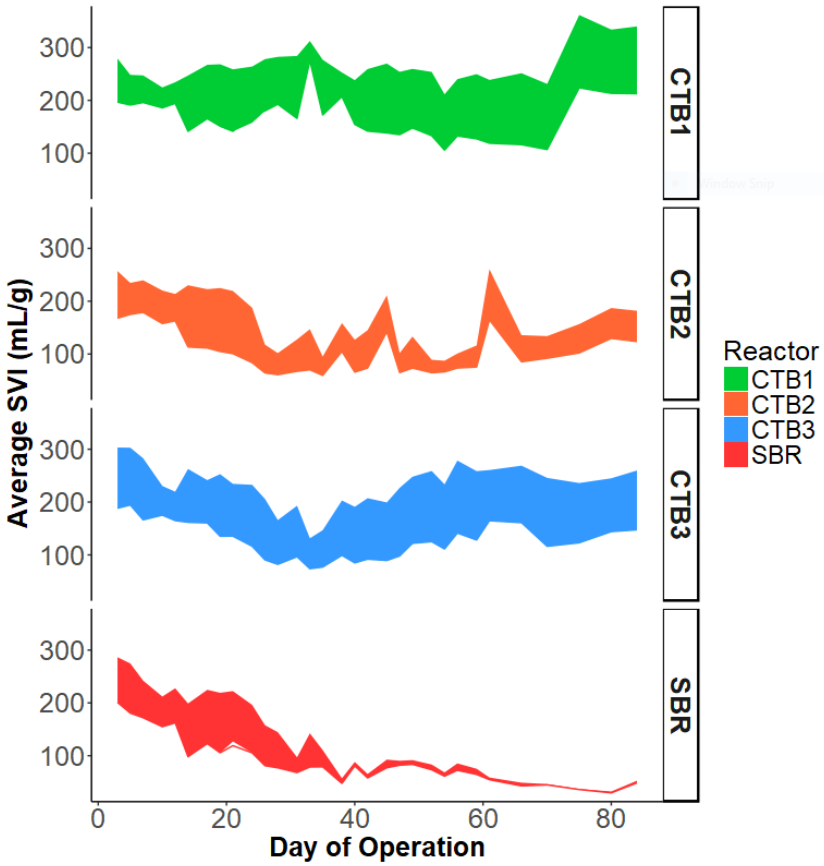

Figure 13. Ribbon plot displaying difference between SVI_5 and SVI_{30}

4-5 Effluent Characteristics

Effluent samples from each reactor had COD, total nitrogen, nitrite, and nitrate measurements taken. COD may be seen in the previous Section 4-2. Over the course of the experiment, the total nitrogen (TN) was within the range of 50-150 mg/L for all reactors (Figure 14). During the second half of the experiment, the SBR effluent had a higher TN than the CTBs. This observation may be due to the biofilm buildup only seen on the walls of the Couette reactors. Though they were cleaned regularly, there was some unavoidable biofilm growth that may have resulted in an anoxic environment where nitrate was converted to nitrogen. As seen in Figure 15 the nitrogen observed in the effluent was primarily present as nitrate. Dips in the CTB1 and CTB2 effluent nitrate (Figure 15), may have been caused by clogs or wear on the

flexible bubble wands which resulted in inadequate oxygen for the autotrophs to oxidize nitrite to nitrate.

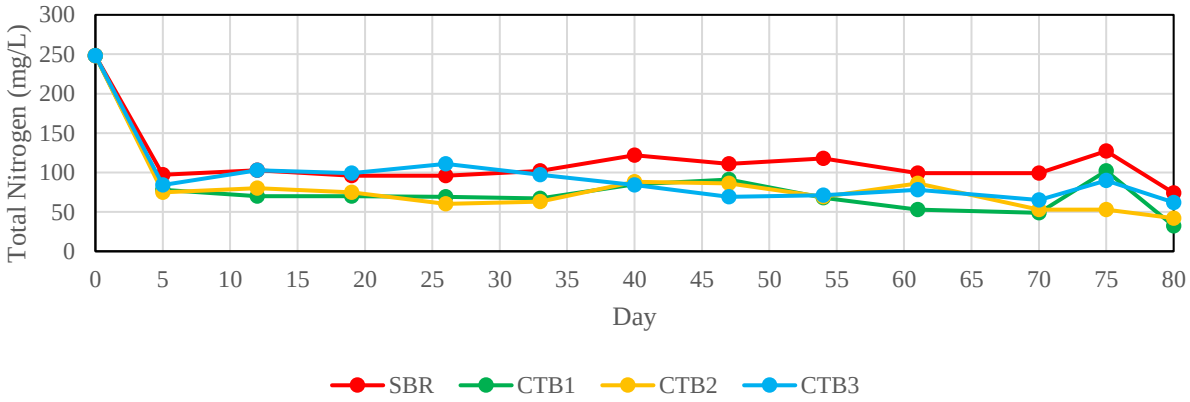

Figure 14. Effluent Total Nitrogen concentrations

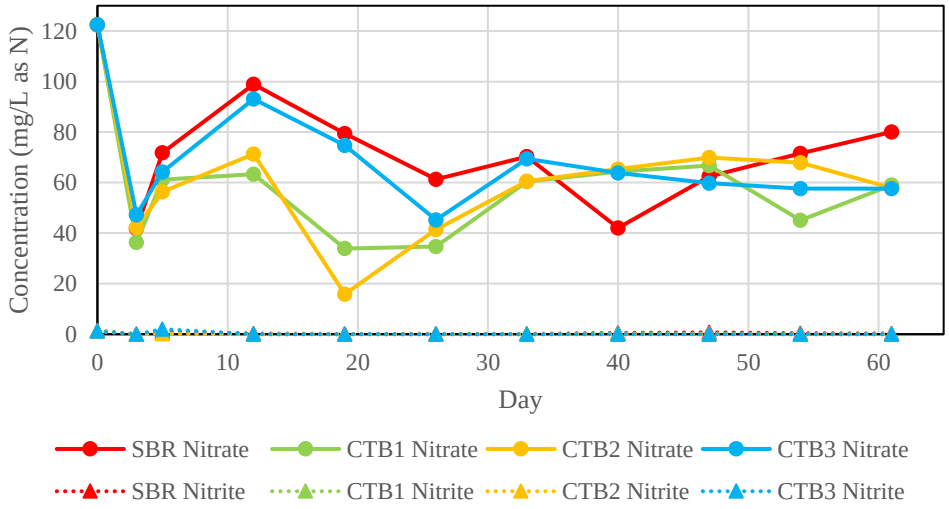

Figure 15. Effluent Nitrite and Nitrate concentrations

All reactors showed relatively high nitrification efficiency. Figure A-1 shows the effluent nitrite concentrations separately from nitrate so the changes during the run may be better observed.

4-6 Image Analysis

Mixed liquor samples, taken from each reactor, were observed using a stereomicroscope and image analysis software to assess particle morphology and granule formation.

4-6.1 Percent Granulation

Generally, literature has classified an aerobic granule as being particles larger than 200 μm with roundness above 0.6, indicating a spherical or elliptical shape (Park, Jung, & Milferstedt, 2017). There are some studies with lower thresholds such as roundness above 0.45 (Adav et al., 2007; Beun et al., 1999). Using R, the image analysis data was sorted so that particles with an equivalent diameter larger than 200 μm and shape factor larger than 0.6 were counted and considered granules. The percentages of these counted particles over the total number of particles on the plate were calculated and are shown in the following sections. The shape factor is an indicator of the roundness of a two-dimensional figure with values from 0, representing an irregular or very elongated ellipse, to one, indicating a circle (Beun, Van Loosdrecht, & Heijnen, 2002). Shape factor was calculated by the following formula:

$$Shape\ Factor = \frac{4\pi A}{p^2} \qquad \text{Eq. 7}$$

Where *A* is the particle area and *P* is the perimeter of the particle.

Due to the differences in reported granule thresholds, a sensitivity analysis regarding the percent of total particles that meet granule qualifications may be used for this experiment. Based on the original granule thresholds, the performance of CTB1, with lower total average shear than the SBR can be seen below in Figure 16. The difference in particles is also visible in the example images that match sampling points on the plot. The SBR achieved >10% granules around day 40

before returning to ~5% granules while CTB1 consistently produced fewer granules than the SBR.

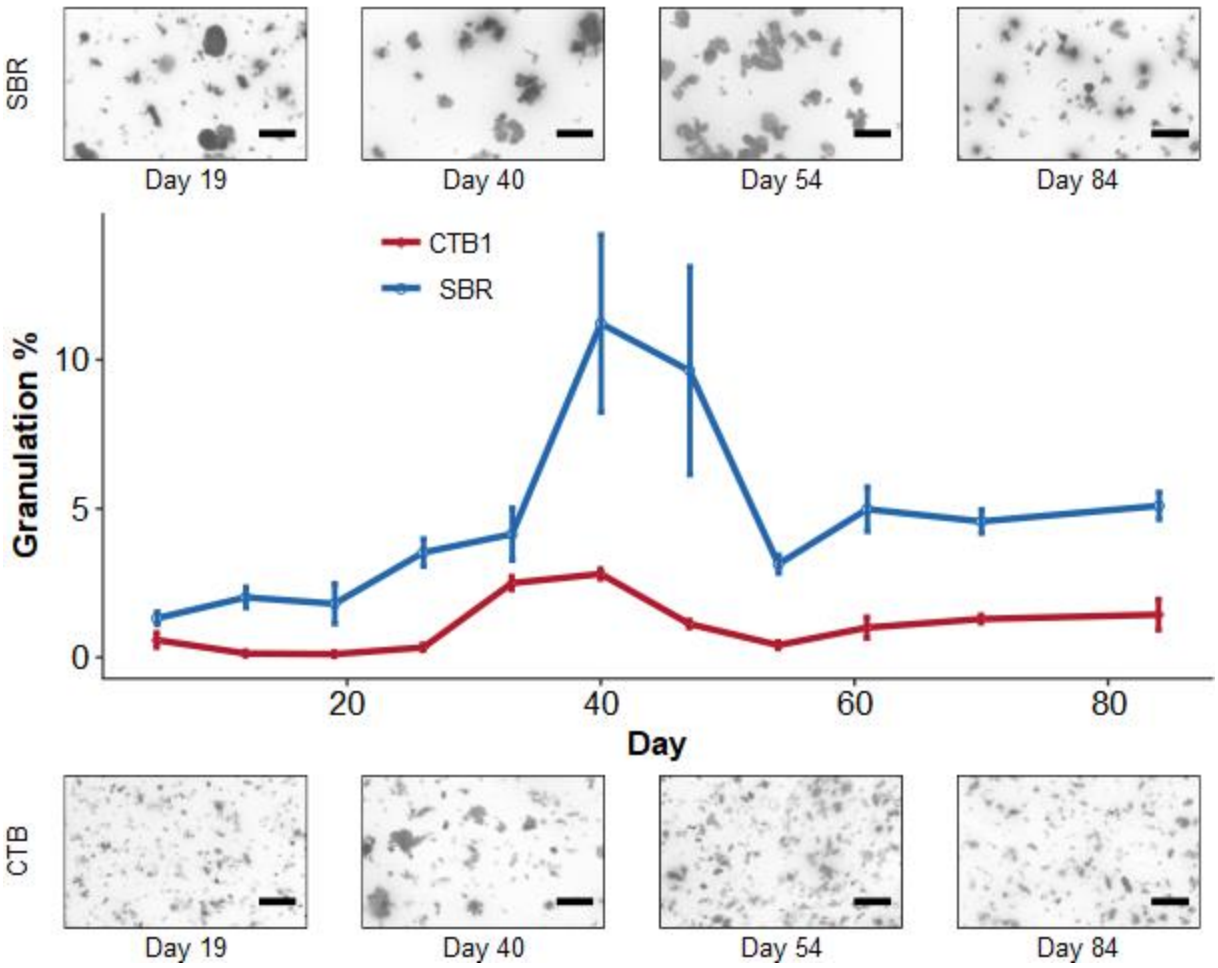

Figure 16. Percent granulation comparison between CTB1 and SBR

When the threshold for granules was changed to size greater than 150 μm and roundness above 0.45 the granules percentages changed (Figure 17). In general, the SBR trends over the course of the run remained the same, though the leading line of the peak in granulation around day 40 became steeper. Under these less selective limits, the SBR achieved around 17.5% granules while CTB1 remained below 5% over the entire course of the run. Since the performance of each reactor, in terms of COD removal, did not change significantly, as seen

previously in Figure 11, it may not be necessary to classify where the threshold for which particles are considered granular is, rather, emphasis may be focused on which conditions may be adjusted to achieve higher percentages of granules and may be translated to full-scale operation.

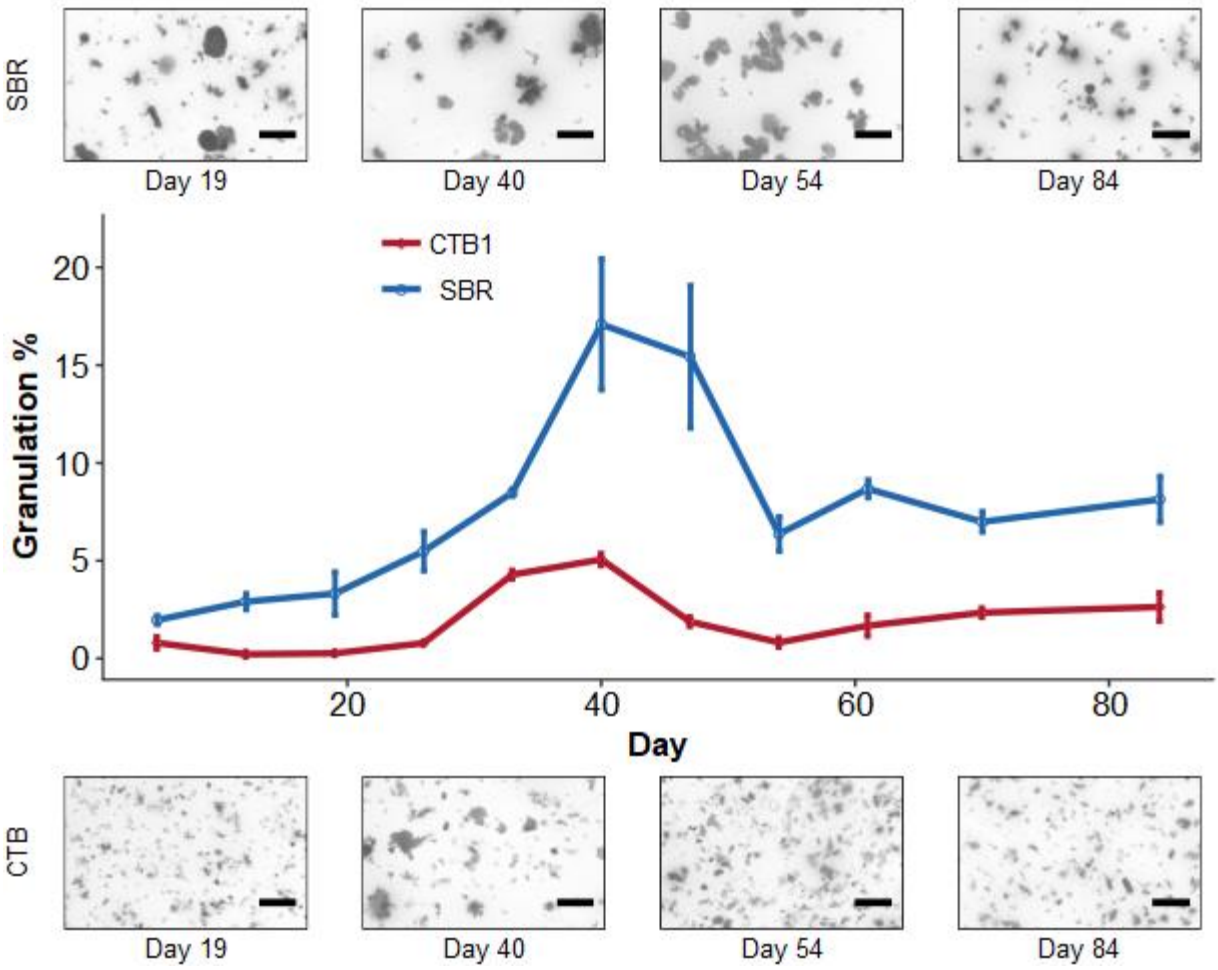

Figure 17. Percent granulation comparison between CTB1 and SBR with less selective granule threshold

The inability of CTB1 to achieve higher percent granulation, regardless of the roundness threshold chosen, may be due to the low shear. With lower shear, there may not be enough fluid movement to encourage aggregation and EPS production between small particles.

The comparison of CTB2, which was operated with equal total shear to the control SBR allows for comparison as to whether only a base shear level is necessary, or if the variation in shear only seen in the SBR is necessary to form aerobic granules. Based on the original granule thresholds, the performance of CTB2 is compared to the SBR in the following Figure 18. From this visualization it is can be seen that the percent of granules within the reactor increases over the run; however, this may be due to an overall increase in the consistent TSS of CTB2 as compared to the decreasing solids content of the SBR. With more particles within the reactor, there is a higher chance that more particles will classify as having a roundness above 0.6.

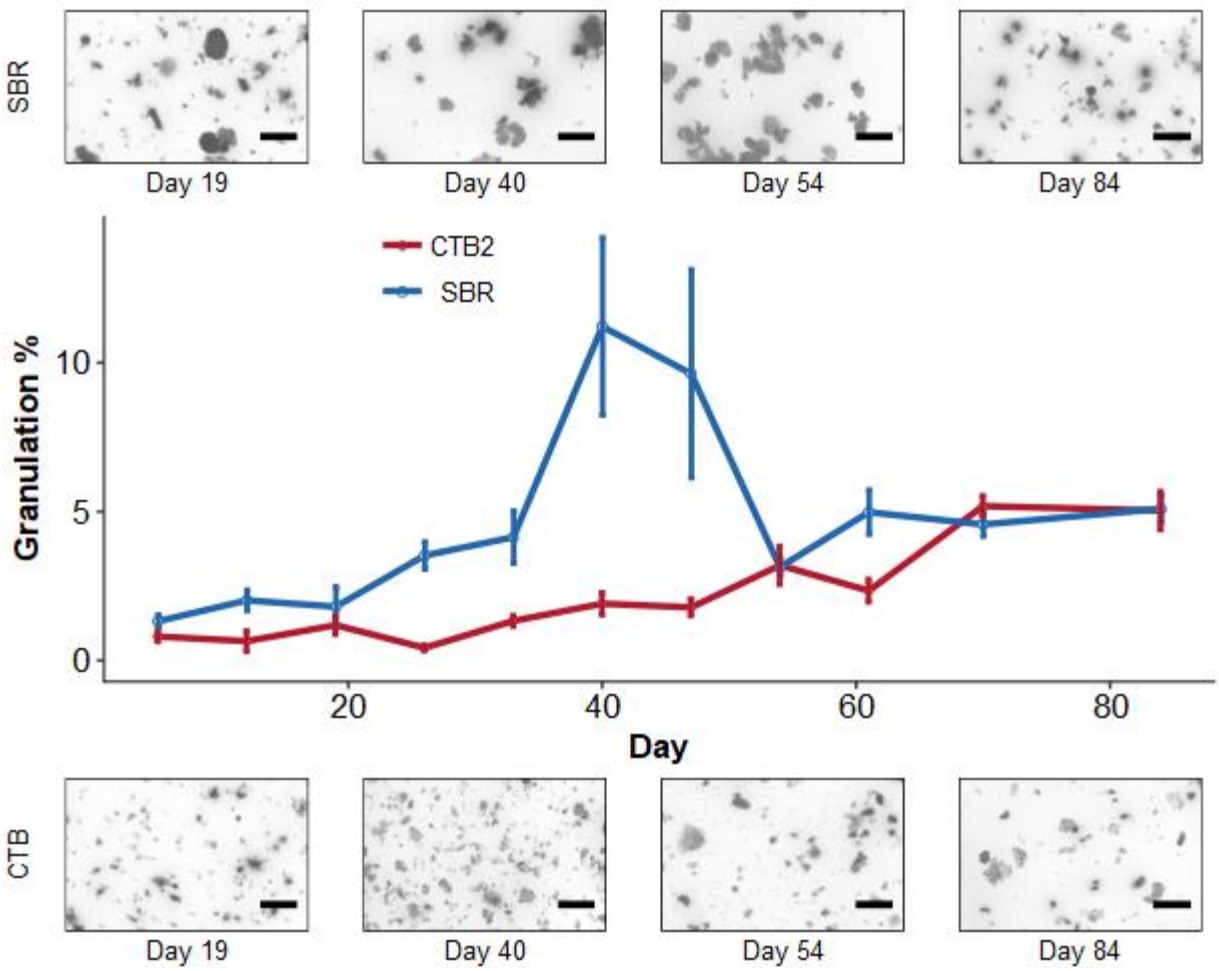

Figure 18. Percent granulation comparison between CTB2 and SBR

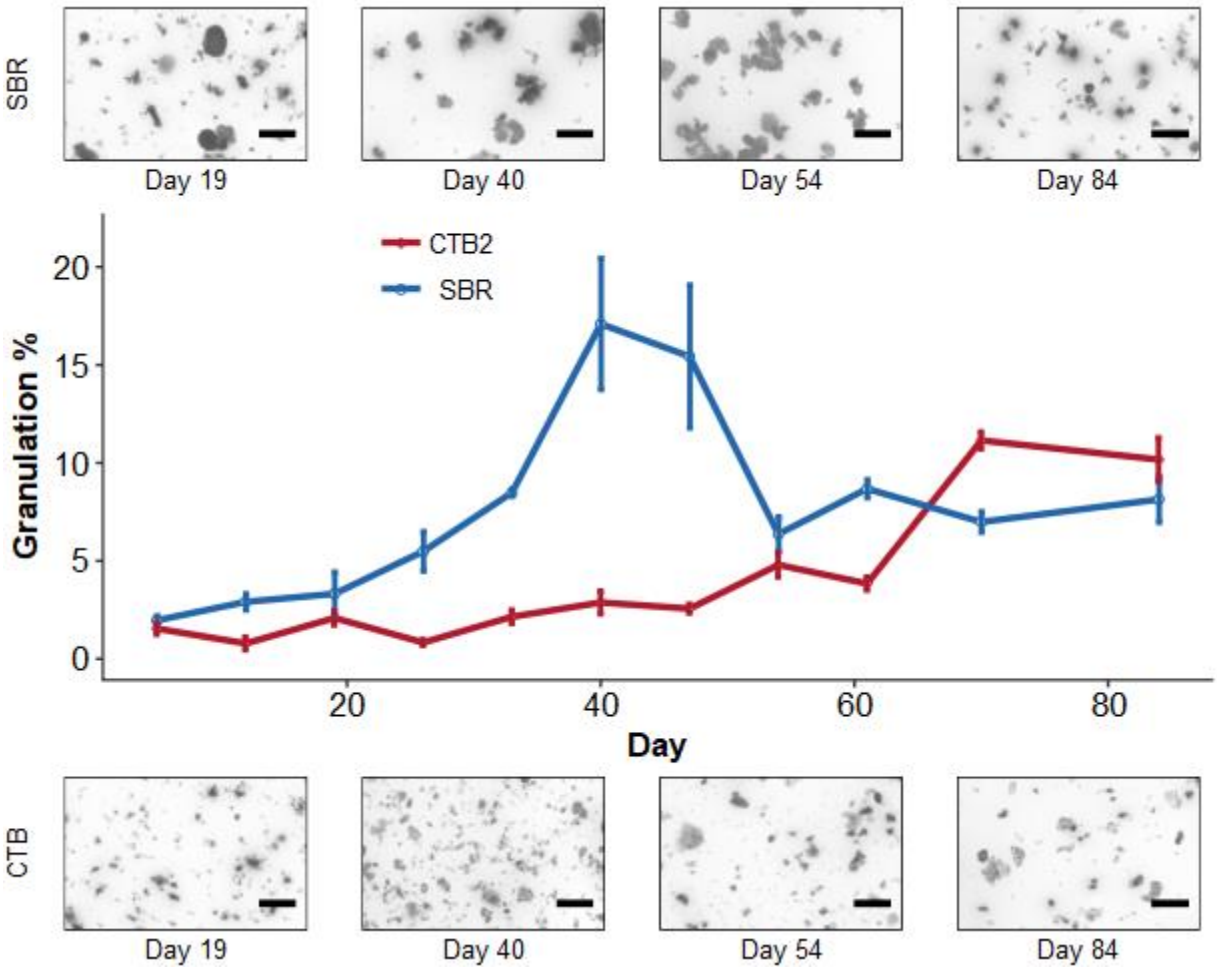

Figure 19. Percent granulation comparison between CTB2 and SBR with less selective granule threshold

Looking at the differences in the the granulation percentages achieved between CTB2 and the SBR by changing the threshold to a roundness of 0.45 increases the CTB2's performance over the SBR after day 65. This indicates that the particles present in the CTB towards the end of the experiment might be larger, but they are still more irregular in shape. This could be due to a looser structure which is supported by the fact that the SVI_5/SVI_{30} difference remains larger than the SBR towards the end of the run, as seen earlier in Figure 13. Visually it appears that the total number of particles remaining in CTB2 decreases over time, when looking at the images in Figure 19, which may also explain the apparent increase in percent granules seen towards the end of the run.

Comparatively, the performance of CTB3 is more similar to that of CTB1 where the percent granules achieved remained low when assessed using the orignal granulation percentage thresholds. The apparent spike of granules seen in CTB3 around day 60 may not be representative of actual aerobic granules in the reactor. This increase may be due to gel-like conditions of the sludge in CTB3 leading to false aggregates being measured as 'granules' when they were short-term flocculent aggregates, not the stable aerobic granules which were desired. The images of the particles in CTB3 support this theory as days 54 and 84 do not show large portions of the particles to be larger and more regularly shaped, expecially when compared with the particles seen in the SBR.

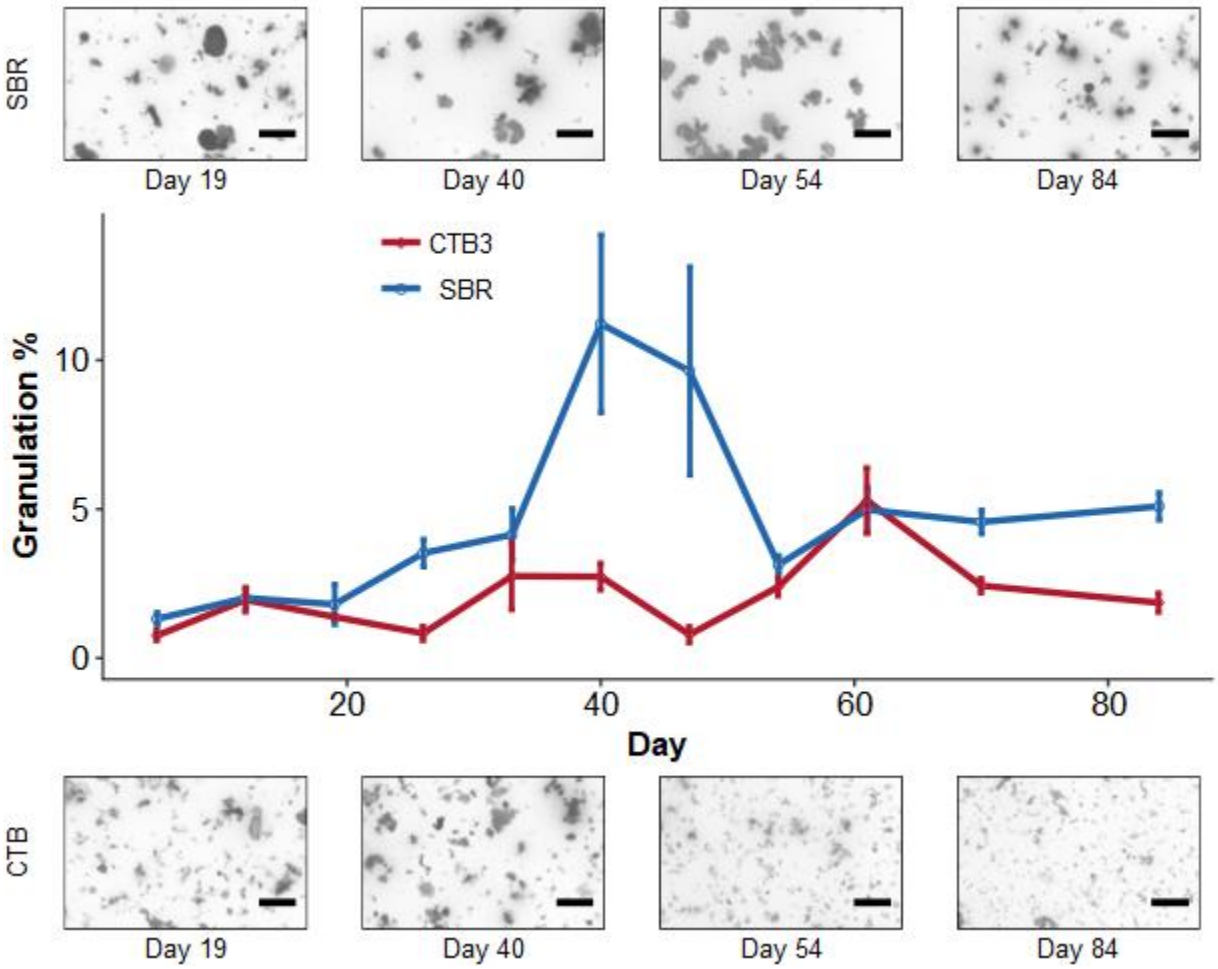

Figure 20. Percent granulation comparison between CTB3 and SBR

With the mean shear rate in CTB3 being higher than that of the SBR, 249 s^{-1} vs. 204 s^{-1}, the shear in the CTB may have been high enough that it promoted the breakage of flocs over aggregation. This hydrodynamic flow behavior would explain why CTB3 did not achieve higher granulation over the course of the run. It appears that every time the particles in CTB3 seemed to be increasing in size and regularity enough to be considered granules, around day 35 and day 60, the particles were broken apart again until they no longer met the criteria to be considered granules. With the less selective threshold criteria, the granulation percentage peak seen at day 60 in CTB3 was less than the percentage seen in the SBR on the same day. This may indicate that the particles seen on day 60 which met the granule requirements were larger than those seen previously, but not as regular as those seen in the SBR, since the change from the original to the less selective threshold was not as large of a jump up as seen in the SBR.

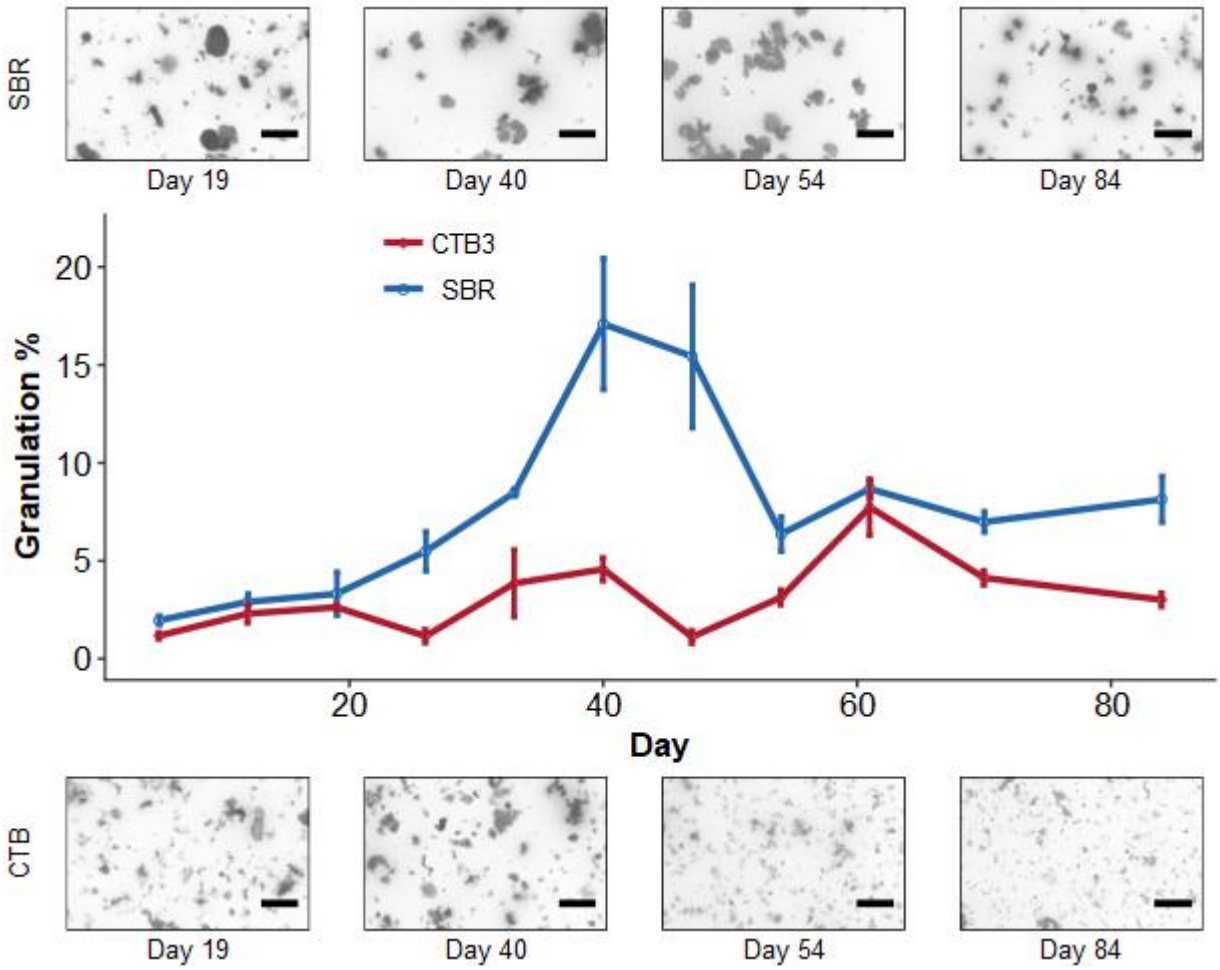

Figure 21. Percent granulation comparison between CTB3 and SBR with less selective granule threshold

4-6.2 Equivalent Diameter and volume moment mean (d_{43})

Assessment of the observed particles sizes, one of the parameters needed for granule classification, was determined by the volume-moment mean value (volume- or weight-moment mean), d_{43}, which could be calculated by the following equation (Kaczmarski & Bellot, 2003).

$$d_{43} = \frac{\sum_i n_i d_i^4}{\sum_i n_i d_i^3} \qquad \text{Eq. 8}$$

Where *n* is the number of particles for sample point *i* and *d* is the equivalent diameter for a particle. Equivalent diameter was calculated by solving for the diameter from the particle area determined during image analysis, shown in the following equation:

$$Equivalent\ Diameter = 2 \times \sqrt{\frac{Area}{\pi}} \qquad \text{Eq. 9}$$

For both the CTB1 and CTB3, the SBR had larger particles for the duration of the run, as seen in Figure 22. Towards the end of run, CTB2 appeared to have larger particles than the SBR, but as seen by Figure 13, these particles do not match the SBR's particles in settling ability. The trends observed in the volume-moment mean are similar to that of the percent granulation, due to the relationship between d_{43} and particle diameter, seen in Eq. 8. The granules observed in this experiment peaked around 150 μm which is smaller than average Nereda® granules and other studies examining factors affecting aerobic granules (Deng et al., 2016; Rewell & Seccombe, 2012; Wei et al., 2012; Xiao et al., 2008).

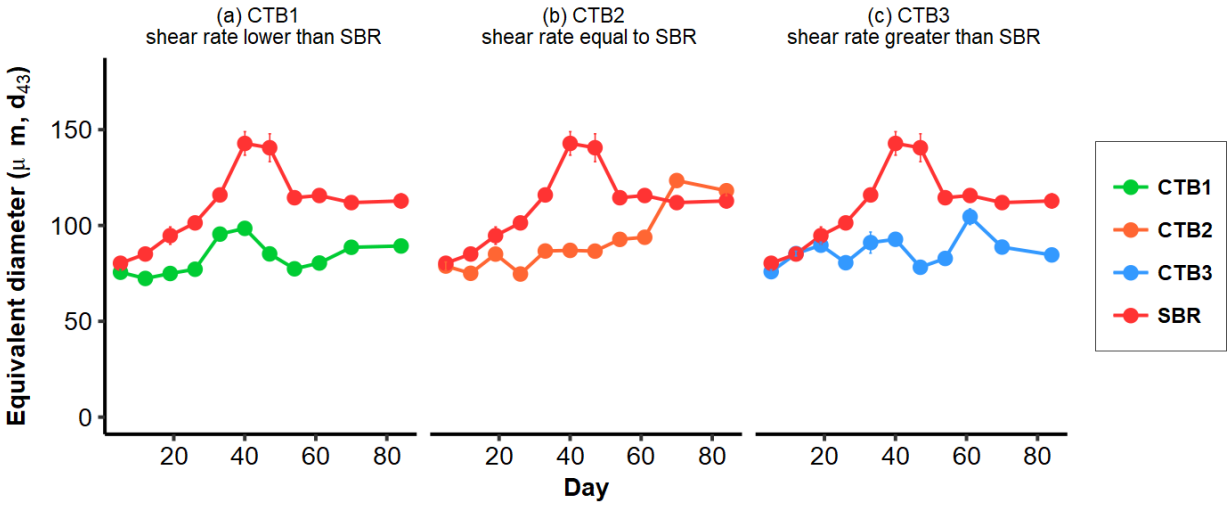

Figure 22. Changes in volume-moment mean (d_{43}) over the course of the run for (a) CTB1, (b) CTB2, and (c) CTB3 as compared to the control SBR

4-7 Extracellular Polymeric Substances (EPS)

The three types of EPS were extracted and analyzed for protein and polysaccharide components according to the procedures listed in Section 3-11. To assess the role of EPS on the aerobic granulation process, the quantities of EPS recorded and the corresponding ratio of PS/PN were plotted with percent granulation achieved within each reactor to determine how shear variation affected the production of EPS. This also allowed further observation regarding the overall presence of each EPS component and the presence or lack of granules within each reactor.

As has been reported, increases in bound EPS, and as seen when some of the CTBs towards the end of the run, could be correlated to decreases in filterability (Z. Wang et al., 2009). This was especially apparent when performing the solids testing, as the time needed to filter mixed liquor samples through the 0.45 μm membranes varied depending on the character of the sludge and bulk liquid.

4-7.1 Soluble EPS (Sol-EPS)

After separation from the biomass by repeated centrifugation, the protein and polysaccharide components of the soluble EPS (Sol-EPS) found in all four reactors were measured and compared as PS/PN ratios (Figure 23). Following the PS/PN ratio in the SBR over the course of the run, we can see that after the peak and initial decline of granulation, the PS/PN ratio nearly doubled from ~100 g carbohydrates/g proteins to over 200 g/g and remained high for the remainder of the run. Though only CTB2, of equal total average shear to the SBR, reached a PS/PN ratio of 200, and not until day 80, the trend seen in the SBR may indicate that after initial granule formation, increases in Sol-EPS may prevent additional granulation. The increased

presence of polysaccharides in the bulk fluid may make the matrix too dense for particles to physically contact each other, preventing aggregation. Additionally, increased polysaccharides may alter the overall charge of the bulk fluid enough that the double layer surrounding each charged particle prevents them from being able to overcome the van der Waals forces.

When comparing the measured Sol-EPS components to LB-EPS and TB-EPS components shown in Section 4-7.2 and 4-7.3, respectively, it is immediately obvious that the Sol-EPS fraction seems much larger than the other types of EPS. However, during our extraction of the soluble EPS by centrifugation, we did not attempt to separate the soluble microbial products (SMP) and the Sol-EPS. SMP are the soluble cellular components that are released during cell lysis, diffuse through the cell membrane, or are lost during synthesis (Laspidou & Rittmann, 2002). SMP are present no matter the granulation process or type of wastewater and typically make up the majority of effluent COD and BOD. EPS and SMP are both organic materials produced by the microbes but are secreted to the exterior of the cells for different reasons. This inherent presence of SMP may be the reason that the Sol-EPS components appear to be so large.

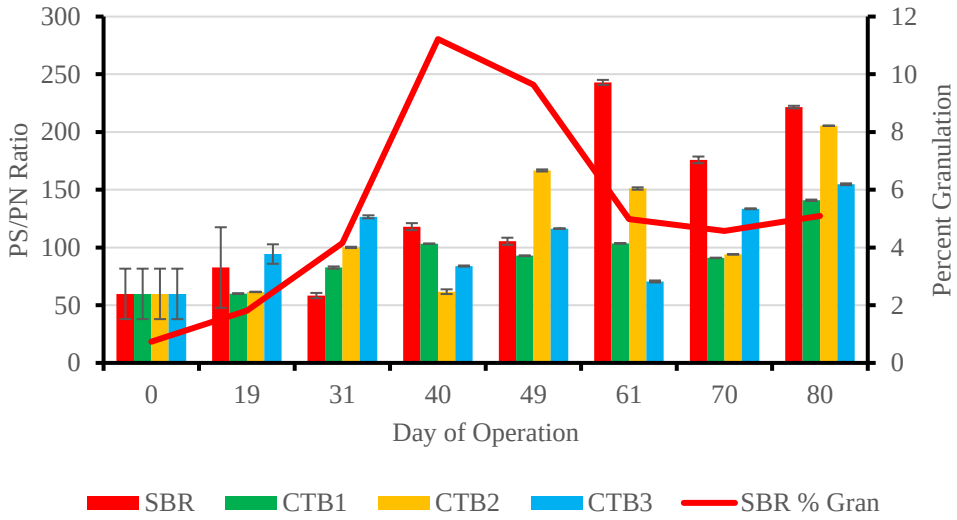

Figure 23. PS/PN ratio for Soluble EPS components from each reactor

Note that on day zero, the sample measured was from the inoculum, not a sample taken individually from each reactor. Samples from each reactor were taken in triplicate and technical triplicates were analyzed for each sampling point on the microplates for protein and carbohydrate analysis.

High polysaccharide content might facilitate cell-to-cell interaction and the resulting matrix may be critical to stronger microbial structures (Y.-Q. Liu et al., 2004).

4-7.2 Loosely Bound EPS (LB-EPS)

The loosely bound EPS (LB-EPS), characterized as the EPS forming an amorphous slime around the granules, whose role is thought to be bonding particle clusters to form stable micro-colonies, was measured and reported similarly to the Sol-EPS (Chen et al., 2017). The magnitude of the PS/PN ratio was about an order of magnitude lower than Sol-EPS for the duration of the run. After day 50 the LB-EPS PS/PN ratio increased from ~2 g/g up to ~6 g/g in all reactors. While this increase of polysaccharides in the CTBs did not correlate to trends in observed percent granules, the increase in carbohydrates in the SBR followed the disintegration of the granules formed. The fluctuation of the polysaccharide component of LB-EPS seen in the SBR, compared to the relatively constant amounts of protein, imply that the polysaccharides in LB-EPS might play a main role in the stability of granular sludge. The PS/PN ratio was consistently above 1, for all four reactors, indicating PS was a dominant component over PN in the sludge in the LB-EPS.

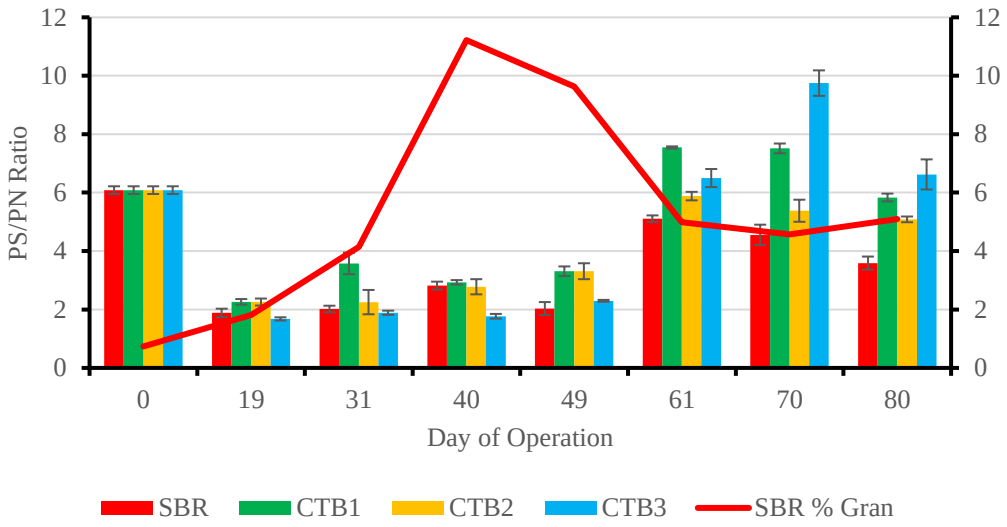

Figure 24. PS/PN ratio for Loosely Bound EPS components from each reactor

4-7.3 Tightly Bound EPS (TB-EPS)

The last component of EPS, measured after the second round of sonication, was tightly bound EPS (TB-EPS). Similar to the LB-EPS component, TB-EPS quantities were about an order of magnitude lower than the corresponding samples of Sol-EPS, though the trends observed with TB-EPS are the opposite of LB-EPS. Generally, each reactor began with higher PS/PN ratios which decreased towards the end of the run. The behavior of the TB-EPS seen in the SBR showed a peak in the PS/PN ratio around the same time that the highest percentage of granules was measured, implying that TB-EPS might be correlated to the formation of aerobic granules. The sharp decrease in the PS/PN ratio of the SBR from >6 g/g to <2 g/g on days 40 and 49 may be the reason the percent granulation of the SBR dropped from ~12% to ~9% to ~3% on days 40, 49, and 61, respectively. This may indicate that a decrease in polysaccharides, the dominant EPS component for each EPS type, of TB-EPS are sufficient to lead to granule disintegration. The lack of new and stable granules after day 50 from any of the reactors, and the PS/PN ratios of TB-EPS remaining below ~3.5 g/g, whereas at the start of the run the ratios had

been >3.5 g/g, may indicate that higher PS/PN ratios are required for granules to form. Previous research has reported TB-EPS, which is attached to the cell surface peripheral capsules, to be a key component keeping cells stuck together in clusters, which corresponds to the absence of granules when TB-EPS decreased (Chen et al., 2017).

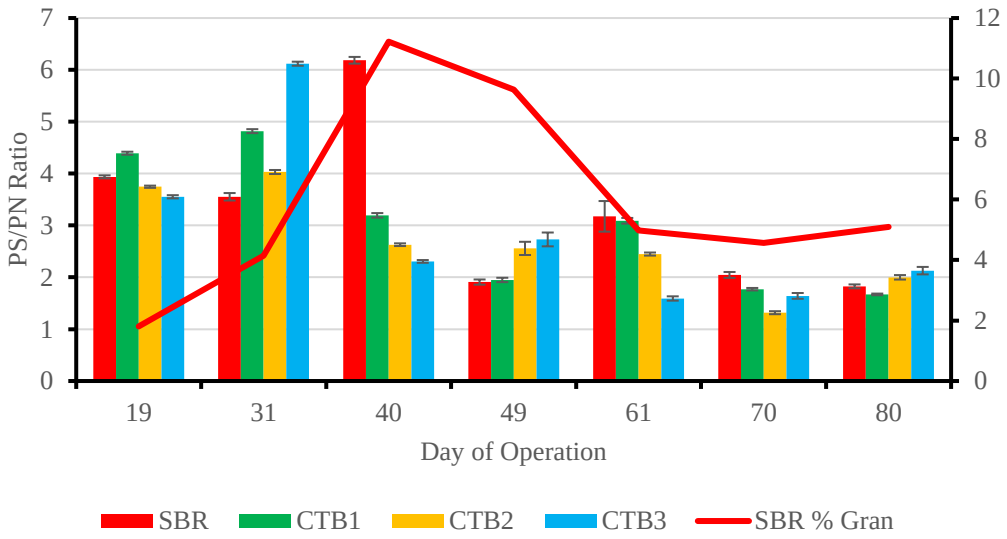

Figure 25. PS/PN ratio for Tightly Bound EPS components from each reactor

While the general trends of the TB-EPS PS/PN ratio seen between the SBR and CTB3 reactors seem similar, the CTB3 reactor also experienced a high level of polysaccharides in Sol-EPS which may have prevented the cells from coming together and benefiting from the higher levels of TB-EPS carbohydrates.

The actual values of the EPS measurements may be found in Table A-02 of the Appendix.

4-7.4 Correlation Analysis

To further explore the relationship between observed granulation and EPS measurements, a correlation analysis was performed. The correlation coefficient, *r*, was calculated by:

$$r = \frac{n\sum xy - \sum x \sum y}{\sqrt{(n\sum x^2 - (\sum x)^2)}(n\sum y^2 - (\sum y)^2)}$$ Eq. 10

Where *x* and *y* are the values of the variables and *n* is the size of the sample. If the value of the correlation coefficient is 1, a perfect positive correlation is indicated; if it is equal to -1, a perfect negative correlation is indicated; if *r* is equal to zero, then there is no correlation between the two values. Comparisons between the achieved percent granulation and average PS/PN ratios determined for each reactor yielded the correlation coefficients in Table 04.

Table 04. Correlation coefficients between percent granulation and PS/PN ratios

		Sol-EPS	**LB-EPS**	**TB-EPS**
% Granulation in	**SBR**	0.169	-0.405	0.327
	CTB1	0.400	-0.188	0.117
	CTB2	0.518	0.409	-0.850
	CTB3	-0.206	0.216	-0.167

These correlation coefficients do not indicate a consistent trend between the PS/PN ratio and percent granulation across all four reactors and most of the determined r-values indicate weak correlation. The relationship between the PS/PN ratio of TB-EPS found in CTB2 had the strongest correlation, a negative correlation indicated by a r-value of -0.850, to percent granulation achieved. The earlier suggestion that higher PS/PN ratios in Sol-EPS may be better for granulation is not strongly supported by the r-values listed in Table 04. Additionally, there is not a consistent positive correlation between TB-EPS and percent granulation across reactors.

Examination of the relationship between the volume-moment mean, d_{43}, and PS/PN ratios showed similar results to those above. The strongest correlation was found to be in the LB- and TB-EPS ratios of CTB2 with a strong positive correlation for the loosely bound and a strong negative correlation for the tightly bound portions of EPS. The strong negative correlation

between the PS/PN ratio of TB-EPS in CTB2 corresponds to the strong negative correlation found between EPS ratio and percent granulation of CTB2, as mentioned above.

Table 05. Correlation coefficients between d_{43} and PS/PN ratios

		Sol-EPS	LB-EPS	TB-EPS
d_{43} of	**SBR**	-0.102	-0.127	0.258
	CTB1	0.374	-0.087	-0.044
	CTB2	0.372	0.731	-0.802
	CTB3	-0.671	0.174	-0.126

The relationship between the protein and polysaccharide components were also examined when paired with percent granulation and d_{43} individually. Table 06 shows the correlation between the protein components and percent granulation and d_{43}, individually. Nearly all of the correlation coefficients for the protein component of Sol-EPS indicate a slight negative correlation to percent granulation and d_{43}. The correlation of protein in LB-EPS is less consistent with the CTB2 displaying strong negative correlation between protein and both percent granulation and d_{43} while, for the most part, the other reactors indicate slight positive correlations. For the protein found in TB-EPS, CTB2 shows strong positive correlation to percent granulation and d_{43} while the other reactors display weak positive correlation.

Table 06. Correlation coefficients between protein and percent granulation and d_{43}

		Sol-EPS	LB-EPS	TB-EPS
SBR	**% Granulation**	-0.560	0.396	0.122
	d_{43}	-0.264	0.407	0.157
CTB1	**% Granulation**	-0.318	0.443	-0.242
	d_{43}	-0.209	0.477	-0.073
CTB2	**% Granulation**	-0.485	-0.811	0.749
	d_{43}	-0.549	-0.845	0.743
CTB3	**% Granulation**	-0.351	-0.195	0.525
	d_{43}	0.465	0.037	0.348

Table 07 similarly shows that the most of the correlation coefficients of polysaccharides in Sol-EPS follow a similar slight negative correlation to both percent granulation and d_{43}. While there was a strong correlation between the polysaccharides in LB-EPS of CTB1 and the resulting d_{43}, overall, there was both weak positive and negative correlation.

Table 07. Correlation coefficients between polysaccharide and percent granulation and d_{43}

		Sol-EPS	**LB-EPS**	**TB-EPS**
SBR	**% Granulation**	-0.438	-0.012	0.458
	d_{43}	-0.212	0.413	0.432
CTB1	**% Granulation**	-0.221	0.265	-0.551
	d_{43}	0.320	0.960	-0.549
CTB2	**% Granulation**	-0.441	-0.211	0.278
	d_{43}	-0.429	0.166	0.230
CTB3	**% Granulation**	-0.457	0.177	0.207
	d_{43}	0.086	0.412	-0.002

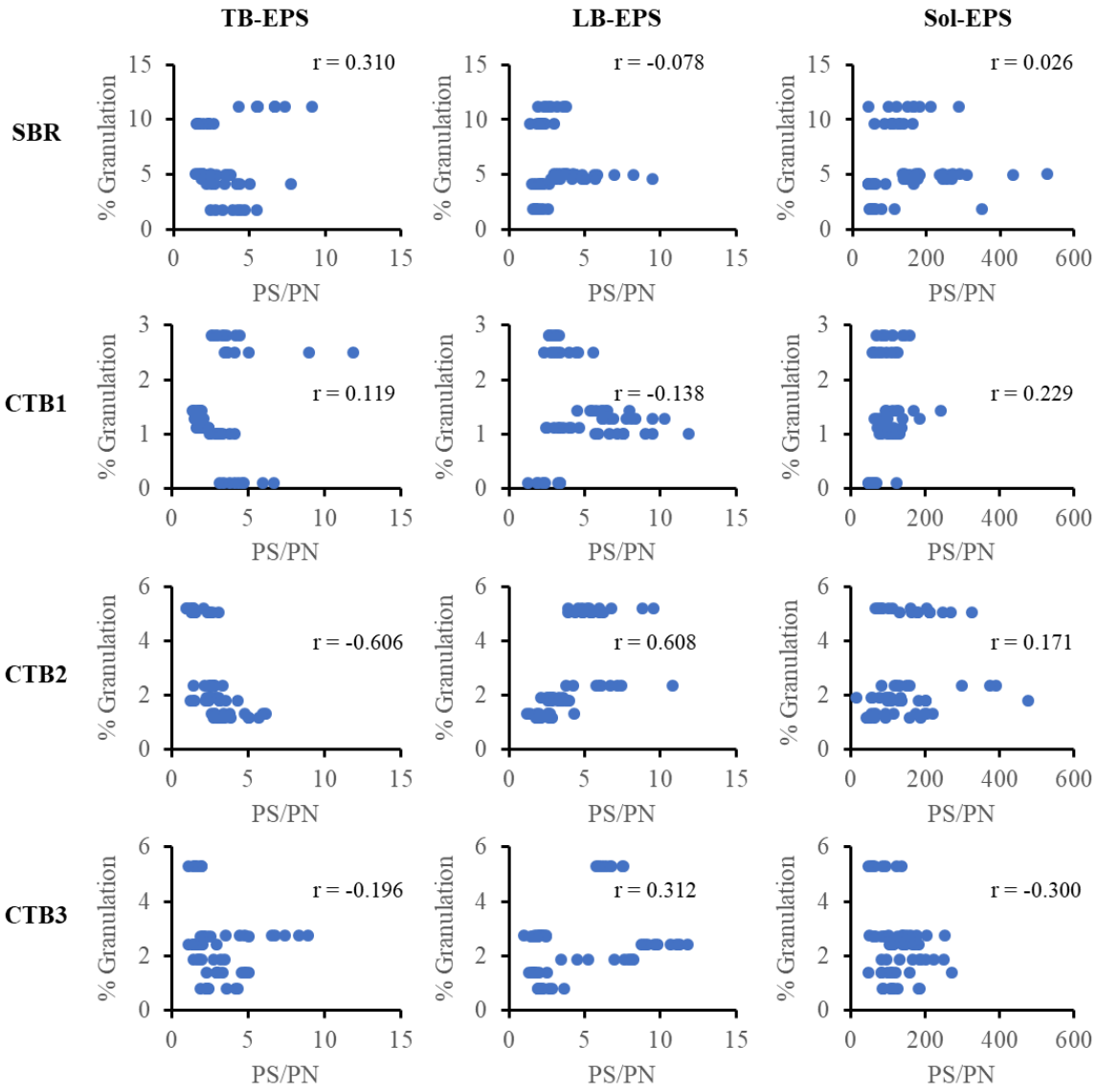

Figure 26. Correlation plots between PS/PN and percent granulation

Figure 26 expands the correlation analysis to include individual replicate data, rather than averages, over the entire course of the run. CTB2 showed strong correlation between PS/PN in TB-EPS and LB-EPS with percent granulation achieved, but this is not consistent among the other reactors. To further analyze correlation, correlation coefficients were calculated for the individual protein and polysaccharide components and percent granulation.

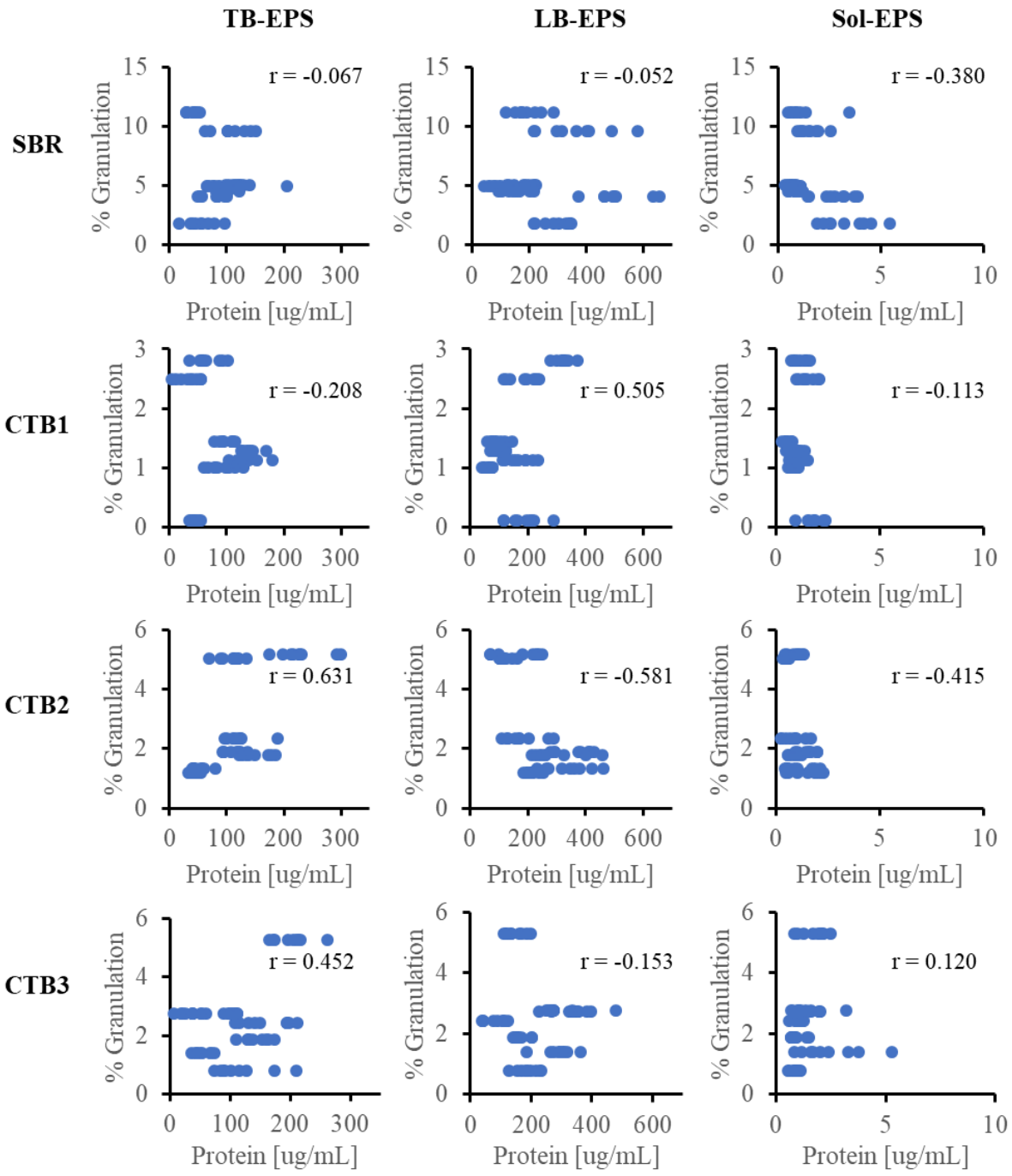

Figure 27. Correlation plots between protein and percent granulation

CTB2 again shows strong correlation between protein in TB-EPS and LB-EPS. Solely examining the protein correlation over the duration of the run, not much consensus may be drawn regarding consistent effects of protein on percent granulation.

With the SBR achieving the best granulation performance during the first 40 days of operation, before a disintegration between days 40 and 80, a separate analysis was done on each time period to isolate changes related to the formation of granules and those changes related to disintegration. Correlation coefficients reflecting these time periods are found in Figure 28. During the formation of the granules seen in the SBR, moderate-to-strong negative correlation was determined between protein in all types of EPS and percent granulation. This indicates that lower amounts of protein within each type of EPS may be necessary for the formation of granules. During the disintegration event, protein in LB- and Sol-EPS displayed strong positive correlation to percent granulation. This provides stronger indication that high levels of protein in EPS is not beneficial for the granulation process. A more detailed analysis would need to be performed to determine whether the protein was released before or after the disintegration event.

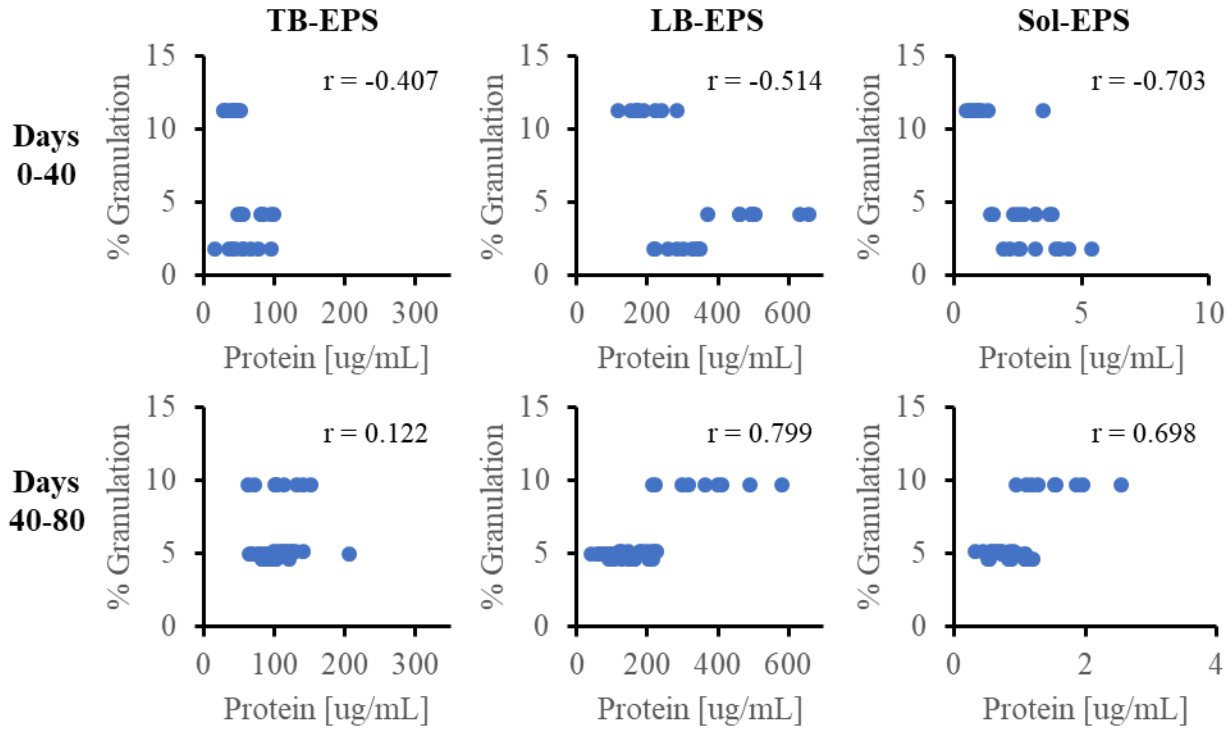

Figure 28. Correlation plots between protein and percent granulation for the SBR, separated by granulation and disintegration events

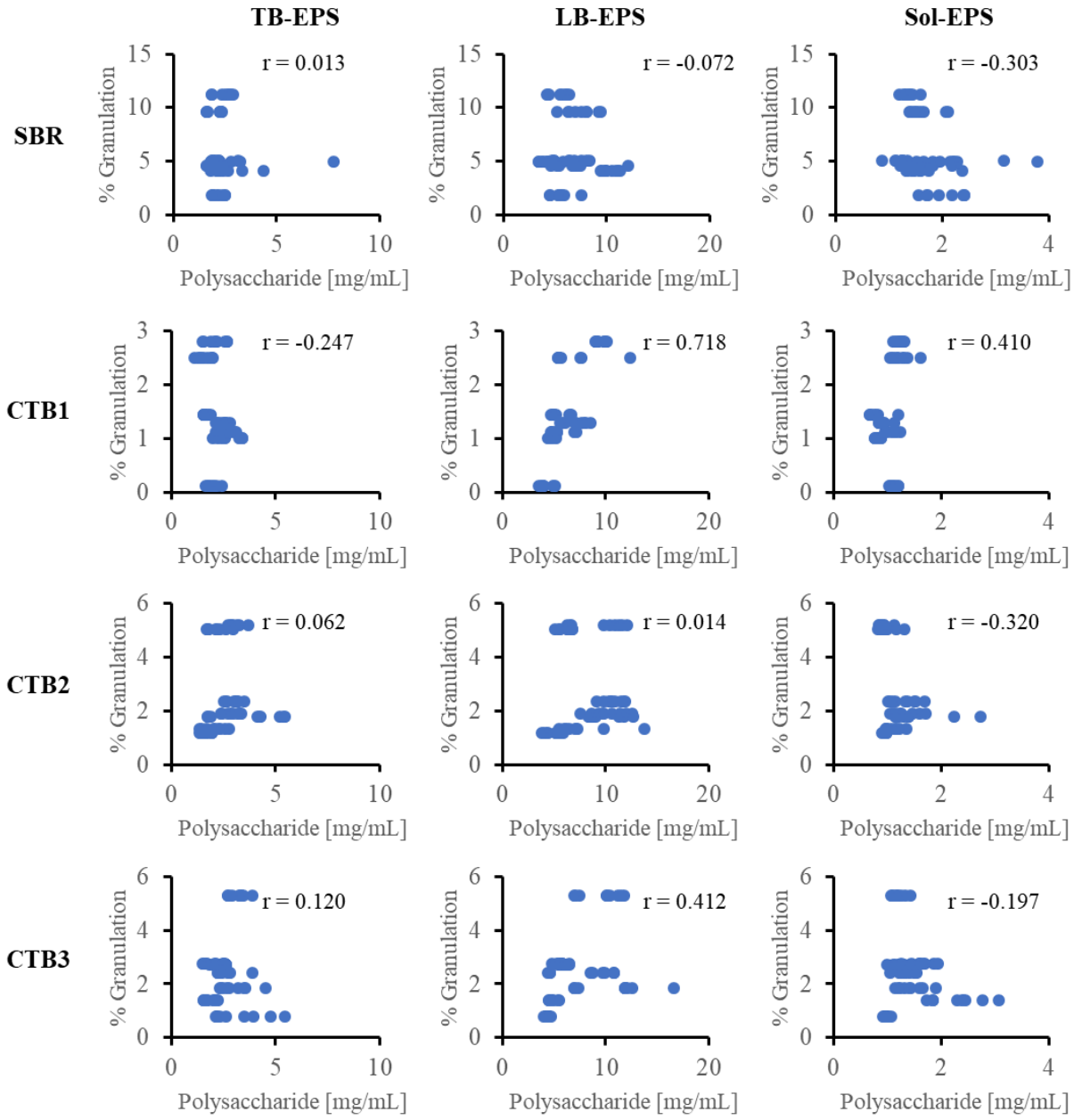

Figure 29. Correlation plots between polysaccharide and percent granulation

Similarly to the correlation coefficients calculated for protein, the relationship between polysaccharides and percent granulation over the entire course of the run was not clear. The results were not consistent across reactors or type of EPS. Thus, further analysis was performed

on the SBR to determine whether trends could be identified between the formation and disintegration of granules.

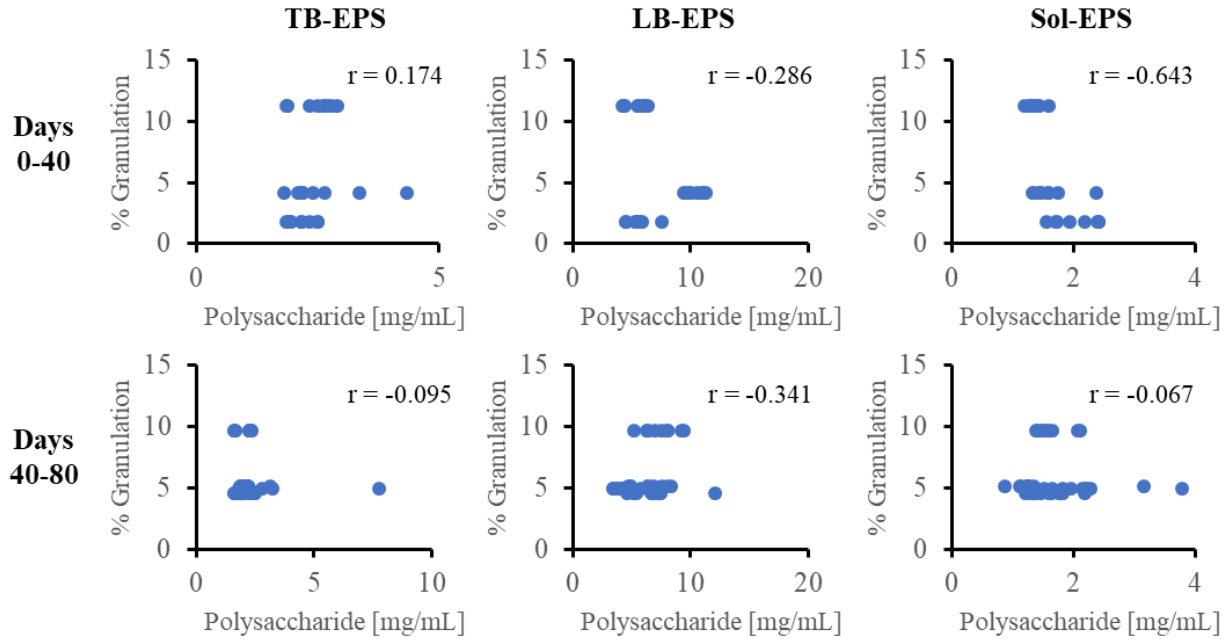

Figure 30. Correlation plots between polysaccharide and percent granulation for the SBR, separated by granulation and disintegration events

From Figure 30 it appears that the polysaccharide component of Sol-EPS had a strong negative correlation to percent granulation during granule formation. This may be because higher levels of polysaccharides make the EPS matrix too dense for particles to effectively aggregate or change the overall charge enough that it prevents cells from coming in contact with one another. A slight negative trend between the polysaccharide level of LB-EPS and percent granulation was identified during both the granulation and disintegration periods. This may indicate the polysaccharide level in LB-EPS plays a role in the formation and stability of granules. The correlation coefficients identified between polysaccharides in TB-EPS and percent granulation were close to zero, indicating that it may not be important to granule formation or stability.

The results from the correlation analysis indicate that protein in all types of EPS and polysaccharides found in Sol-EPS may be inhibitory towards the formation of aerobic granules. Low achieved granulation in the SBR makes it difficult to draw strong conclusions regarding the effect of EPS on the performance of the reactors.

4-8 Parameters over a single cycle

To analyze performance over a single cycle in the reactor and better understand the behavior of the communities in each reactor. Parameters were also measured during the 5 minute feeding time, causing the COD values from the first 5-10 minutes of the cycle to reflect the mixing of the feed within the reactor.

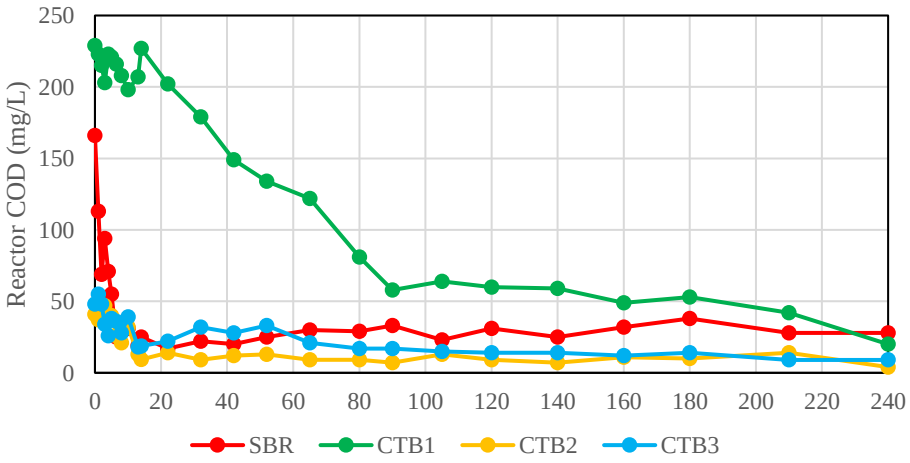

Figure 31. Reactor COD over a cycle

Figure 31 indicates that the SBR, CTB2, and CTB3 had similar COD removal behavior, with CTB2 and CTB3 consuming the influent CTB slightly faster than the SBR. In contrast, it took CTB1 the whole cycle to achieve the same >90% COD removal.

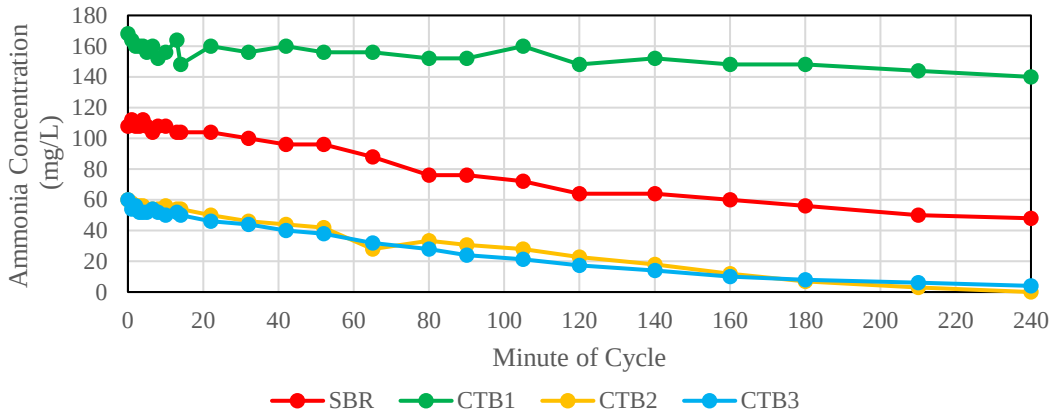

Figure 32. Reactor Ammonia over a cycle

Figure 32 shows the ammonia concentrations within the reactors, with CTB2 and CTB3 being the only reactors to achieve ammonia removal during the run. At the end of the cycle, the ammonia concentration in the SBR and CTB1 were 48 mg/L and 140 mg/L, respectively. The free ammonia (FA) remaining in the SBR and CTB1 may be inhibiting the nitrification process, which can inhibit ammonia oxidizing bacteria (AOB) at threshold concentrations of 10-150 mg/L and can inhibit nitrite oxidizing bacteria (NOB) 0.1-1.0 mg/L (Ford, 1980; Kim, Lee, & Keller, 2006). The free ammonia concentration is a function of ammonia concentration, pH, and the operation temperature as seen in the following equation (Davis L. Ford, 1980):

$$FA\left(as\ NH_3, \frac{mg}{L}\right) = \frac{17}{14} * \frac{\left(total\ NH_3 as\ N \frac{mg}{L}\right) * 10^{pH}}{\frac{K_b}{K_w} + 10^{pH}} \quad \text{Eq. 11}$$

Where the ionization constant of ammonia (K_b) and water (K_w) is calculated by the following;

$$\frac{K_b}{K_w} = e^{\frac{6334}{273+T(℃)}} \quad \text{Eq. 12}$$

Assuming that the operational temperature of all four reactors was 25°C, and using the pH measured on the day the parameters were measured over a cycle, the FA of each reactor can be found in Table 04. The FA concentrations for the SBR is within the range of 0.1-1.0 mg/L

which inhibits the NOBs, explaining the accumulation of nitrite in the SBR, seen in Figure 33. Although CTB1 also displayed high FA concentrations, there was not a corresponding nitrite accumulation. CTB3 showed an accumulation of nitrite towards the beginning of the cycle, but nearly all the nitrite was oxidized by the end of the cycle. The high ammonia concentrations seen in the SBR and CTB1 could also be due to smaller populations of ammonia oxidizing bacteria in those particular reactors or potentially low dissolved oxygen within the reactors due to blockage of the air diffusers, though such blockages were not observed.

Table 08. Free Ammonia concentrations in each reactor

Reactor	**Ending Ammonia Concentration [mg/L]**	**pH**	**Free Ammonia [mg/L as NH_3]**
SBR	48	6.65	0.15
CTB1	140	7.14	1.36
CTB2	0	6.75	0.00
CTB3	4	6.67	0.01

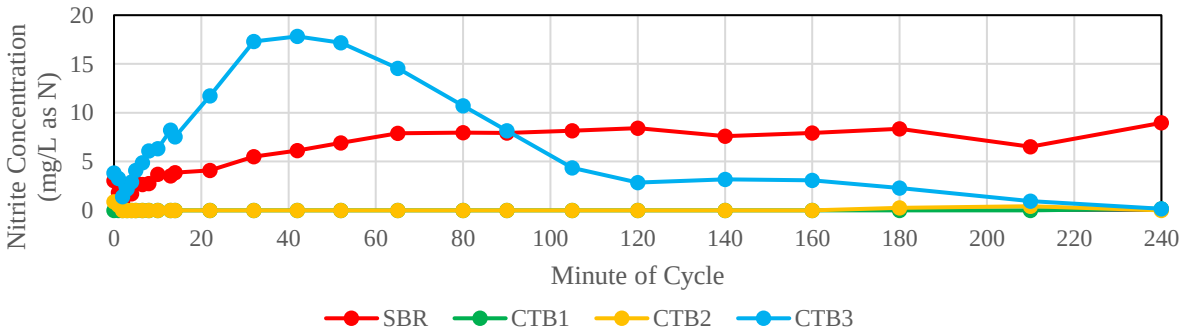

Figure 33. Reactor Nitrite over a cycle

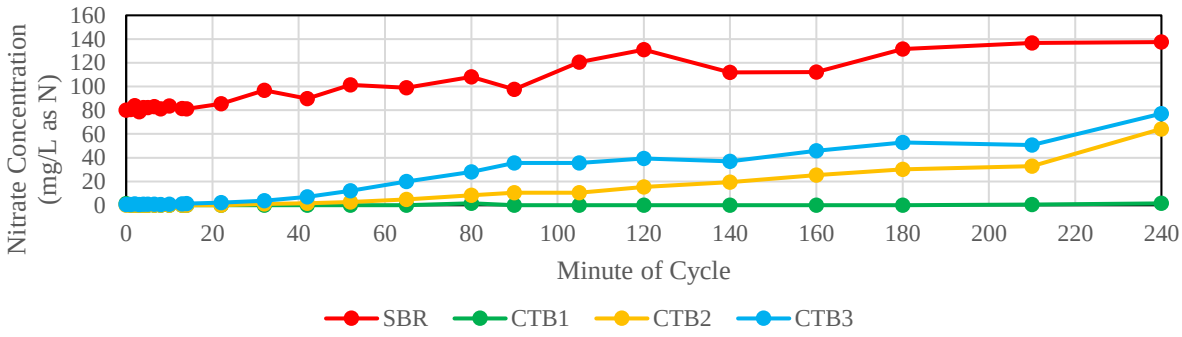

Figure 34. Reactor Nitrate over a cycle

4-9 Lessons from Operation

The following were unanticipated lessons learned during the operation and monitoring of the reactors for this experiment.

- The use of buffer addition to control the pH of the reactors was needed due to the observation of continued pH decreases, particularly in CTB2 and CTB3. The pH for all reactors stabilized around day 45 and the addition of buffer was no longer needed.
- The flexible bubble wands used to provide fine-bubble aeration to the Couette reactors must be periodically checked when the CTBs are not rotating. The hard, plastic caps on the end of the bubble wands wear down due to the constant motion of the outer cylinder, eventually forming a hole in the wand. This hole in the wand allows a secondary release for the pressure needed to push air through the fine holes, altering the air flow rate into the reactors. Flexible bubble wands should be replaced before this occurs.
- Due to the consistent rotation necessary for the Couette reactors and the additional weight of the reactor and working volume of sludge and influent on the pottery wheels, slight misbalancing can cause the axel to permanently shift due to friction, rendering the pottery

wheel unusable. It is ideal to have a backup pottery wheel for when this happens. Worn down wheels are kept for spare parts.

- Attached biofilm growth on the walls of the Couette reactors may be cleaned by gliding a long 25 mL bulb pipet through the annular gap.
- All four reactors achieved good COD removal throughout the course of the run. During batch testing, the SBR, CTB2, and CTB3 achieved >90% COD removal within the first 10 minutes of the cycle. At the time of the batch test, it took the CTB1 longer to significantly remove the majority of the COD from the influent.
- Determined by image analysis, equivalent diameter and roundness, the SBR produced over 10% granules while no Couette reactor reached more than 5%. These results support the hypothesis that the shear distribution only seen in the SBR is necessary for the formation of granules. The variation of shear present in tall, narrow SBRs may be why past research using this type of reactor has shown the most successful aerobic granule formation.
- Sonication showed successful extraction of loosely-bound and tightly-bound EPS as determined by the anthrone-sulfuric acid method with D-Glucose as a standard for determining polysaccharide content and the Lowry method with BCA standards for protein measurement. It is necessary to filter the EPS samples through a 0.45 μm filter prior to the 0.20 μm filtration to prevent the smaller pore sizes from clogging. Further analysis should be performed to determine whether the soluble EPS portions gathered contained high levels of soluble microbial products, giving a false high measurement.

- Additional EPS extraction on samples taken during the first 40 days, where granulation was observed in the SBR would help identify whether stronger trends may be observed between each type of EPS and achieved granulation.
- Further exploration of the individual components that comprise the protein and polysaccharide components of each type of EPS may help explain the characteristics and behavior of the particles over time. Additional colorimetric methods or standards may be useful in identifying the individual components within extracted EPS samples.

CHAPTER FIVE – Conclusions and Future Work

Based on the original granule qualifications (particle diameter greater than or equal to 200 μm and a shape factor greater than or equal to 0.6), the SBR produced the highest percent granules for the majority of the run in comparison to the three CTBs with lower, equal, and higher total average shear. The peak in the percent granulation of the SBR seen around day 40 correlated to an increase in the PS/PN ratio of tightly bound EPS. As the observed percent granules in the SBR decreased, the PS/PN ratio of tightly bound EPS decreased while the PS/PN ratio of loosely-bound EPS sand soluble EPS were observed. These trends may indicate that tightly-bound EPS is important for the aggregation and growth of granular particles and high PS/PN ratios of loosely-bound and soluble EPS may be counteractive to the aerobic granulation process.

To use aerobic granular sludge in existing treatment plants, the technology needs to be adapted from batch reactors to continuous reactors. The main problems research groups have found in trying to create granules under continuous settings is how to direct the settling pressure within the reactor to keep granules and purge the smaller particles with the effluent supernatant stream. Currently, lab-scale experiments are being done using a long plug-flow section, for kinetic and metabolic settling pressure, and baffles to select larger and faster-settling particles, settling selection pressure, for the RAS line. Another difficulty lies in the fact that since flow is continuous, there can be issues with controlling the loads presented to the microbes at any given time which can lead to shock loads or toxic shock conditions that damage the desired microbial community and affect granule growth or stability. An area of this project that could be examined further is the settling selection pressure. Compared to past research, our lowest settling time of

10 minutes could be made more aggressive to provide a higher selection pressure and push the sludge communities towards greater granule formation.

Additional work needs to be done to assess the microbial community structure within a reactor during the granulation process. Understanding the key players within a reactor and how the populations fluctuate in relation to each other as granules are formed would help researchers and operators understand know whether they are forming desirable granules that keep the ability to simultaneously remove nitrogen and phosphorous. If the community can be determined periodically, knowledge about which species could be important would also allow a crude warning system to be developed for operators to know whether their granules may be at risk of breaking.

Examination of the 16S rRNA from samples corresponding to EPS quantification dates should be performed to observe correlations between the appearance and dominance of certain species and associated changes in the protein and carbohydrate components of EPS. This will aid understanding of whether a certain species is necessary for the majority of the EPS production or whether EPS may be reliably produced by all microbes present in any granular sludge.

CHAPTER SIX – Overall Mechanism of Granulation related to Shear Variation and EPS Production

6-1 The role of shear variation

Early aerobic granulation research suggested that reductions in shear stress experienced under conventional activated sludge processes were necessary to prevent excess shear from preventing aggregation. The first reported aerobic granules, by Mishima et al. (1991), were formed in an Aerobic Upflow Sludge Blanket (AUSB) with mild vertical stress from the upflow and horizontal stress from the agitator rotation. This project was placed in contrast to the strong shear stresses due to aeration and sludge return pumping experienced in conventional activated sludge processes. The suggested lower shear of the AUSB would allow filamentous bacteria to grow and become tangled with another particle's filamentous, accelerating the granulation process (Mishima & Nakamura, 1991).

More recent research tends to suggest that high shear force helps to form dense granules (Adav et al., 2007). The primary reasoning behind this theory is that the high shear encourages the production of EPS, which promotes better aggregation between cells due to the excreted sticky matrix of protein, polysaccharides, nucleic acids, humic acids, and lipids. However, it is important to note that hydrodynamic shear and EPS production are not directly correlated; once shear becomes too high, the structure of aggregates or granules may be sheared apart, leading to disintegration events. A balance between high and low shear must be found to allow for microbial growth, EPS production, and surface erosion to keep granules dense and regularly shaped. The presence of areas of high and low shear is only seen in the SBR, which had the best production of granules in this experiment. The presence of constant shear within each of the Couette reactors is the most likely reason why these three reactors had trouble producing aerobic

granules. The uniform shear of the Couette reactors either was not enough to induce EPS excretion or it was high enough to encourage EPS excretion, but not to force the particles close enough together for the EPS to aid in aggregation.

6-2 The role of EPS

Excreted because of environmental stress, mainly hydrodynamic shear, EPS is a protective layer against toxins, a way for cells to remain stable, and a place where nutrients may be captured for easy access. The products, apart from polysaccharides, found in EPS tend to originate as intracellular polymers that are released due to cell lysis. On granules, EPS may be separated into three groups, soluble, loosely-bound, and tightly-bound EPS using many different methods. The total EPS content of granules has been found to be higher than that of flocculant particles and biofilms and the composition of the EPS depends on the present species, substrate, oxygen limitation, ionic strength, temperature, hydrodynamic shear, among other parameters.

Thus far, the composition of each type of EPS has not been determined for aerobic granules. This project measured total protein (PN) and polysaccharide (PS) contents of each EPS type. Coupled with image analysis of the particles to follow the granulation process within each reactor, trends in the EPS production were identified. Results showed that high PS/PN ratios in the Sol-EPS may have inhibited granule formation within both the SBR and CTBs. The PS/PN ratio of TB-EPS followed the general granulation pattern, indicating that it may be important to the aggregation and granulation process. During granulation, there was a strong positive correlation coefficient between the protein component of Sol-EPS in the SBR and achieved granulation. During disintegration, strong negative correlation was found between protein in the LB-EPS and Sol-EPS of the SBR and achieved granulation, indicating that there may be a higher levels of protein in these components may be related to the disintegration of aerobic granules.

6-3 Proposed granulation mechanisms

The presence of hydrodynamic shear variation appeared to benefit the aerobic granulation process with the SBR producing a higher percentage of granules than any of the CTBs. Previous experiments performed with the same setup suggested that the travel time between the areas of high and low shear was important in allowing both EPS extraction and coalescence between particles (Karami, 2012). The figure below illustrates different lengths of time as a particle travels between high and low shear zones if the particles are assumed to travel at the same velocity along the trajectory indicated by the arrows in both (a) and (b). Within the tall, narrow SBR, which has been the most successful reactor configuration for producing granules, a variation in shear and movement similar to Figure 30 is observed, which supports the idea that this mechanism is necessary for granulation.

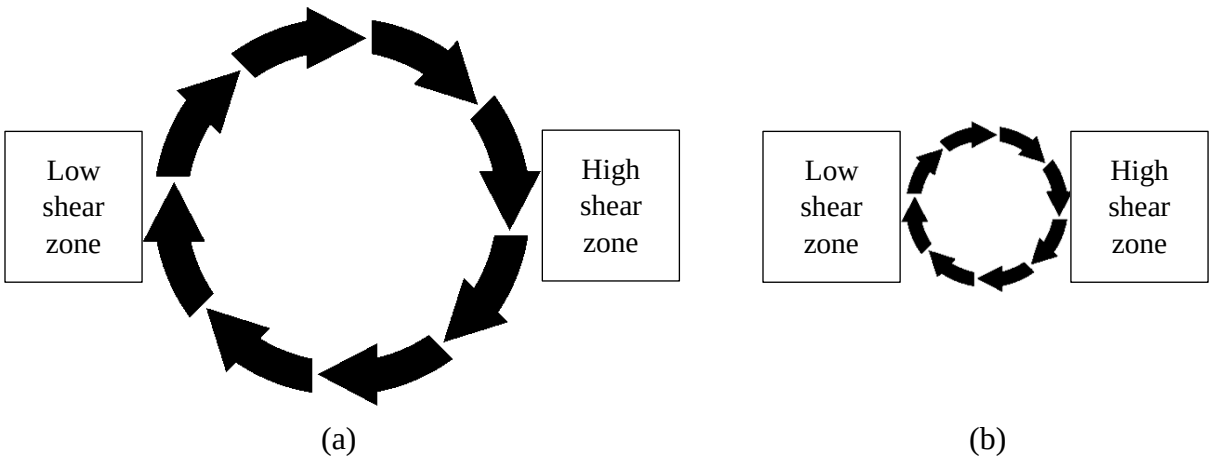

Figure 35. Proposed mechanism for the presence of shear variation in a bioreactor; (a) longer cycle time between low and high shear zones (b) shorter cycle time between high and low shear zones (Karami, 2012)

The results of EPS quantification suggest that higher levels of polysaccharides in the TB-EPS benefits the formation of aerobic granules. Minimal Sol-EPS excreted or released due to cell lysis was also shown to be beneficial, likely because higher levels of polysaccharides within the bulk liquid prevents the particles from colliding and aggregating to form larger granules. Further

microbial community analysis will help in understanding whether the source of EPS is from a select number of species or from the overall communities present and which conditions lead to changes in EPS production.

6-4 Conclusions

Future projects should consider the proposed mechanism of movement between high and low shear zones within a reactor during the design phase, especially under continuous conditions, to allow granulation to occur. Coupled with extracellular polymeric substance monitoring for increases in the polysaccharide content of tightly bound EPS and low overall soluble EPS, we propose that this mechanism is necessary for successful aerobic granule formation. Further research is needed to develop reactors conducive to the proposed granulation mechanisms that may run under continuous operation. This project and further research will help further the understanding of how settling pressures, operating conditions, hydrodynamic shear, and extracellular polymeric substances may lead to successful aerobic granulation which will help existing plants retrofit granulation technology.

REFERENCES

Adav, S. S., Lee, D. J., & Lai, J. Y. (2007). Effects of aeration intensity on formation of phenol-fed aerobic granules and extracellular polymeric substances. *Applied Microbiology and Biotechnology*, *77*(1), 175–182. https://doi.org/10.1007/s00253-007-1125-3

Beun, J. J., Hendriks, A., Van Loosdrecht, M. C. M., Morgenroth, E., Wilderer, P. A., & Heijnen, J. J. (1999). Aerobic granulation in a sequencing batch reactor. *Water Research*, *33*(10), 2283–2290. https://doi.org/10.1016/S0043-1354(98)00463-1

Beun, J. J., Van Loosdrecht, M. C. M., & Heijnen, J. J. (2002). Aerobic granulation in a sequencing batch airlift reactor. *Water Research*, *36*(3), 702–712. https://doi.org/10.1016/S0043-1354(01)00250-0

Cammarota, M. C., & Sant'Anna, G. L. (1998). Metabolic blocking of exopolysaccharides synthesis: Effects on microbial adhesion and biofilm accumulation. *Biotechnology Letters*, *20*(1), 1–4. https://doi.org/10.1023/A:1005394325549

Chen, C., Bin, L., Tang, B., Huang, S., Fu, F., Chen, Q., & Wu, L. (2017). Cultivating granular sludge directly in a continuous-flow membrane bioreactor with internal circulation. *Chemical Engineering Journal*, *309*, 108–117. https://doi.org/10.1016/j.cej.2016.10.034

Cornea, T., Cr, I., & Dinu, I. (2013). INCREASING ENERGY EFFICIENCY OF WASTEWATER TREATMENT PLANTS BY UPGRADING THE CONVENTIONAL TREATMENT PROCESS WITH NEREDA TECHNOLOGY, *12*(4), 651–656.

Davis L. Ford, R. L. C. and J. W. K. (1980). Comprehensive Analysis of Nitrification of Chemical Processing Wastewaters. *Journal (Water Pollution Control Federation)*, *52*(11), 2726–2746. https://doi.org/10.2307/25040952

Deng, S., Wang, L., & Su, H. (2016). Role and in fl uence of extracellular polymeric substances on the preparation of aerobic granular sludge. *Journal of Environmental Management*, *173*, 49–54. https://doi.org/10.1016/j.jenvman.2016.03.008

Eliosov, B., & Ellis, T. G. (2002). Extant Respirometric Kinetic Parameter Estimation Procedure Training Manual. *Proceedings of SPIE - The International Society for Optical Engineering*, *4575*, 12–22. Retrieved from http://www.scopus.com/inward/record.url?eid=2-s2.0-0035764181&partnerID=40&md5=d80bef36c5e0f433abdfa58b69b2ee70

Fang, H. H. P., Liu, H., & Zhang, T. (2002). Characterization of a hydrogen-producing granular sludge. *Biotechnology and Bioengineering*, *78*(1), 44–52. https://doi.org/10.1002/bit.10174

Feng, Q., Xiao, Y., Wang, X., Li, J., Wu, Y., Xue, Z., … Oleyiblo, J. O. (2016). The influences of shear stress on Extracellular Polymeric Substances of activated sludge. *Desalination and Water Treatment*, *3994*(January), 15835–15842. https://doi.org/10.1080/19443994.2015.1079254

Frølund, B., Palmgren, R., Keiding, K., & Nielsen, P. H. (1996). Extraction of extracellular polymers from activated sludge using a cation exchange resin. *Water Research*, *30*(8), 1749–1758. https://doi.org/10.1016/0043-1354(95)00323-1

Fukuzaki, S., Nishio, N., & Nagai, S. (1995). High rate performance and characterization of granular methanogenic sludges in upflow anaerobic sludge blanket reactors fed with various defined substrates. *Journal of Fermentation and Bioengineering*, *79*(4), 354–359. https://doi.org/10.1016/0922-338X(95)93994-U

Grady Jr., C. P. L., Diagger, G. T., Love, N. G., & Filipe, C. D. M. (2011). *Biological Wastewater Treatment* (Third). Boca Raton, FL: CRC Press, Taylor and Francis Group.

Kaczmarski, K., & Bellot, J. C. (2003). Effect of Particle-Size Distribution and Particle Porosity Changes on Mass-Transfer Kinetics. *Acta Chromatographica*, *13*(13), 22–37.

Kang, A. J., & Yuan, Q. (2017). Bioresource Technology Long-term stability and nutrient removal efficiency of aerobic granules at low organic loads. *Bioresource Technology*, *234*, 336–342. https://doi.org/10.1016/j.biortech.2017.03.057

Karami, B. (2012). *Effect of Hydrodynamics on Aerobic Granulation*. North Carolina State University.

Kim, D. J., Lee, D. I., & Keller, J. (2006). Effect of temperature and free ammonia on nitrification and nitrite accumulation in landfill leachate and analysis of its nitrifying bacterial community by FISH. *Bioresource Technology*, *97*(3), 459–468. https://doi.org/10.1016/j.biortech.2005.03.032

Laspidou, C. S., & Rittmann, B. E. (2002). A unified theory for extracellular polymeric substances, soluble microbial products, and active and inert bi omass. *Water Research*, *36*, 2711–2720. https://doi.org/10.1016/S0043-1354(01)00413-4

Li, J., Ding, L. Bin, Cai, A., Huang, G. X., & Horn, H. (2014). Aerobic sludge granulation in a full-scale sequencing batch reactor. *BioMed Research International*, *2014*. https://doi.org/10.1155/2014/268789

Liang, Z., Li, W., Yang, S., & Du, P. (2010). Extraction and structural characteristics of extracellular polymeric substances (EPS), pellets in autotrophic nitrifying biofilm and activated sludge. *Chemosphere*, *81*(5), 626–632. https://doi.org/10.1016/j.chemosphere.2010.03.043

Liu, Y.-Q., Liu, Y., & Tay, J.-H. (2004). The effects of extracellular polymeric substances on the formation and stability of biogranules. *Applied Microbiology and Biotechnology*, *65*(2), 143–148. https://doi.org/10.1007/s00253-004-1657-8

Liu, Y. Q., & Tay, J. H. (2007). Characteristics and stability of aerobic granules cultivated with different starvation time. *Applied Microbiology and Biotechnology*, *75*(1), 205–210. https://doi.org/10.1007/s00253-006-0797-4

Liu, Y., & Tay, J. H. (2002). The essential role of hydrodynamic shear force in the formation of biofilm and granular sludge. *Water Research*, *36*(7), 1653–1665. https://doi.org/10.1016/S0043-1354(01)00379-7

Martins, A. M. P., Pagilla, K., Heijnen, J. J., & Van Loosdrecht, M. C. M. (2004). Filamentous bulking sludge - A critical review. *Water Research*, *38*(4), 793–817. https://doi.org/10.1016/j.watres.2003.11.005

Masuda, H. (2018). Flow Dynamics in Taylor – Couette Flow Reactor with Axial Distribution of Temperature, *64*(3), 1075–1082. https://doi.org/10.1002/aic.15972

Mishima, K., & Nakamura, M. (1991). Self-Immobilization of Aerobic Activated Sludge-a Pilot Study of the Aerobic Upflow Municipal Sewage Treatment. *Water Sci. Technol.*, *23*, 981–990.

More, T. T., Yadav, J. S. S., Yan, S., Tyagi, R. D., & Surampalli, R. Y. (2014). Extracellular polymeric substances of bacteria and their potential environmental applications. *Journal of Environmental Management*, *144*, 1–25. https://doi.org/10.1016/j.jenvman.2014.05.010

Mota, C. R., Head, M. A., Williams, J. C., Eland, L., Cheng, J. J., & de los Reyes, F. L. (2014). Structural integrity affects nitrogen removal activity of granules in semi-continuous reactors. *Biodegradation*, *25*(6), 923–934. https://doi.org/10.1007/s10532-014-9712-3

Park, C., Jung, J., & Milferstedt, K. (2017). ScienceDirect Biogranules applied in environmental engineering, *2*. https://doi.org/10.1016/j.ijhydene.2017.07.176

Pellicer-Nàcher, C., Domingo-Félez, C., Mutlu, A. G., & Smets, B. F. (2013). Critical assessment of extracellular polymeric substances extraction methods from mixed culture biomass. *Water Research*, *47*(15), 5564–5574. https://doi.org/10.1016/j.watres.2013.06.026

Pronk, M., de Kreuk, M. K., de Bruin, B., Kamminga, P., Kleerebezem, R., & van Loosdrecht, M. C. M. (2015). Full scale performance of the aerobic granular sludge process for sewage treatment. *Water Research*. https://doi.org/10.1016/j.watres.2015.07.011

Qiao, J., Yan, W., Teoh, J. H., Tong, Y. W., & Wang, C. (2018). Experimental and computational studies of oxygen transport in a Taylor- Couette bioreactor. *Chemical Engineering Journal*, *334*(October 2017), 1954–1964. https://doi.org/10.1016/j.cej.2017.11.137

Quarmby, J. (Birmingham U., & Forster, C. F. (Birmingham U. (1995). An examination of the structure of UASB granules. *Water Research*, *29*(11), 2449–2454.

Rewell, S., & Seccombe, D. Nereda , Netherlands ® (2012).

Sánchez Pérez, J. A., Rodríguez Porcel, E. M., Casas López, J. L., Fernández Sevilla, J. M., & Chisti, Y. (2006). Shear rate in stirred tank and bubble column bioreactors. *Chemical Engineering Journal*, *124*(1–3), 1–5. https://doi.org/10.1016/j.cej.2006.07.002

Sarma, S. J., & Tay, J. H. (2018). Aerobic granulation for future wastewater treatment technology: challenges ahead. *Environmental Science: Water Research & Technology*. https://doi.org/10.1039/C7EW00148G

Sarma, S. J., Tay, J. H., & Chu, A. (2016). Finding Knowledge Gaps in Aerobic Granulation Technology. *Trends in Biotechnology*, *35*(1), 66–78. https://doi.org/10.1016/j.tibtech.2016.07.003

Sheng, G. P., Yu, H. Q., & Li, X. Y. (2010). Extracellular polymeric substances (EPS) of microbial aggregates in biological wastewater treatment systems: A review. *Biotechnology Advances*, *28*(6), 882–894. https://doi.org/10.1016/j.biotechadv.2010.08.001

Sponza, D. T. (2002). Extracellular polymer substances and physicochemical properties of flocs in steady- and unsteady-state activated sludge systems. *Process Biochemistry*, *37*(9), 983–998. https://doi.org/10.1016/S0032-9592(01)00306-5

Tay, H., & Liu, S. (2001). The effects of shear force on the formation , structure and metabolism of aerobic granules, 227–233. https://doi.org/10.1007/s002530100766

Tay, J. H., Liu, Q. S., & Liu, Y. (2001). The role of cellular polysaccharides in the formation and stability of aerobic granules. *Letters in Applied Microbiology*, *33*(3), 222–226. https://doi.org/10.1046/j.1472-765X.2001.00986.x

Tay, J. H., Liu, Q. S., & Liu, Y. (2002). Aerobic granulation in sequential sludge blanket reactor. *Water Science and Technology*, *46*(4–5), 13–18. https://doi.org/10.1046/j.1365-2672.2001.01374.x

Wang, Z., Wu, Z., & Tang, S. (2009). Extracellular polymeric substances (EPS) properties and their effects on membrane fouling in a submerged membrane bioreactor. *Water Research*, *43*(9), 2504–2512. https://doi.org/10.1016/j.watres.2009.02.026

Wang, B. Bin, Chang, Q., Peng, D. C., Hou, Y. P., Li, H. J., & Pei, L. Y. (2014). A new classification paradigm of extracellular polymeric substances (EPS) in activated sludge: Separation and characterization of exopolymers between floc level and microcolony level. *Water Research*, *64*, 53–60. https://doi.org/10.1016/j.watres.2014.07.003

Wei, Y., Ji, M., Li, G., & Qin, F. (2012). Microbial and hydrodynamic properties of aerobic granules in a sequencing batch reactor treating landfill leachate. *Journal of Zhejiang University SCIENCE A*, *13*(3), 219–229. https://doi.org/10.1631/jzus.A1100153

Williams, J. C. (2004). Initial Investigations of Aerobic Granulation in an Annular Gap Bioreactor. *Science*.

Xiao, F., Yang, S. F., & Li, X. Y. (2008). Physical and hydrodynamic properties of aerobic granules produced in sequencing batch reactors, *63*, 634–641. https://doi.org/10.1016/j.seppur.2008.07.002

Zhang, L. L., Chen, J. M., & Fang, F. (2008). Biodegradation of methyl t-butyl ether by aerobic granules under a cosubstrate condition. *Applied Microbiology and Biotechnology*, *78*(3), 543–550. https://doi.org/10.1007/s00253-007-1321-1

Zhuang, W. Q., Tay, J. H., Yi, S., & Tay, S. T. L. (2005). Microbial adaptation to biodegradation of tert-butyl alcohol in a sequencing batch reactor. *Journal of Biotechnology*, *118*(1), 45–53. https://doi.org/10.1016/j.jbiotec.2005.02.014

APPENDIX

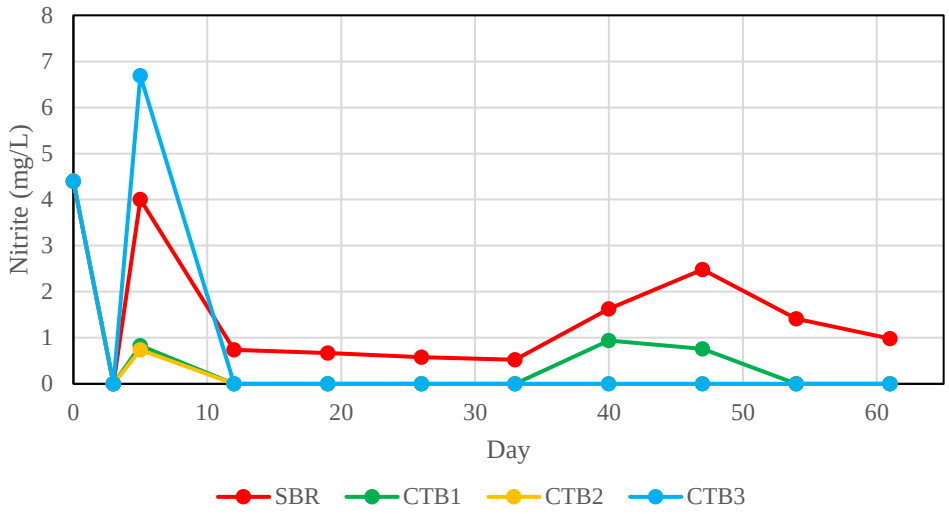

Figure A-01. Effluent Nitrite concentrations

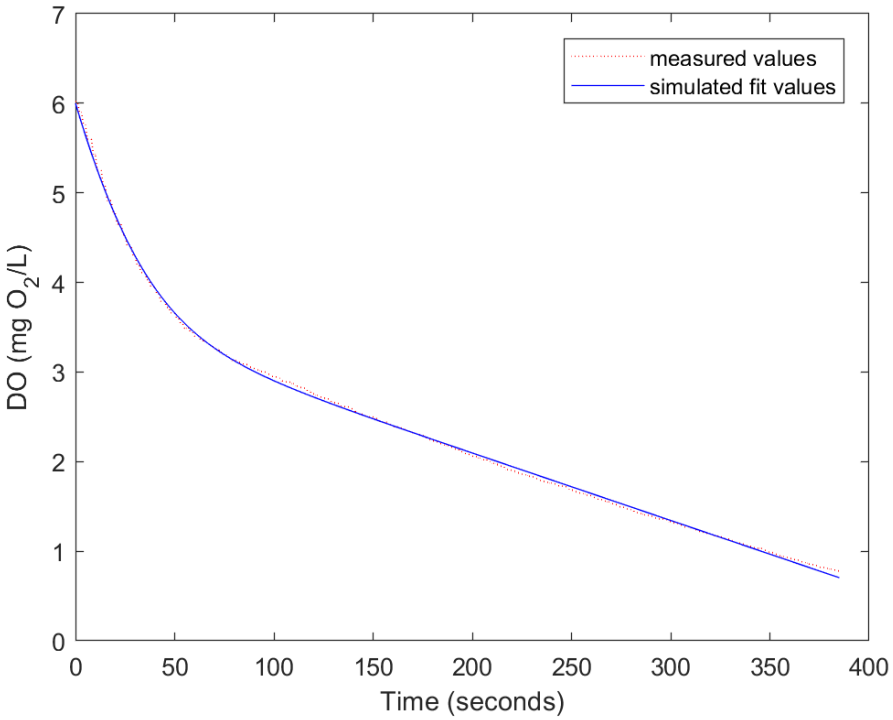

Figure A-02. Least squares curve fit for SBR during respirometry test

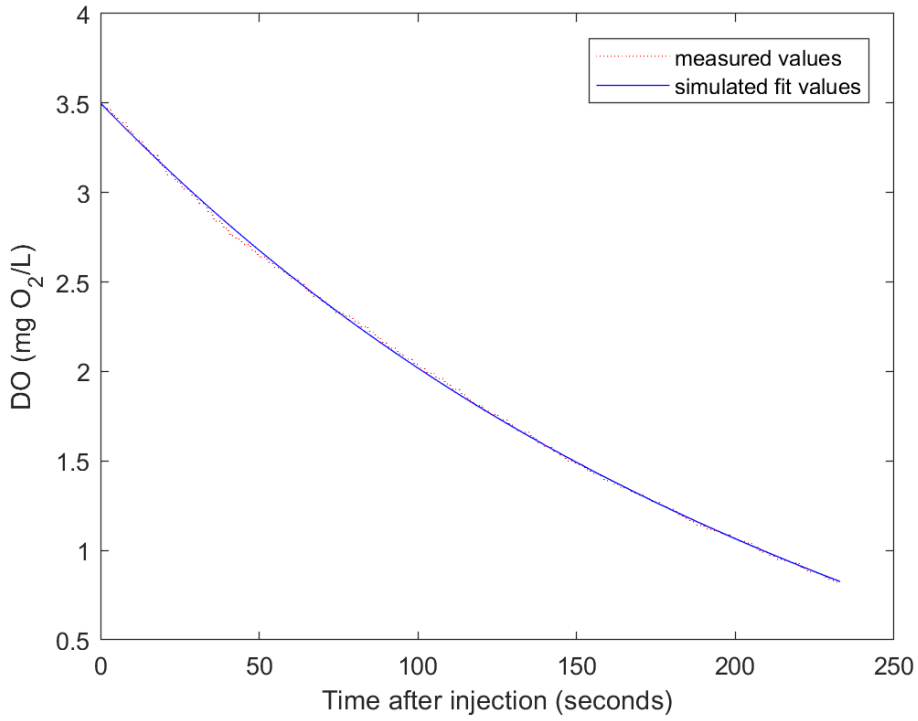

Figure A-03. Least squares curve fit for CTB1 during respirometry test

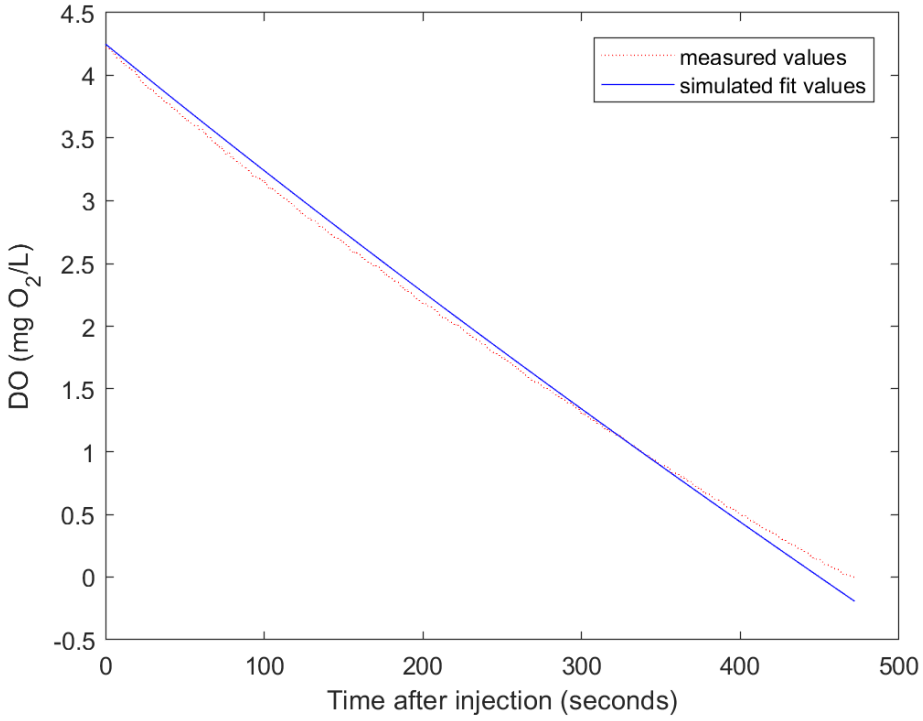

Figure A-04. Least squares curve fit for CTB2 during respirometry test

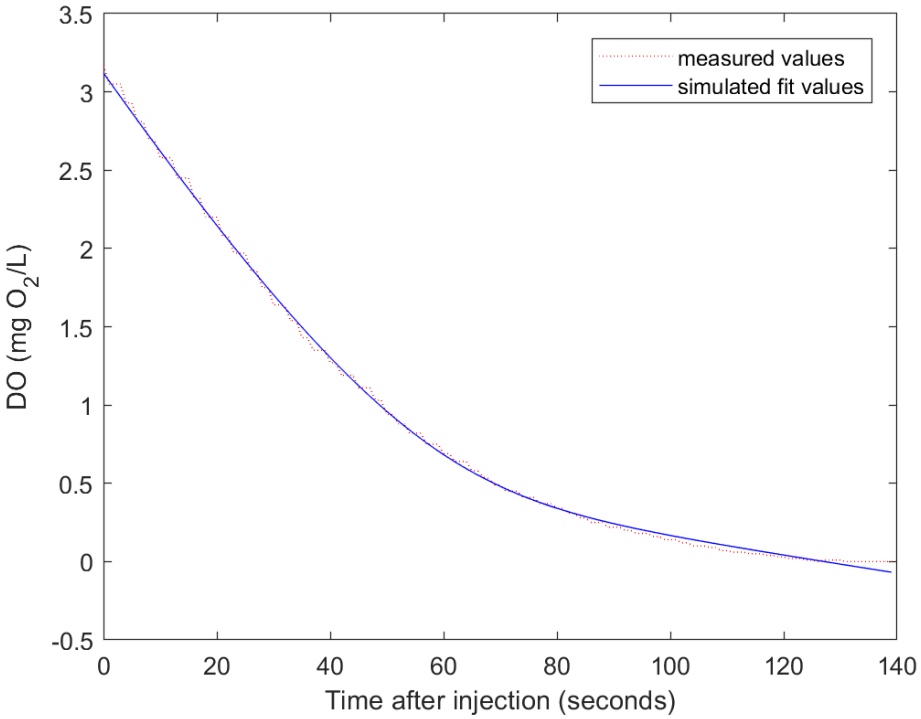

Figure A-05. Least squares curve fit for CTB3 during respirometry test

Table A-02. Average EPS measurements

Protein [mg EPS/g VSS]

			Sol-EPS		
Date	**Day**	**SBR**	**CTB1**	**CTB2**	**CTB3**
5/19/2017	0	2.14842	2.14842	2.14842	2.14842
6/7/2017	19	1.144709	0.648013	0.487425	0.842966
6/19/2017	31	0.738425	0.55183	0.26233	0.352371
6/28/2017	40	0.590704	0.353039	0.446409	0.400403
7/7/2017	49	0.692588	0.386903	0.221833	0.270188
7/19/2017	61	0.416795	0.235393	0.243686	0.575198
7/28/2017	70	0.518238	0.301779	0.259897	0.323185
8/7/2017	80	0.17947	0.230983	0.138424	0.277474
			LB-EPS		
Date	**Day**	**SBR**	**CTB1**	**CTB2**	**CTB3**
5/19/2017	0	64.88647	64.88647	64.88647	64.88647
6/7/2017	19	99.16457	65.38094	66.80055	99.6282
6/19/2017	31	137.5717	68.35241	81.48024	81.2839
6/28/2017	40	97.94812	96.45161	77.69676	92.00308
7/7/2017	49	163.6021	56.04382	70.85673	60.67103
7/19/2017	61	37.72966	18.17686	51.45345	49.81962
7/28/2017	70	86.54727	28.30715	47.22604	26.17871
8/7/2017	80	50.91266	38.20662	34.97214	49.19056

		TB-EPS			
Date	**Day**	**SBR**	**CTB1**	**CTB2**	**CTB3**
5/19/2017	0				
6/7/2017	19	18.39646	15.58242	13.50259	18.40987
6/19/2017	31	19.62703	12.14249	12.21916	9.052078
6/28/2017	40	20.46378	19.98878	23.76237	27.01556
7/7/2017	49	48.55015	43.78343	35.74389	37.94828
7/19/2017	61	41.90196	26.5071	34.53381	68.08833
7/28/2017	70	55.23619	41.63658	61.78577	51.17023
8/7/2017	80	33.40722	40.25607	30.92353	42.87677

Carbohydrate [mg EPS/g VSS]

		Sol-EPS			
Date	**Day**	**SBR**	**CTB1**	**CTB2**	**CTB3**
5/19/2017	0	1283.919	1283.919	1283.919	1283.919
6/7/2017	19	945.943	388.945	299.5858	794.62
6/19/2017	31	430.6754	455.5984	262.4282	445.9043
6/28/2017	40	697.204	364.4974	275.3136	335.9148
7/7/2017	49	729.6951	359.108	369.7887	314.3033
7/19/2017	61	1012.796	243.635	368.082	405.7379
7/28/2017	70	911.4746	274.3789	244.2999	431.4961
8/7/2017	80	397.6889	325.3977	284.4042	429.4543
		LB-EPS			
Date	**Day**	**SBR**	**CTB1**	**CTB2**	**CTB3**
5/19/2017	0	3948.224	3948.224	3948.224	3948.224
6/7/2017	19	1867.361	1478.703	1506.398	1671.505
6/19/2017	31	2774.831	2444.332	1835.27	1534.526
6/28/2017	40	2758.215	2827.237	2157.993	1626.568
7/7/2017	49	3325.974	1854.214	2345.281	1393.697
7/19/2017	61	1926.588	1371.726	3026.05	3238.014
7/28/2017	70	3941.083	2127.034	2540.675	2552.117
8/7/2017	80	1826.856	2228.475	1778.166	3257.774
		TB-EPS			
Date	**Day**	**SBR**	**CTB1**	**CTB2**	**CTB3**
5/19/2017	0				
6/7/2017	19	724.3759	684.576	505.9154	654.1171
6/19/2017	31	697.4036	585.1723	492.5594	553.9143
6/28/2017	40	1265.783	638.6724	624.7375	623.1993
7/7/2017	49	926.6266	853.473	914.193	1036.205
7/19/2017	61	1330.672	819.2892	845.5368	1083.774
7/28/2017	70	1130.19	737.3539	814.1738	840.1551
8/7/2017	80	609.9302	672.2741	618.4547	912.5917

Appendix A-1: Image capture and analysis procedures

1. Prepare bacto agar gel at 15 g/L concentration in 500 mL batches. Heat at intervals in microwave and gently swirl to dissolve all agar granules in deionized water.
2. Add 11 mL of warm agar to 15 mL centrifuge tube containing 1 mL of mixed liquor sample (total 12 mL). Use a transfer pipette with the tip cut to make a larger hole to ensure the correct amount of agar is added to each tube.
3. Add 10-20 μL of methylene blue dye to each tube. Cap the 15 mL centrifuge tube and invert gently 15 times to mix thoroughly.
4. Pour the sample + agar + dye mix into a petri dish, gently rotating the dish as you pour to ensure that the mix spreads evenly. Minimize the number of times the dish is swirled to prevent sludge particles from migrating towards the wall of the dish.
5. Prop the petri dish cover halfway over the dish to prevent dust from the falling into the dish while the agar cools to room temperature, about 30 minutes.
6. After samples are cooled, fully cap the petri dishes and store inverted in a plastic bag, with all samples from the same day, to prevent condensation from dripping onto the gel. If analysis will not be done immediately, samples may be stored at 4°C for up to a week.
7. Images of the floc and granule particles within the sample may be captured using the image capture CCD camera found on the Nikon SMA-2T stereomicroscope in the Dark Room in the Broughton Hall Environmental Engineering Laboratory.
8. To begin capturing the images of the plate, turn on the lightbox (under microscope) and the corresponding computer. Open the ToupView program on the computer and make sure it is connected to the camera.
9. Place a 1 mm ruler on the light box below the microscope and camera and adjust magnification using the coarse and fine focus knobs until the ruler may be clearly seen.
10. Once in focus, select ‘Options’ then ‘Calibration.’ The calibration name may be arbitrary as it does not save after exiting the program.
11. Adjust the red line to two points on the ruler using the camera view and take note of the actual length between the two points and the number of pixels the program measures between the two points (i.e. 1 mm, 900000 pixels). From this point on, only use the fine focus to get images in focus. Changing the coarse focus will change the magnification and the program will need to be recalibrated.
12. Capture ~10-20 images per plate using the scroll functions on the light box to get a ‘train’ of images that overlap and may be stitched together. The ToupView program will slow down if more than 10 images are open in the program at one time. Use the ‘Batch Save’ function, under ‘File’ to save all images that are open at once (example file name: 2017-04-06-SBR-A-9000x.png). The program will add a number on the end of the specified name. Save all images as .png or .tiff – never as .jpg!
13. Once all images for a sample batch have been taken and saved, turn off the light box to preserve the bulb and exit out of the ToupView program.
14. To stitch the images together, use the Microsoft Image Composite Editor (ICE) under default settings (no correction for perspective). Crop the image after stitching to remove the jagged edges which are a remnant from the images not being perfectly aligned. The

color of the stitched images (typically a pink to blue gradient) will not affect the image analysis.

15. Convert the stitched images to 8-bit using the Fiji ImageJ program using a threshold of (0,184). Threshold was decided on in order to achieve the most accurate conversion of particles (to not allow shading due to due or shadow to affect the 8-bit particle size).
16. After the images have been converted to black and white (8-bit) the 'Analyze Particles' function in ImageJ may be used to outline the particles and calculate area, size, and other general parameters of the images.
17. Save the resulting data tables as .csv files.
    a. The following macro code may be used to convert multiple stitched images to binary and to process them using the 'Analyze Particles' function of ImageJ at one time:

```
title = getTitle();
run("8-bit");
setAutoThreshold("Default");
//run("Threshold...");
//setThreshold(0, 184);
setOption("BlackBackground", false);
run("Convert to Mask");
run("Set Measurements...", "area mean min center perimeter shape feret's
integrated limit display redirect=None decimal=3");
run("Analyze Particles...", "  show=Outlines display exclude summarize");
close();
save(title+"fiji");
close();
```

18. Follow the R code listed in Appendix A-2 to process the collected data.

Appendix A-2: Code for plotting percent granulation, equivalent diameter, ribbon plots for SVI_5/SVI_{30} in R

Calculating percent granulation & equivalent diameter code:

```
# Include the libraries we need
library("ggplot2")
library("directlabels")

# Handy library which eases split, apply, and combine (SAC) operations on data
library("plyr")
library("dplyr")

library("readr")
library("lubridate")

# Antialised plots in windows
library("Cairo")

# Handy for looking at dataframes  (e.g. whatis)
library("YaleToolkit")

# For helping identify parameters from naming strings
library("stringr")

# Needed to read and combine many tidy data files
library("tidyr")
library("purrr")

# Nice default ggplot2 aesthetic theme
theme_set(theme_bw())

# Identify the directories that we'll be working with
projDir="C:/Users/Jacqueline Yeh/Documents/Research/Aerobic_Proj/R2/Data/"
dataDir="/Data"
outDir="/Outputs"

# Remember to set the working directory to the overall file with all the saved images

# Read in files output from ImageJ software with all the necessary data for particle size analysiss
particles <- c("C:/Users/Jacqueline Yeh/Documents/Research/Aerobic_Proj/R2/Data/2017-05-19-inocA-results.csv", … all other file names to be read in, if there are >25 files to be read in, split them into groups labeled 'particles1', 'particles2', etc.)
```

```
particles

# From the serialmentor.com page about "Reading and combining many tidy data files in R"
data <- data_frame(filename=particles) %>%
  mutate(file_contents=map(filename,~read_csv(.))) %>%  #originally ...file.path(files, .))))
  unnest()

# Need to create new column to have dates in in order for future functions to work
# This uses the library(stringr)
datePat <- "[:digit:]{4}-[:digit:]{2}-[:digit:]{2}"
dateStr <- str_extract(data$filename,datePat)
data$Date <- sapply((dateStr), function(x)x)

data$Date

ReactorPat <- "[:alpha:]{3}[:digit:]*[:alpha:]-results"
ReactorStr <- str_extract(data$filename,ReactorPat)
data$Reactor <- sapply(str_split(ReactorStr,"[:alpha:]-"), function(x)x[1])

data$Reactor

reppat <- "[:alpha:]{3}[:digit:]*[:alpha:]-"
repStr <- str_extract(data$filename,reppat)
data$Rep <- sapply(str_split(repStr,"[:digit:]{1}"), function(x)x[2])

data$Rep

# Labeling each date as a number of days since the beginning of the experiment (begin)
begin <- ymd("2017-05-19")
data$Date.x <- ymd(data$Date)
data$ExpDay <- data$Date.x-begin

# Total volume in each run and volfrac per element
data <- ddply(data, c("Reactor","ExpDay","Rep"), transform,
          totalarea    = sum(Area))
data$volfrac <- data$Area/data$totalarea

# Combine R objects by Rows or Columns
cbind(area = 0, data)
# Calculating particle area, equivalent diameter, d43, geometric mean
unique(data$totalarea)
data$area <- (data$Area*((1/915867*(10^-6))^2))
```

```
data$EquivDiameter <- 2*sqrt(data$Area/pi)
data$d43 <- (data$EquivDiameter^4)/(data$EquivDiameter^3)
data$geomMean <- (data$Round*data$Solidity*data$Solidity*data$Circ.)^(1/4)

# Subsetting the data to those with equivalent diameter > 50, 0.1 < roundness < 1
data <- subset(subset(data,EquivDiameter>50),Round>0.1 | Round <1)

# Creating a granule column where equivalent diameter >100 and geometric mean > 0,5
#data$isGranule <- (data$EquivDiameter > 100) & (data$geomMean > 0.5)

# Creating a new dataset with 200 size threshold (updating 'isGranule' column)
# granule = equivalent diameter (d43) > 200um and shape factor (roundness) > 0.6
data$isGranule <- (data$EquivDiameter > 200) & (data$Round > 0.6)
pctgrans200a <- summarise(group_by(data, Reactor, ExpDay, Rep),
                  granules=sum(isGranule),
pctGranule=100*sum(isGranule)/(sum(!isGranule)+sum(isGranule)))
pctgrans200a$sizeThresh=200
##

# Inserting the reactor label into the pctgrans dataset previously developed
pctgransall$Reactor <- factor(pctgransall$Reactor, levels=c("SBR","CTB1","CTB2","CTB3"))

#data$d43avg <-
d43a <- summarise(group_by(data, Reactor, ExpDay, Rep),
               totalED=sum(d43), pctED=100*sum(d43)/(sum(!d43)+sum(d43)),
               avgED=mean(d43))

d43a <- factor(d43a$Reactor, levels=c("SBR","CTB1","CTB2","CTB3"))
```

Plotting percent granulation with images code:

```
library(ggplot2)
install.packages('png')
library(png)
install.packages('caTools')
library(caTools)
library(grid)
library(plyr)
library(dplyr)
library('Cairo')
CairoWin()

# Change the project directory to match where the scripts/csv data came from
```

```
projDir="C:/Users/Jacqueline Yeh/Documents/Research/Aerobic_Proj/R2/Data"
#projDir="Dropbox/Bahareh Thesis to Manuscript/"
dataDir="C:/Users/Jacqueline Yeh/Documents/Research/Aerobic_Proj/R2/Data"
#dataDir="/CSV Data"

# Remember set working directory to the one with the files and images that will be used in the
plots

# Reference and run the summary code that calculates standard error from 3 replications for error
bars
#   Remember that the source file needs to be in the same folder as the R script, csv file, and the
images
#   AKA the source file needs to be in the working directory
source('summarySE.r') # ‘summarySE.r’ code may be found online

# Begin plotting phase#, use Cairo to put plot outside the R window
# Remember to change the 'phase' in the corresponding .csv file as well in order to plot the
desired reactor
plotPhase='I'
Cairo(file="PG_ssetEDgt50_EDgt200_Rgt0.4_all.png",
      type="png",
      units="in",
      width=7*1.75, # 7
      height=5*1.75, # 5
      bg="white",
      dpi=600)

# Read in the filename where the percent granules csv comes from
# filename="percent_granules_jy_CTB1.csv"
filename="PG ssetEDgt50 Rgt0.4.csv"
fdat <- read.csv(filename,sep=",")

# Organizing the replicate data (modeled after the percent_granules.csv file in the shared
Dropbox folder)
reps <- c("1","2","3")
repLabels <- c("Rep1","Rep2","Rep3")
fdat <- reshape(fdat, varying = repLabels, v.names = "pctGran",
                timevar = "Rep", times = reps, direction = "long")

# Use the summary R file to calculate standard error for groupings based on Reactor, Days, and
Phase
# install.packages('Rmisc') <- don't need to install Rmisc if you use the syntax below
```

```
fdat_s <- Rmisc::summarySE(data=fdat, measurevar="pctGran",
groupvars=c("Reactor","ExpDay","Phase"),
            na.rm=FALSE, conf.interval=0.95, .drop=TRUE)
fdat_s

# Dodge overlapping objects side-to-side
pd <- ggplot2::position_dodge(0.1)

# In R, an expression vector is a list of calls, symbols etc.
# Remember to change according to which reactors are being plotted
ctbLeg <- expression(paste("CTB1"))
ctbLeg2 <- expression(paste("CTB2"))
ctbLeg3 <- expression(paste("CTB3"))
sbrLeg <- expression(paste("SBR"))

# Colors used in the plot (CTB and SBR)
cbbPalette <- c("#00CC33","#FF6633","#3399FF","#FF3333")

# Begin the basics of the plot window (Cairo)
CairoWin(width = 6.4*1.75, height = 5*1.75, pointsize = 30, # sum up total width and height of
viewports created, 6.4, 5, 12
        rescale = c("R", "fit", "fixed"), xpinch, ypinch, bg =
          "transparent", canvas = "white", gamma = getOption("gamma"),
        xpos = NA, ypos = NA, buffered = getOption("windowsBuffered"),
        restoreConsole = TRUE)

# Organize the middle plot which shows the % Granules over the course of the run for the paired
SBR and CTB
pg <- ggplot(fdat_s[which(fdat_s$Phase==plotPhase),], aes(x=ExpDay, y=pctGran)) +
  geom_line(aes(color=Reactor),size=1.2*1.75) + #1.2
  geom_point(aes(color=Reactor,shape=Reactor),fill="white",size=1) +
  geom_errorbar(aes(ymin=pctGran-se,
ymax=pctGran+se,color=Reactor),width=1,position=pd,size=1) +
  xlab("Day") +
  ylab("Granulation %") +
  expand_limits(y=c(0,20)) +
#1.15*1.1*max(fdat_s[which(fdat_s$Phase==plotPhase),]$pctGran))) +
  theme(panel.grid.major = element_blank(), panel.grid.minor = element_blank(),
        panel.background = element_blank(),
        axis.line.x = element_line(colour = "black"),
        axis.title.x = element_text(size = 34),
        axis.line.y = element_line(colour = "black"),
        axis.title.y = element_text(size = 34)) +
```

```
  theme(axis.title=element_text(face="bold",colour="black",size=34)) +
  theme(axis.text=element_text(colour="black",size=34)) +
  theme(legend.position=c(0.1, 0.80), #0.3,0.9 -> change if it overlaps plot
        legend.text=element_text(face="bold",colour="black",size=30),
        legend.title=element_blank()) +
  scale_colour_manual(name  ="Reactor",
                      breaks=c("CTB1", "CTB2", "CTB3", "SBR"),
                      labels=c(ctbLeg, ctbLeg2, ctbLeg3, sbrLeg),
                      values=cbbPalette) +
  scale_shape_manual(name  ="Reactor",
                     breaks=c("CTB1", "CTB2", "CTB3", "SBR"),
                     labels=c(ctbLeg, ctbLeg2, ctbLeg3, sbrLeg),values=c(23,21,19,17)) +
  theme(legend.key = element_rect(fill = NA, colour = NA, size = 0.25))
pg

# Set the size of the viewports that will make up the final comparison plot with called images of
reactor particles
size = unit((7/4-0.2)*1.75, "in") # 7/4-0.2
hsize = unit(0.8*1.75, "in") # 0.8
hsize2 = unit(3*1.75, "in") # 3
hsize3 = unit(0.2*1.75, "in") # 0.2

# Set up the layout for grid of images that will make the whole comparison plot
heights = unit.c(hsize,hsize3,hsize2,hsize,hsize3)
widths = unit.c(hsize3,size,size,size,size)
lo = grid.layout(5, 5,widths,heights) # change according to setup of grid of viewports

# Show the layout to make sure the grid sets up as desired
grid.show.layout(lo)

# Position the elements within the viewports:
#   pushViewport() adds viewports to the tree
#   popViewport() removes viewports form the tree
#   There is only ever one current viewport(nested drawing contexts), which is the current
position within the viewport
#   The viewports can be used to overlay plots, images, or text on each other (?)
grid.newpage()
pushViewport(viewport(layout = lo))

# The plot
pushViewport(viewport(layout.pos.row=3, layout.pos.col = c(1,5)))
print(pg, newpage=FALSE)
popViewport()
```

```
sCap<-textGrob("SBR",rot=90,hjust=0.5,vjust=0.5,gp=gpar(fontsize=30, face="bold"))
# The logo
pushViewport(viewport(layout.pos.row=1, layout.pos.col =1 ))
print(grid.draw(sCap), newpage=FALSE)
popViewport()

# Adjust the following titles to reflect the days an image is chosen to represent the SBR particles
sCap<-textGrob("Day 19",hjust=0.5, gp=gpar(fontsize=30))
# The logo
pushViewport(viewport(layout.pos.row=2, layout.pos.col =2 ))
print(grid.draw(sCap), newpage=FALSE)
popViewport()

sCap<-textGrob("Day 40",hjust=0.5, gp=gpar(fontsize=30))
# The logo
pushViewport(viewport(layout.pos.row=2, layout.pos.col =3 ))
print(grid.draw(sCap), newpage=FALSE)
popViewport()

sCap<-textGrob("Day 54",hjust=0.5, gp=gpar(fontsize=30))
# The logo
pushViewport(viewport(layout.pos.row=2, layout.pos.col =4 ))
print(grid.draw(sCap), newpage=FALSE)
popViewport()

sCap<-textGrob("Day 84",hjust=0.5, gp=gpar(fontsize=30))
# The logo
pushViewport(viewport(layout.pos.row=2, layout.pos.col =5 ))
print(grid.draw(sCap), newpage=FALSE)
popViewport()

img <- readPNG("C:/Users/Jacqueline Yeh/Documents/Research/Aerobic_Proj/R2/Data/Rescale
0-33 output gscale/2017-06-07-SBRa-stitch.png")
g <- rasterGrob(img)
# The logo
pushViewport(viewport(layout.pos.row=1, layout.pos.col =2 ))
print(grid.draw(g), newpage=FALSE)
popViewport()
# Pulling the images up to put in the plot - correspond to the days of the titles in the previous
section
```

```
img <- readPNG("C:/Users/Jacqueline Yeh/Documents/Research/Aerobic_Proj/R2/Data/Rescale
0-33 output gscale/2017-06-28-SBRa-stitch.png")
g <- rasterGrob(img)
# The logo
pushViewport(viewport(layout.pos.row=1, layout.pos.col =3 ))
print(grid.draw(g), newpage=FALSE)
popViewport()

img <- readPNG("C:/Users/Jacqueline Yeh/Documents/Research/Aerobic_Proj/R2/Data/Rescale
0-33 output gscale/2017-07-12-SBRa-stitch.png")
g <- rasterGrob(img)
# The logo
pushViewport(viewport(layout.pos.row=1, layout.pos.col =4 ))
print(grid.draw(g), newpage=FALSE)
popViewport()

img <- readPNG("C:/Users/Jacqueline Yeh/Documents/Research/Aerobic_Proj/R2/Data/Rescale
0-33 output gscale/2017-08-11-SBRa-stitch.png")
g <- rasterGrob(img)
# The logo
pushViewport(viewport(layout.pos.row=1, layout.pos.col =5 ))
print(grid.draw(g), newpage=FALSE)
popViewport()

# Now these are the day titles for the images pulled for the CTB reactor
sCap<-textGrob("CTB",rot=90,hjust=0.5,vjust=0.5,gp=gpar(fontsize=30, face="bold"))
# The logo
pushViewport(viewport(layout.pos.row=4, layout.pos.col =1 ))
print(grid.draw(sCap), newpage=FALSE)
popViewport()

sCap<-textGrob("Day 19",hjust=0.5, gp=gpar(fontsize=30))
# The logo
pushViewport(viewport(layout.pos.row=5, layout.pos.col =2 ))
print(grid.draw(sCap), newpage=FALSE)
popViewport()

sCap<-textGrob("Day 40",hjust=0.5, gp=gpar(fontsize=30))
# The logo
pushViewport(viewport(layout.pos.row=5, layout.pos.col =3 ))
print(grid.draw(sCap), newpage=FALSE)
popViewport()
```

```
sCap<-textGrob("Day 54",hjust=0.5, gp=gpar(fontsize=30))
# The logo
pushViewport(viewport(layout.pos.row=5, layout.pos.col =4 ))
print(grid.draw(sCap), newpage=FALSE)
popViewport()

sCap<-textGrob("Day 84",hjust=0.5, gp=gpar(fontsize=30))
# The logo
pushViewport(viewport(layout.pos.row=5, layout.pos.col =5 ))
print(grid.draw(sCap), newpage=FALSE)
popViewport()

# The following section pulls the corresponding CTB reactor particle images to the days titled
above
img <- readPNG("C:/Users/Jacqueline Yeh/Documents/Research/Aerobic_Proj/R2/Data/Rescale
0-33 output gscale/2017-06-07-CTB1a-stitch.png")
g <- rasterGrob(img)
# The logo
pushViewport(viewport(layout.pos.row=4, layout.pos.col =2 ))
print(grid.draw(g), newpage=FALSE)
popViewport()

img <- readPNG("C:/Users/Jacqueline Yeh/Documents/Research/Aerobic_Proj/R2/Data/Rescale
0-33 output gscale/2017-06-28-CTB1a-stitch.png")
g <- rasterGrob(img)
# The logo
pushViewport(viewport(layout.pos.row=4, layout.pos.col =3 ))
print(grid.draw(g), newpage=FALSE)
popViewport()

img <- readPNG("C:/Users/Jacqueline Yeh/Documents/Research/Aerobic_Proj/R2/Data/Rescale
0-33 output gscale/2017-07-12-CTB1a-stitch.png")
g <- rasterGrob(img)
# The logo
pushViewport(viewport(layout.pos.row=4, layout.pos.col =4 ))
print(grid.draw(g), newpage=FALSE)
popViewport()

img <- readPNG("C:/Users/Jacqueline Yeh/Documents/Research/Aerobic_Proj/R2/Data/Rescale
0-33 output gscale/2017-08-11-CTB1a-stitch.png")
g <- rasterGrob(img)
# The logo
pushViewport(viewport(layout.pos.row=4, layout.pos.col =5 ))
```

```
print(grid.draw(g), newpage=FALSE)
popViewport()

# Close out the Cairo viewing window
popViewport()

dev.off()
```

Plotting the SVI ribbon plot (SVI_5/SVI_{30}):

```
# Set up libraries needed to plot
library("ggplot2")
library("directlabels")
library("plyr")
library("dplyr")
library("Cairo")
library("stringr")
library("gridExtra")

# Nice default ggplot2 aesthetic theme
theme_set(theme_bw())

# Setup project directory
projDir="C:/Users/Jacqueline Yeh/Documents/Research/Aerobic_Proj/R2"
dataDir="/Data"
outDir="/Outputs"

# Remember to set working directory to be the folder you are working in

# Call in *.csv files of data so R can read them
#svidata <- read.csv("C:/Users/Jacqueline
Yeh/Documents/Research/Aerobic_Proj/R2/AG&EPS_R2_SVI.csv",header=TRUE)
svisbr <- read.csv("C:/Users/Jacqueline
Yeh/Documents/Research/Aerobic_Proj/R2/AG&EPS_R2_SVI_SBR_v2.csv",header=TRUE)
svictb1 <- read.csv("C:/Users/Jacqueline
Yeh/Documents/Research/Aerobic_Proj/R2/AG&EPS_R2_SVI_CTB1.csv",header=TRUE)
svictb2 <- read.csv("C:/Users/Jacqueline
Yeh/Documents/Research/Aerobic_Proj/R2/AG&EPS_R2_SVI_CTB2.csv",header=TRUE)
svictb3 <- read.csv("C:/Users/Jacqueline
Yeh/Documents/Research/Aerobic_Proj/R2/AG&EPS_R2_SVI_CTB3.csv",header=TRUE)

# Check that leafdata has correct files
svisbr
```

```
svictb1
svictb2
svictb3

# Individual plots for each reactor
svi_sbr <- ggplot(data=svisbr, aes(x=Day,y=SVIavg_sbr), Reactor=sbr) +
  geom_ribbon(aes(ymin=(svi30avg_sbr), ymax=SVI5avg_sbr),fill="red") +
  geom_line(aes(y=SVIavg_sbr)) +
  xlab("Day of Operation") + ylab("Average SVI (mL/g)")
svi_sbr

svi_ctb1 <- ggplot(data=svictb1, aes(x=Day,y=SVIavg_ctb1), Reactor=ctb1) +
  geom_ribbon(aes(ymin=SVI30avg_ctb1, ymax=SVI5avg_ctb1),fill="green") +
  geom_line(aes(y=SVIavg_ctb1)) +
  xlab("Day of Operation") + ylab("Average SVI (mL/g)")
svi_ctb1

svi_ctb2 <- ggplot(data=svictb2, aes(x=Day,y=SVIavg_ctb2), Reactor=ctb2) +
  geom_ribbon(aes(ymin=SVI30avg_ctb2, ymax=SVI5avg_ctb2),fill="orange") +
  geom_line(aes(y=SVIavg_ctb2)) +
  xlab("Day of Operation") + ylab("Average SVI (mL/g)")
svi_ctb2

svi_ctb3 <- ggplot(data=svictb3, aes(x=Day,y=SVIavg_ctb3), Reactor=ctb3) +
  geom_ribbon(aes(ymin=SVI30avg_ctb3, ymax=SVI5avg_ctb3),fill="blue") +
  geom_line(aes(y=SVIavg_ctb3)) +
  xlab("Day of Operation") + ylab("Average SVI (mL/g)")
svi_ctb3

# Using command from library("gridExtra") to stack each of the SVI plots on top of one another
grid.arrange(svi_sbr,svi_ctb1,svi_ctb2,svi_ctb3,ncol=1)
# Colour-filled stacked SVI plot
#     2018-01-30: Currently getting the following, Error: Aesthetics must be either length 1 or the
same as the data (172): ymin, ymax, fill, x, y
svi_combo2 <- ggplot(data=svicombo, aes(x=Day[Day<125], y=SVIavg)) +
  geom_ribbon(aes(ymin=SVI30avg, ymax=SVI5avg, fill=Reactor)) +
    scale_fill_manual(values=c("#00CC33","#FF6633","#3399FF","#FF3333")) +
  geom_line(aes(y=SVIavg, colour=Reactor)) +
    scale_colour_manual(values=c("#00CC33","#FF6633","#3399FF","#FF3333")) +
  facet_grid(Reactor~.) +
  xlab("Day of Operation") + ylab("Average SVI (mL/g)") + theme_classic() +
  # Font made larger for the 2018 Symposium poster
  theme(strip.text.y=element_text(size=24, face="bold")) +
```

```
  theme(axis.text=element_text(size=24), axis.title=element_text(size=24, face="bold")) +
  theme(legend.text=element_text(size=22), legend.title=element_text(size=24))

svi_combo2
ggsave("SVI-allreactors-color.png", width=8, height=8)

# Colour-filled SIDE-BY-SIDE SVI plot
CairoWin()
Cairo(file="SVIRibbon_sbs.png", # not sure if this is supposed to name the image? haven't seen
where they've been saving if that's what this is for...
      type="png",
      units="in",
      width=8,
      height=3,
      bg="white",
      dpi=600)

CairoWin(width = 15, height = 5, pointsize = 30, # sum up total width and height of viewports
created, 6.4, 5, 12
         rescale = c("R", "fit", "fixed"), xpinch, ypinch, bg =
           "transparent", canvas = "white", gamma = getOption("gamma"),
         xpos = NA, ypos = NA, buffered = getOption("windowsBuffered"),
         restoreConsole = TRUE)

svi_combo2 <- ggplot(data=svicombo, aes(x=Day[Day<125], y=SVIavg)) +
  geom_ribbon(aes(ymin=SVI30avg, ymax=SVI5avg, fill=Reactor)) +
  scale_fill_manual(values=c("#00CC33","#FF6633","#3399FF","#FF3333")) +
  geom_line(aes(y=SVIavg, colour=Reactor)) +
  scale_colour_manual(values=c("#00CC33","#FF6633","#3399FF","#FF3333")) +
  facet_grid(.~Reactor) +
  xlab("Day of Operation") + ylab("Average SVI (mL/g)") + theme_classic() +
  # Font made larger for the 2018 Symposium poster
  theme(strip.text.y=element_text(size=24, face="bold")) +
  theme(strip.text.x=element_text(size=24, face="bold")) +
  theme(axis.text=element_text(size=24), axis.title=element_text(size=24, face="bold")) +
  theme(legend.text=element_text(size=22), legend.title=element_text(size=24))

svi_combo2
```

Appendix A-3: Full EPS extraction and quantification procedures

Separation of EPS components by sonication

EPS sonication protocol follows the Pellicer-Nacher et al. (2013) team's it needed to be adapted to fit our sonicator output of 500W and the volume of our samples.

Reagents (extraction buffer, EB):

2 mM Trisodium phosphate (Na3PO4), 4 mM Monosodium phosphate (NaH2PO4), 9 mM Sodium chloride (NaCl), 1 mM Potassium chloride (KCl) at pH 7

$$\frac{2\ mmol\ Na_3PO_4}{L\ H_2O} \times \frac{1\ mol}{1000\ mmol} \times \frac{163.94\ g\ Na_3PO_4}{1\ mol\ Na_3PO_4} = \frac{0.327\ g\ Na_3PO_4}{L\ H_2O}$$

$$\frac{4\ mmol\ NaH_2PO_4}{L\ H_2O} \times \frac{1\ mol}{1000\ mmol} \times \frac{119.98\ g\ NaH_2PO_4}{1\ mol\ NaH_2PO_4} = \frac{0.479\ g\ NaH_2PO_4}{L\ H_2O}$$

$$\frac{9\ mmol\ NaCl}{L\ H_2O} \times \frac{1\ mol}{1000\ mmol} \times \frac{58.44\ g\ NaCl}{1\ mol\ NaCl} = \frac{0.526\ g\ NaCl}{L\ H_2O}$$

$$\frac{1\ mmol\ KCl}{L\ H_2O} \times \frac{1\ mol}{1000\ mmol} \times \frac{74.55\ g\ KCl}{1\ mol\ KCl} = \frac{0.075\ g\ KCl}{L\ H_2O}$$

Procedure:

1. Soluble EPS separation
    a. Centrifuge 14 mL mixed liquor samples for 1.5 minutes at 5000g in a swinging bucket rotor, then for 10 minutes at 12,000g in a fixed-angle rotor, then for 15 minutes at 5000g in a fixed angle rotor to separate the Sol-EPS from the biomass.
    b. Filter the supernatant through 0.2 μm pore size filters and store at -21°C in 1.5 mL microcentrifuge tubes until further analysis.
        i. Note for each type of EPS extracted, it is helpful to filter supernatant through 0.45 μm filter membranes using a vacuum pump prior to syringe filtration through the 0.2 μm filters.
    c. Resuspend the remaining pellets to the original volume in extraction buffer.
2. Loosely-Bound (LB) EPS extraction
    a. Minimize temperature rise of samples during sonication by keeping them on ice.
    b. Gently homogenize the 15 mL centrifuge tubes of biomass resuspended in extraction buffer at 50 J/mL using a sonifer (Emmerson, USA) equipped with a 1/8" tapered microtip (for our sonicator: 14 seconds at 20% of 500 W on 50% duty cycle).
    c. Right after sonication, add 6 μL of 100% formamide per mL of sample (84 μL/14 mL sample).
    d. Incubate samples for 1 hour in a horizontal position at 4°C in an orbital shaker rotating at 300 rpm.

        i. If this type of shaker is unavailable, can mix slowly using a vertical mixer.
    e. Centrifuge the incubated and mixed samples for 10 minutes at 12,000g (10,000 rpm on floor-model ultracentrifuge).
    f. Filter the supernatant through 0.2 um pore size filters and store at -21°C in 1.5 mL microcentrifuge tubes until further analysis.
    g. Resuspend the remaining pellets to the original volume in extraction buffer.
3. Tightly-Bound (TB) EPS extraction
    a. Sonicate the resuspended pellets in extraction buffer from the last LB-EPS extraction step on ice at 150 J/mL using a sonifer (Emmerson, USA) equipped with a 1/8" tapered microtip (for our sonicator: 42 seconds at 20% of 500 W on 50% duty cycle).
    b. Centrifuge the sonicated samples for 1.5 minutes at 4500 rpm, 10 minutes at 10,000 rpm, and 15 minutes at 6500 rpm, all at 4°C.
    c. Filter the supernatant through 0.2 μm pore size filters and store at -21°C in 1.5 mL microcentrifuge tubes until further analysis.
    d. Resuspend the remaining pellets to the original volume in extraction buffer.

Carbohydrate quantification: Anthrone and sulfuric acid method

Following the Pellicer-Nàcher et al., 2013 protocol, the Anthrone method from Frølund et al., 1996 was used and adapted for flat bottom 96-well microplates (ours are not flat-bottomed) used with a microplate reader. D-Glucose was used as a standard for carbohydrate measurements. From Frølund et al., 1996:

Reagents:

0.125% anthrone (w/v); 94.5% Sulfuric acid (v/v); D-Glucose

Procedure:

1. Put a waste container (for pipette tips) and a glass dish in the hood for the anthrone-sulfuric acid reagent mixture to be pulled using the multipipetter.
2. Cover a glass vial for storage of anthrone/sulfuric acid reagent storage with aluminum foil to protect the light-sensitive (slightly) mixture.
3. Under a hood, measure 100 mL of concentrated (>94.5%) sulfuric acid and pour into prepped glass vial. *Always* work with exposed sulfuric acid under the hood.
4. Add 0.125 grams of anthrone to 100 mL of concentrated (>94.5%) sulfuric acid. Gently swirl to mix. Place to the side of the hood until ready to add to samples. Note that the reagent mixture must be used within 12 hours to produce accurate readings.
5. Prepare blind values (DI water) without the anthrone reagent (typically 10% of sample values).
6. Prepare standards using D-Glucose.
    a. Each plate has space for 6 standards (A4 to A9). Tailor the standards to the range of the samples to be analyzed.
7. Pipette 0.08 mL (80 μL) of DI water into the designated wells for blank replicates.

8. Pipette 0.08 mL (80 µL) of each D-Glucose standard into the designated wells to create the standard curve. Do this for each plate to ensure that the minute differences between plates do not affect the readings.
9. Pipette 0.08 mL (80 µL) of carbohydrate-containing samples into appropriate well on plate. See 96-well sample organization table to check placement of the sample.
10. Add 0.16 mL (160 µL) anthrone/sulfuric acid reagent to each well. Direct the stream of acid to the liquid surface rather than the side of the wells to quickly obtain good mixing. Gently mix exactly 15 times using multipipetter (*consistency is key*).
11. Place plate with samples in PCR cycler to incubate at 100°C for 14 minutes to hydrolyse the polysaccharides to monosaccharides by the strong acid. The monosaccharides are then dehydrated to furfural derivatives by the anthrone which causes the bluish-green complex to form.
12. When incubation has finished, remove plate from the PCR cycler and cool at 4°C for 5 minutes on ice under the hood.
13. Measure absorbance at 620 nm using microplate reader.
    a. If the fluorescence filter is in place, carefully open the filter door and replace with the correct absorbance filter (620 nm should be the fourth filter). Never push or force the filter into the machine, the microplate reader should draw the filter into the correct position like a CD.
    b. Setup the microplate reader software with the brand of the 96-well plate, wells to be measured, and the absorbance desired.
14. Save and export file from microplate reader as an Excel file. Be sure to include "Carbohydrate" plate ID, project, and initials in the file name so it can be easily identified by someone else.

Protein quantification: microplate procedure with BCA standards

Procedure following that listed in the ThermoFisher procedure that comes with the Pierce BCA Protein Assay kit for the microplate procedure (sample to WR ratio = 1:8).

Reagents:

BCA Reagent A, BCA Reagent B, Albumin Standard (2 mg/L)

Procedure:

1. Determine volume working reagent (WR) required using the following formula:
$$(\#\ standards + \#\ unknowns) \times (\#\ replicates) \times (volume\ of\ WR\ per\ sample) = total\ volume\ WR\ reqired$$
Note that for the microplate procedure, 200 µL of WR are required for each sample.
2. Prepare WR by mixing 50 parts of BCA Reagent A with 1 part of BCA Reagent B (50:1, Reagent A:B). Note when Reagent B is first added to Reagent A, turbidity is observed that quickly disappears upon mixing to yield a clear, green WR. Prepare sufficient volume of WR based on the number of samples to be assayed. The WR is stable for several days when stored in a closed container at room temperature.

3. Bring a waste container for pipette tips, petri dish for the WR (to use multipipette), and labelled 0.2 mL 96-well microplate (suitable for microplate reader) to a hood.
4. Pipette 25 µL of each standard or unknown sample replicate into a microplate well (working range = 20-2000 µg/mL).
5. Add 200 µL of the WR to each well and mix plate thoroughly on a plate shaker for 30 seconds.
6. Cover plate and incubate at 37°C for 30 minutes.
7. Cool plate to RT. Measure the absorbance at or near 562 nm on a plate reader.
8. Subtract the average 562 nm absorbance measurement of the blank standard replicates from the 562 nm measurements of all other individual standard and unknown sample replicates.
9. Prepare a standard curve by plotting the average blank-corrected 562 nm measurement for each BSA standard vs. its concentration in µg/mL. Use the standard curve to determine the protein concentration of each unknown sample. Note if using curve-fitting algorithms associated with a microplate reader, a four-parameter (quadratic) or best-fit curve will provide more accurate results than a purely linear fit. If plotting results by hand, a point-to-point curve is preferable to a linear fit to the standard points.